# Dispersal of Mountain Pine Beetle and Impacts of Management

by

Shaun Strohm

B.Sc. Hons., The University of British Columbia, 2008

A THESIS SUBMITTED IN PARTIAL FULFILLMENT OF
THE REQUIREMENTS FOR THE DEGREE OF

DOCTOR OF PHILOSOPHY

in

The College of Graduate Studies

(Mathematics)

THE UNIVERSITY OF BRITISH COLUMBIA

(Okanagan)

July 2013

# Abstract

In this thesis, we use a reaction-diffusion equation with chemotaxis to model the interaction between Mountain Pine Beetle (MPB, Dendroctonius ponderosae), Mountain Pine Beetle pheromones, and susceptible trees. The goal is to understand how the movement and attack of MPB is affected by management activities.

We investigate the spatial pattern formation of attack clusters in a system for Mountain Pine Beetle. Mathematical analysis is utilized to discover the spacing between beetle attacks on the susceptible landscape. The model predictions are verified by analyzing aerial detection survey data of Mountain Pine Beetle Attack from the Sawtooth National Recreation Area. We find that the distance between Mountain Pine Beetle attack clusters predicted by our model and observed in the Sawtooth National Recreation Area are the same. These results clarify the spatial mechanisms controlling the transition from incipient to epidemic populations and may eventually lead to control measures which protect forests from MPB outbreaks.

Our next avenue of investigation is using an experimental study and theoretical work to help understand the effects of habitat fragmentation on the movement of the MPB. The experimental study consists of trap catch data for MPB in different domains of fragmented habitat. We simulate the experimental system using our mathematical model, testing different hypothesis on initial position of MPB emergence and diffusion speed. Our study provides support for the hypothesis that MPB may move faster in harvested landscapes, and that MPB emerge uniformly over the landscape.

Finally, we use a multi-year spatially explicit model to test the effectiveness of the management strategies of baiting and tree-removal and prescribed burning. We find that baiting and tree-removal is successful at reducing

MPB density and forest impact, as long as MPB emergence densities are not too small. We predict that tree removal without baiting can be more successful than combined baiting and tree removal if the searched area has a large density of MPB. Finally, analysis of our model indicates that prescribed burning can be more effective than clearcutting given certain assumptions about the reproductive output and attractiveness of burned trees.

# Preface

- The mathematical model was constructed by Shaun Strohm. To ensure biological relevance we consulted with MPB biologist Mary Reid (University of Calgary) and Kurt Trzcinski (Department of Fisheries and Oceans, Dartmouth, NS).

- Chapter 2 is a study of the attack patterns formed by MPB at incipient epidemic levels. Mountain Pine Beetle attack data from the Sawtooth National recreation area were provided by Jim Powell (Utah State University). More specifically, the data are USDA Forest Service aerial detection survey; full details are provided in Crabb et al. [CPB12]. Analysis of the data and mathematical analysis of the model were done by Shaun Strohm. This work has been accepted in the Bulletin of Mathematical Biology and is currently in press. Jim Powell, our co-author, provided valuable insight into this project.

- Chapter 3 is an elucidation of Mountain Pine Beetle trap catch data through a simulation study of the mathematical model. The data were provided by Mary Reid. All simulation work and analysis were done by Shaun Strohm. Mary Reid was consulted regularly on this project.

- Chapter 4 is a study of the effects of different management activities on Mountain Pine Beetle Movement. All mathematical analysis and simulation work was done by Shaun Strohm. To maintain relevance to management and MPB biology we consulted with Mary Reid and a representative from Parks Canada in Banff, Jane Park.

- The simulation model was written using a Fortran code base developed originally by Rebecca Tyson, and heavily modified by Shaun Strohm

to solve the Mountain Pine Beetle model equations. The model uses CLAWpack, a program which is capable of solving very stiff hyperbolic systems with high accuracy. This program is developed by Randall LeVeque [LT96, LeV97].

– All the research subprojects above were completed under the supervision of Rebecca Tyson. My committee members Dan Coombs and Sylvie Desjardins also provided feedback and helpful suggestions.

– All thesis text is original, unpublished, and was written exclusively by Shaun Strohm.

# Table of Contents

# List of Tables

# List of Figures

# Acknowledgements

I would like to acknowledge the support of my supervisor, Rebecca Tyson. Her amazing guidance and support allowed this work to be possible. Collaborators Mary Reid and Jim Powell provided very helpful discussions and direction for the work. Other helpful ideas came from discussions with Dan Coombs, Sylvie Desjardins, Jane Park, and Kurt Trzcinski. Critical to the numerical analysis was Clawpack, developed by Randall LeVeque. Computing assistance for HPC was provided by Steve Cundy and Wade Klaver. I would like to also acknowledge helpful discussions from Alan Law and the members of the Tyson Lab group, past and present, including Ben Wilson, Carly Rozins, Meghan Dutot, Garrett Culos, Alex Blaessle, Chris Coutts, and Katrina Williams. Finally, I must acknowledge the amazing support of my wife, Elizabeth, as well as my family (especially my parents, Chris and Dianne) and friends. I would also like to acknowledge my funding sources NSERC, PIMS IGTC, MITACS, and UBC Okanagan.

# Dedication

I would like to dedicate this thesis to my wife, Elizabeth Strohm, and my parents, Chris and Dianne Strohm.

# Chapter 1

# Introduction

The Mountain Pine Beetle (MPB, *Dendroctonius ponderosae*) is an aggressive bark beetle that has had a major economic impact on the Western Canadian and United States forestry industries. At endemic (low population) levels this beetle is a minor pest, killing trees weakened by drought, root rot, or lightning strikes [PKW+00]. In contrast, at epidemic levels, thousands of acres of healthy, vigorous trees can be rapidly eradicated [PKW+00].

The MPB preferentially uses lodgepole pine as its host [SW06]. What distinguishes MPB from other tree pests is that it must kill the host to successfully reproduce. The beetles land on the host tree, then burrow into the bark to reach the nutrient-rich phloegm, where they dig vertical galleries. The eggs laid in the galleries produce larvae which feed on the phloegm, cutting off the nutrient pathways of the tree. If consumption of the phloegm tissue is sufficiently extensive, the tree dies and develops a red-top by the following summer. MPB also have a mutualistic relationship with blue stain fungus [SW06], and can introduce the fungus to attacked trees, which can cause dessication and interrupt transpiration in the host tree. This combination can severely impede the nutrient and water movement (more than just the MPB alone) within the tree and induce mortality in the host tree.

The lodgepole pine has a defense mechanism against beetle attack: It produces resin, that fills the holes in the bark produced by the nesting MPBs and crystallizes around the beetles, effectively killing them. Furthermore, the tree can produce oleoresin, which is capable of killing the MPB eggs. The MPB must therefore mass attack in sufficient numbers to overcome host defenses and kill the tree.

The life cycle of the MPB is generally univoltine (one generation per

year) [SW06] and is very dependent upon ambient temperature. Eggs are generally laid from late July to mid-August, and these eggs hatch and develop through four larval instars over the winter. The fourth larval instar develops into a pupa by June and then matures into an adult by late June to mid-July. These adults emerge from the tree in mid-July to mid-August, fly around until they find a suitable host, and then attack it and lay their eggs. The flight of these beetles is very interesting since the movement is not governed by simple diffusion but also incorporates chemotactic movement due to semiochemicals produced by the MPBs and the host trees (See White and Powell and references therein [WP97]).

Due to the importance of the MPB to the forestry industry, the interaction between MPBs and lodgepole pine trees has been extensively studied and modeled by several authors. The beetle phenology and the impact of temperature on the beetle life cycle has been modeled by Gilbert et al [GPLB04] and Powell et al [PJLB00, PL05, PB09]. Shore and Safranyik [SS92] developed a susceptibility model for stands of trees. Susceptibility models are important in forest management since they can assist in the identification of high-risk stands of lodgepole pine. A computer model for population dynamics was developed by Raffa et al [RB86]. Discrete models for the spatial movement of MPB were developed by Burnell [Bur77] and Geiszler et al [GGG80]. Burnell [Bur77] incorporated both beetle dispersal and aggregation, while Geiszler et al [GGG80] incorporated the dynamics of beetle pheromone and modeled variable wind speeds. A discrete model for MPB growth and lodgepole pine attack in a 1 ha stand was developed by Safranyik et al [SBTR99]. The purpose of the model was to evaluate the effectiveness of different management strategies. The authors investigated stand removal, stand thinning, single-tree application of MSMA (a chemical designed to induce mortality of the MPB), and the use of attractive and repulsive pheromone. Since this model was not spatially explicit it neglected the spatial variation in the landscape and its effects on the management activities. To make the MPB model more usable for forestry management, the model was extended to the stand scale by Riel et al [RFSS04], and then extended further to the landscape level [RFSS04]. At the stand and land-

scape levels, tree removal and green-attack detection were the management activities investigated. Riel et al [RFSS04] did not investigate the use of pheromone baiting at these larger spatial scales.

These studies were followed by work using continuous models, such as the ordinary differential equation models of Berryman et al [BSW84] and Nelson et al [NPL$^+$08]. The Berryman et al [BSW84] model uses two coupled ODEs to describe the interaction between the lodgepole pine forest and the MPB. The Nelson et al [NPL$^+$08] model focuses on the interaction of a single tree with the MPB. It incorporates the damage to trees done by MPBs, which allows the trees to be weakened for attacks by MPBs in subsequent years. The Berryman et al paper [BSW84] focuses on the spatial movement of the beetle while the work of Nelson et al [NPL$^+$08] focuses on the beetle biology.

There have been other models that incorporate both the beetle biology and the spatial movement of the beetle. Polymenopoulos and Long [PL90] introduced a MPB model with diffusive movement and a simple discrete linear growth term. They made the model more complex through incorporation of directed movement of beetles toward trees with larger phloem. Later, an integro-difference model developed by Heavilin et al [HP08], which is continuous in space and discrete in time, was used to model the spread of the beetle infestation by considering simply the transmission of "infection" from one tree to another, without regard for the details of the beetle dynamics. This model did not explicitly consider the spatial movement of beetles due to chemotaxis, which can be done by using a more complex spatially explicit partial differential equation model, as developed by Powell et al [PMW98, WP97]. It did, however, incorporate the biology and spatial movement of the MPB, and the interaction between lodgepole pine trees and beetles at the stand scale of the forest. An individual-based approximation of this model was developed by Hughes et al [HFSL06] to investigate the effect of different landscapes on the spatial movement of the MPB.

Previous modelling efforts have generally investigated beetle dynamics over a single season. Few models have looked at beetle populations across multiple years. Of those that have looked at multiple-year dynamics, there are no models of which we are aware that explicitly model both population

dynamics and dispersal, including the interactions between beetles, beetle pheromones, tree kairomones, and the forest landscape. These interactions are extremely important as they are major determinants of the MPB spread dynamics over the landscape.

In this thesis, we build a multi-year spatially explicit mathematical model that incorporates the interactions between beetles, beetle pheromones, tree kairomones, and the forest landscape. Our model investigates the beetle dynamics on the stand scale of 1 ha - 1 $km^2$. We are not aware of this type of spatially explicit modelling work at this scale investigating the effects of management.

We use our model to address three different questions about MPB spread and subsequent tree damage. In Chapter 2, we use our mathematical model to investigate the spacing between clusters of MPB attack on the forest landscape. To verify the predictions of our mathematical model we utilize aerial detection survey data from the Sawtooth National Recreation Area (SNRA), and then discuss the management implications of our results. Chapter 3 focuses on the effects of habitat fragmentation on MPB movement. We use our theoretical model to explain results obtained in an experimental MPB study. Specifically, we consider a landscape with pheromone traps on either side of a boundary between mature and harvested forest. The fragmented habitat contains different combinations of dense, thinned, and clearcut forest regions. This work is extremely important as MPB movement in fragmented habitats is not well understood [BAL93].

These first two chapters provide a basic framework for the more complex study and predictions presented in Chapter 4. In this last chapter, we are interested in understanding the impact of various direct and indirect management strategies on limiting the spread of MPB. The management strategies we investigate are pheromone baiting, tree-removal, clearcutting, and prescribed burning. We find that the optimal management strategy changes with MPB density and depends on the properties of MPB movement and reproduction.

# Chapter 2

# Pattern Formation in a Model for Mountain Pine Beetle Dispersal: Linking Model Predictions to Data

## 2.1 Introduction

Pattern formation is ubiquitous in biology [Mur03]. Nature provides a diverse array of systems with spatial patterns. Examples include static spatial patterns such as those found on butterfly wings and mammalian coats, and spatiotemporal patterns such as those exhibited by predator-prey populations [Mur03]. What is even more interesting is that reaction-diffusion systems can exhibit all of these various patterns given the correct range of parameter values. Pattern arises in these systems through diffusion-driven instability, which was first observed by Turing [Tur52]. An essential element for spatial patterning is local activation with long-range inhibition [Mur03].

Not all pattern formation is due to diffusion-driven instability. Pattern formation can also occur in reaction-diffusion equations with chemotaxis. Examples include models for snake pigmentation patterns and spatial patterns formed by colonies of growing bacteria [Mur03]. In particular, Budrene and Berg [BB91, BB95] found very diverse and interesting patterns formed by the bacteria *Escherichia Coli* and *S. typhimurium*. Tyson et al [TLM99] were able to reproduce these interesting patterns using a reaction diffusion model that incorporated chemotaxis.

A very interesting insect to study in regard to pattern formation is the Mountain Pine Beetle (*Dendroctonus ponderosae* Hopkins, MPB). This bark beetle has had a major economic impact on the Western Canada and United States forestry industries [SW06]. Many characteristics of the spread and spatial synchrony of MPB have been well researched at both large [HLZ$^+$08, GH08, BS03, PLBW02] and small [RNJ$^+$09, MP91] scales. These studies have illuminated the factors driving the spatial patterns in beetle spread, such as weather, elevation, and proximity to nearby MPB attacked areas. Additionally, models for MPB movement have been developed to describe the spread and aggregative behaviour of MPB [LWBP98, BPL96, PD11, PL90, SW06, Bur77, GGG80, SBTR99, RFSS04, HP08, PMW98, WP97, HFSL06]. In this paper, we will focus on the spot formation that occurs at intermediate spatial scales. Previous cluster analysis focused on either large scales (kms) or very small scales (100m regions). In this study we are interested in the pattern formation of clusters at intermediate scales, with distances between clusters falling within the 0-1000m range. We also focus our search to investigate spot formation in a single year rather than the change in spot formation across multiple years.

Successful aggregation of MPB (in response to a suite of pheromones) is crucial for reproduction and survival of the species. At incipient epidemic population levels, the pattern of attack of MPB on a landscape is small isolated spots [SW06]. In contrast there can be high mortality of host trees over thousands of contiguous acres at epidemic population levels. We are interested in understanding the pattern formed by MPB during the transition from incipient epidemic to frank outbreaks. To do this work we investigate pattern formation via a spatially explicit model for MPB dispersal [WP97]. We then compare the model predictions to 19 years of data from MPB attack in the Sawtooth National Recreation Area (SNRA), in Idaho, USA. We find that the distance between MPB attack clusters predicted by our model and observed in the SNRA are the same. This indicates that the biological behaviours in our model are sufficient to explain the observed attack pattern.

We first introduce our mathematical model in Section 2.2. In Section 2.3,

we determine the wavelength in between MPB attack clusters as predicted by our mathematical model using pattern formation analysis. We then calculate the wavelength between clusters of MPB attack in the data from the SNRA in Idaho, USA and compare it to the model predictions in Section 2.4. The management implications of our results are in Section 2.5. Discussion and future work can be found in Section 2.6.

## 2.2 Mathematical Model

We are interested in the period of emergence, dispersal, and attack of the MPB. These events all occur over the space of one summer: adults emerge from their host trees, then aggregate on new hosts where they mount an attack and, if successful, lay new eggs. The period between egg-laying and adult emergence occurs during the winter, and is not relevant to the modelling exercise here. That is, we are interested in understanding the attack pattern that results from the dispersal and aggregation stages of the MPB life cycle in a single summer. We thus require a model for MPB movement through forest habitat that incorporates the interaction between the beetle and its pheromones in a continuous framework over space and time. The choice of model structure is based on theoretical work by Powell et al [PMW98]. The model equations are

$$\frac{\partial P}{\partial t} = \overbrace{\mu_p \nabla^2 P}^{\text{diffusion}} - \overbrace{\nabla\left[\left(\nu_a \frac{b_0 - A}{b_0 + A/b_1}\nabla A\right) P\right]}^{\text{chemotaxis}} - \overbrace{\delta_p P}^{\text{death}} - \overbrace{\lambda(x) P \frac{P^2}{P^2 + (k_p)^2}}^{\text{nesting}} + \overbrace{\gamma(x,t)}^{\text{emergence}}, \tag{2.1a}$$

$$\frac{\partial Q}{\partial t} = \overbrace{-\delta_q Q}^{\text{death}} + \overbrace{\lambda(x) P \frac{P^2}{P^2 + (k_p)^2}}^{\text{nesting}}, \tag{2.1b}$$

$$\frac{\partial A}{\partial t} = \overbrace{\mu_a \nabla^2 A}^{\text{diffusion}} + \overbrace{a_1 Q}^{\text{synthesis}} - \overbrace{\delta_a A}^{\text{degradation}}, \tag{2.1c}$$

where our three variables are $P$ - the density of flying MPB, $Q$ - the density of nesting MPB, and $A$ - the concentration of beetle pheromone. The model we have chosen allows us to investigate the dynamics of MPB attack in a single summer season where the emergence rate, $\gamma(x,t)$, is determined by the position and severity of MPB attacks in the previous year. That is, given the pattern of MPB attacks in the previous year, we can predict the emergence rate of flying MPB and the resulting pattern of attacks in the current year.

The movement of MPB is described by two processes: diffusion and chemotaxis. These are the first two terms in (2.1a). The diffusion component describes the random movement of flying MPB, while the chemotaxis describes the attraction and repulsion of MPB according to the concentration of MPB pheromones. MPB have a biological mechanism whereby the pheromone suite is attractive at low densities and repulsive after the concentration becomes too high [WP97]. As a result, the density of beetles attacking a given tree stays below overcrowding levels (though in epidemic situations, when tree resources are limiting, beetles will attack in higher, suboptimal densities) [RB83].

Our model is structurally similar to the model in Powell et al [PMW98], but differs in that the detailed interaction between MPB and lodgepole pine trees in the original model (holes and resin dynamics) has been replaced by a sigmoidal curve, $P^2/(P^2 + {k_p}^2)$, multiplied by a random landing rate, $\lambda(x)$. We discuss both of these terms in some detail here, as they frame a novel description of the MPB response to the pheromone and susceptible tree landscape. The random landing rate, $\lambda(x)$, is spatially dependent based on the density of susceptible trees on the landscape. A lower susceptible tree density results in a lower landing rate $\lambda$. In this manner, we can include the effects of spatial heterogeneity on the MPB aggregation behaviour. We expect this heterogeneity to affect the spatial distribution of MPB attacks. The type 3 functional response term assumes that the MPB must attack in sufficient densities to successfully nest in a lodgepole pine tree [SW06]. This function is defined such that a low density of attacking beetles has a very low success rate until the MPB density reaches a population threshold, at

Table 2.1: Table of parameter values for the dimensional model (2.1). Note that the unit 'fh' refers to flight hour of MPB.

| Parameter | Description | Units | Value |
|---|---|---|---|
| $\mu_p$ | diffusion of flying MPB | $\frac{ha}{fh}$ | 1 |
| $\mu_a$ | diffusion of beetle pheromones | $\frac{ha}{fh}$ | 0.648 |
| $\nu_a$ | beetle pheromone attractiveness | $\frac{ha^2}{\mu g * fh}$ | 5.7 |
| $b_0$ | concentration of pheromones at which dissipation occurs | $\frac{\mu g}{ha}$ | 5.4 |
| $b_1$ | concentration at which pheromone is saturated | $n/a$ | 1 |
| $\lambda$ | random landing rate of flying MPB | $\frac{ha}{trees * fh}$ | 0.16 |
| $a_1$ | rate of pheromone increase due to nesting MPB | $\frac{\mu g}{fh * mpb}$ | 0.02 |
| $k_p$ | flying beetle density required for 50 percent success of mass attack | $\frac{mpb}{ha}$ | 250000 |
| $\delta_p$ | death rate of flying MPB | $fh^{-1}$ | 0.014 |
| $\delta_q$ | death rate of nesting MPB | $fh^{-1}$ | 0.001 |
| $\delta_a$ | degradation of beetle pheromone | $fh^{-1}$ | 180 |

which point the success of the MPB increases dramatically. This population density threshold is $k_p$, the MPB density required for 50% attack success rate. This parameter was estimated based on the empirical data provided in Raffa et al. [RB83]. All other parameters were based on estimates by Biesinger et al. [BPBL00].

We assume that nesting MPB (at density $Q$) have a small linear death rate, $\delta_q$, since they have successfully penetrated the tree defenses. Once MPB nest they do not move spatially and therefore (2.1b) contains only reaction terms. The suite of MPB pheromones, $A$, undergoes three processes. The pheromones undergo movement through diffusion. Furthermore, the pheromones are produced by nesting MPB and degrade naturally at a linear rate, $\delta_a$.

Previous theoretical and empirical work [BPBL00, RB83] informed the selection of parameter values chosen for this study. These values are displayed in Table 2.1.

### 2.2.1 Non-dimensionalization

To simplify model analysis we non-dimensionalize the model. The dimensionless variables are:

$$\begin{aligned} Q &= \frac{b_0\delta_a}{a_1}\overline{Q}, \quad P = \frac{b_0\delta_a}{a_1}\overline{P}, \quad A = b_0\overline{A}, \\ t &= \frac{1}{\delta_a}\overline{t}, \quad (x,y) = \sqrt{\frac{\mu_a}{\delta_a}}(\overline{x},\overline{y}). \end{aligned} \tag{2.2}$$

The choice of non-dimensional scalings can be interpreted biologically. The density of nesting MPB, $Q$, and the concentration of MPB pheromones, $A$, were scaled by the density of nesting MPB, 48600 MPB/ha, and the concentration of pheromone ($b_0$) required for the pheromone to switch from attractive to repulsive, respectively. The density of flying MPB, $P$, was scaled by the same factor as $Q$ to remain consistent. Time was scaled by the average degradation time of the chemical pheromone. Space was scaled by the average distance that the pheromone will spread before degradation.

Inspection of the parameters in Table 2.1 reveals order of magnitude differences in the parameter values. We therefore defined a scaling parameter that identifies parameters as relatively small or large when compared to other parameter values. We chose the scaling parameter describing the relative persistence of a pheromone plume, $\frac{1}{\delta_a}$, and the life expectancy of the dispersing MPB, $\frac{1}{\delta_p}$.

$$\epsilon = \frac{\delta_p}{\delta_a}.$$

Since $\delta_p$ (death rate of flying MPB) is very small compared to $\delta_a$ (degradation rate of MPB pheromone), this ratio is a very small quantity. This order parameter allows us to identify parameters that work over fast and slow scales, respectively. With this scaling parameter we define the following

Table 2.2: Table of parameter values for the non-dimensional model (2.4).

| Parameter | Value |
|---|---|
| $\overline{\mu_p}$ | 1.54 |
| $\overline{\nu_a}$ | 47.5 |
| $\epsilon$ | 0.0000778 |
| $\overline{k_p}$ | 5.14 |
| $\overline{\delta_q}$ | 0.0714 |
| $\overline{\lambda}$ | 11.4 |

new dimensionless parameters:

$$\begin{aligned} \overline{\mu_p} = \frac{\mu_p}{\mu_a}, \quad \overline{\nu_a} = \frac{\nu_a b_0}{\mu_a}, \quad \overline{k_p} = \frac{k_p a_1}{b_0 \delta_a}, \\ \overline{\gamma} = \frac{\gamma a_1}{b_0 \delta_a^2}, \quad \epsilon\overline{\delta_q} = \frac{\delta_q}{\delta_a}, \quad \epsilon\overline{\lambda} = \frac{\lambda}{\delta_a} \end{aligned} \tag{2.3}$$

Values of the non-dimensional parameters (2.3) are shown in Table 2.2. Substituting the non-dimensional parameters (2.3) and variables (2.2) into (2.1), we arrive at

$$\frac{\partial \overline{P}}{\partial \overline{t}} = \overline{\mu_p}\nabla^2\overline{P} - \overline{\nu_a}\nabla\left(\frac{1-\overline{A}}{1+\overline{A}/b_1}\overline{P}\nabla\overline{A}\right) - \epsilon P - \epsilon\overline{\lambda}\frac{\overline{P}^3}{\overline{P}^2 + \overline{k_p}^2} + \overline{\gamma}, \tag{2.4a}$$

$$\frac{\partial \overline{A}}{\partial \overline{t}} = \nabla^2\overline{A} + \overline{Q} - \overline{A}, \tag{2.4b}$$

$$\frac{\partial \overline{Q}}{\partial \overline{t}} = -\epsilon\overline{\delta_q}\overline{Q} + \epsilon\overline{\lambda}\frac{\overline{P}^3}{\overline{P}^2 + \overline{k_p}^2}, \tag{2.4c}$$

For the remainder of the chapter we will drop the bars above the nondimensional quantities and assume that we are using the nondimensional variables and parameter values to simplify notation. The model becomes,

$$\frac{\partial P}{\partial t} = \mu_p\nabla^2 P - \nu_a\nabla\left(\frac{1-A}{1+A/b_1}P\nabla A\right) - \epsilon P - \epsilon\lambda\frac{P^3}{P^2 + k_p{}^2} + \gamma, \tag{2.5a}$$

$$\frac{\partial A}{\partial t} = \nabla^2 A + Q - A, \tag{2.5b}$$

$$\frac{\partial Q}{\partial t} = -\epsilon\delta_q Q + \epsilon\lambda\frac{P^3}{P^2 + {k_p}^2}. \tag{2.5c}$$

In certain PDE models that include chemotaxis the system of equations can exhibit unrealistic unbounded solutions due to finite-time blow up [HP09]. The proof that our system of equations, (2.5), exhibit global existence in two dimensions is outside of the scope of this work. However, we conjecture that the chemotaxis and repulsion of pheromone at high concentrations is a similar mechanism to the volume-filling equations in Hillen and Painter [HP09], which are known to not exhibit finite-time blow up.

## 2.3 Model Pattern Formation

The type of pattern formation we investigate is diffusion and chemotaxis-driven instability of a spatially uniform steady state [Mur03]. Biologically, this amounts to assuming that early in the season emerging MPB are uniformly dispersed on a landscape devoid of chemical information and that hot spots of infestation will develop at spatial scales on which the natural processes of dispersal, attack, and pheromone production/dissipation resonate. Often the distribution of previously attacked trees is clustered and non-uniform. Early in the season, however, when beetles are just beginning to emerge, there is no pre-existing chemical information. Consequently, the random dispersal of emerging MPB, coupled with a brief maturation period during which beetles are not in search of nesting sites [HFSL06], together generate a largely uniform distribution of beetles. The distribution is clearly not completely uniform, and the spacing of previously attacked trees should have some effect on the spatial pattern of attack in the following year. This pre-pattern, however, would most likely amplify and accelarate the pattern of MPB attack clusters through a forcing of the inherent spatial resonance. In other words, it is less surprising to see a spatial pattern emerge when it is seeded with a pre-pattern than when it is seeded with no pattern at all. We therefore take the more parsimonious assumption, and set attack and emergence rates to be spatially uniform $\lambda(x) = \lambda$ and $\gamma(x,t) = \gamma(t)$. We

additionally set our emergence rate to be constant over time, $\gamma(t) = \gamma$. To investigate potential pattern formation, we find the spatially uniform steady state in Section 2.3.1, then linearize about this steady state and add spatial perturbations to find the dispersion relation in Section 2.3.2 [Mur03]. This dispersion relation relates the temporal growth of perturbations to the wavenumber of the pattern. This dispersion relation is studied analytically and numerically to determine the dominant wavenumber of the pattern, in Sections 2.3.3 and 2.3.4, respectively. This dominant wavenumber predicts the expected spacing between MPB attacks in a given year.

### 2.3.1 Spatially Uniform Steady State

To find spatially uniform steady states for (2.5), all spatial and temporal derivatives are set to zero. The spatially uniform steady state of the model, (2.5), is the solution to the system

$$0 = -\epsilon P - \epsilon\lambda \frac{P^3}{P^2 + {k_p}^2} + \gamma, \tag{2.6a}$$

$$0 = Q - A, \tag{2.6b}$$

$$0 = -\epsilon\delta_q Q + \epsilon\lambda \frac{P^3}{P^2 + {k_p}^2}, \tag{2.6c}$$

Solving (2.6b) and (2.6c), we find that there is a spatially uniform steady state given by

$$(P^*, A^*, Q^*) = \left(P^*, \frac{1}{\delta_q}\lambda\frac{(P^*)^3}{(P^*)^2 + k_p^2}, \frac{1}{\delta_q}\lambda\frac{(P^*)^3}{(P^*)^2 + k_p^2}\right). \tag{2.7}$$

$P^*$ is unknown. Rearranging (2.6a), we obtain a cubic equation,

$$P^3 - \frac{\gamma}{\epsilon(1+\lambda)}P^2 + \frac{k_p^2}{1+\lambda}P - \frac{\lambda k_p^2}{\epsilon(1+\lambda)} = 0. \tag{2.8}$$

The real positive root of this cubic equation (2.8) will give us the steady state density of flying MPB, $P^*$. The first derivative of (2.6a) is always

negative and therefore there is only one possible real root. This steady state is positive by inspection of (2.6a). Emergence rate, $\gamma$, is determined exogenously by the density of MPB attack in the previous year and the temperature (phenology) [BPL96], which will then determine the unique density of dispersing MPB.

This system exhibits three distinct behaviours as the emergence rate, $\gamma$, is varied. For very low $\gamma$, the flying MPB density, $P^*$, is very low. At these population levels we have essentially the trivial steady state and the MPB do not successfully attack any trees in the susceptible landscape. If $\gamma$ is $O(1)$, the largest root scales like $P^* \propto \frac{1}{\epsilon}$. Using this scale one finds the steady state is approximately

$$(P^*, A^*, Q^*) = \left( \frac{\gamma}{\epsilon(1+\lambda)}, \frac{\lambda}{\delta_q} P^*, \frac{\lambda}{\delta_q} P^* \right). \tag{2.9}$$

At these emergence rates, $P^*$ is at epidemic densities, and therefore the MPB is successful at inducing mortality in any healthy tree. In contrast, when $\gamma$ is small, $O(\epsilon)$, the roots of $P^*$ are $O(1)$. When $\gamma$ is at these values, the population of MPB is not large enough to kill susceptible trees easily, and must successfully aggregate to overcome tree defenses. We will show through our analysis that for a specific intermediate range of $\gamma$ values, our unique real steady state is an unstable critical point in the presence of diffusion and chemotaxis. Thus, when spatial factors are included, perturbations of the uniform steady state lead to the formation of a spatial pattern. This scale of aggregation will determine the spacing between MPB attacks on a susceptible landscape.

The bifurcation plot of these behaviours around the single steady state is discussed later in Section 2.5 and is shown in Figure 2.4.

### 2.3.2 Linear Analysis

Linearizing about the spatially uniform steady state, we define $f = \nu_a \left( \frac{1-Q^*}{1+Q^*/b_1} \right) P^*$ and $g = \epsilon\lambda \frac{(P^*)^4 + 3(P^*)^2 k_p^2}{((P^*)^2 + k_p^2)^2}$. Note that since $Q^* = A^*$, we replace $A^*$ by $Q^*$ in our equations. We add small spatial perturbations by

substituting $P = P^* + \delta P_1$, $Q = Q^* + \delta Q_1$, and ($\delta << 1$) $A = A^* + \delta A_1$, into (2.5) to obtain the perturbation equations,

$$\frac{\partial P_1}{\partial t} = \mu_p \nabla^2 P_1 - f\nabla^2 A_1 - \epsilon P_1 - gP_1, \tag{2.10a}$$

$$\frac{\partial Q_1}{\partial t} = -\epsilon\delta_q Q_1 + gP_1, \tag{2.10b}$$

$$\frac{\partial A_1}{\partial t} = \nabla^2 A_1 + Q_1 - A_1. \tag{2.10c}$$

Note that we do not drop terms with $\epsilon$ in our linearization, (2.10), and thus the $\epsilon$ contained within $g$ has no effect on the linearization or future analysis.

**Method of Annihilators to find dispersion relation**

Our analysis focusses on one dimensional results, where we do not differentiate between the possible differential characteristic distances in between clusters of attack in the $x$ and $y$ directions. We assume that the domain is large with respect to the insect dispersal distance, and therefore there is no limitation on possible wavenumbers over the domain. Our analysis in this section would be largely unchanged in two dimensions, other than the wavenumber found would consist of both $x$ and $y$ components. For further details see Tyson [Tys96]. Our first-order analysis does not require statement of boundary conditions, although any non-linear analysis (higher-order) would require boundary conditions.

Beginning with (2.10), we can rewrite these equations in terms of linear differential operators [NSS05]:

$$L_1[P_1] = -fL_2[A_1], \tag{2.11a}$$

$$L_3[Q_1] = g[P_1], \tag{2.11b}$$

$$L_4[A_1] = [Q_1], \tag{2.11c}$$

where $L_1 = (\partial_t - \mu_p\partial_{xx} + (\epsilon + g))$, $L_2 = \partial_{xx}$, $L_3 = (\partial_t + \epsilon\delta_q)$, and $L_4 =$

$(\partial_t - \partial_{xx} + 1)$.

From (2.11) we deduce that $L_1 L_3 L_4[A_1] = -gf L_2[A_1]$. If the linear operators are then expanded, we have the equation:

$$(\partial_t - \mu_p \partial_{xx} + (\epsilon + g))(\partial_t + \epsilon\delta_q)(\partial_t - \partial_{xx} + 1)[A_1] = -gf\partial_{xx}[A_1]. \quad (2.12)$$

We assume that the perturbations have an exponential solution of the following form, $A_1 = c_1 e^{\sigma t + i\nu_m x}$. This substitution in (2.12) produces the dispersion relation that links the temporal growth rate, $\sigma$, of patterns to their spatial wavenumber, $\nu_m$,

$$(\sigma + \mu_p\nu_m^2 + (\epsilon + g))(\sigma + \epsilon\delta_q)(\sigma + \nu_m^2 + 1) = gf\nu_m^2. \quad (2.13)$$

If the polynomial (2.13) is expanded in terms of powers of $\sigma$, we have,

$$\begin{aligned}&\sigma^3 + \sigma^2(\epsilon + \mu_p\nu_m^2 + \nu_m^2 + g + 1 + \epsilon\delta_q) + \sigma(\epsilon\nu_m^2 + \epsilon\delta_q + \mu_p\nu_m^4 + \\ &\mu_p\nu_m^2\epsilon\delta_q + \mu_p\nu_m^2 + g\nu_m^2 + g + g\epsilon\delta_q + \nu_m^2\epsilon\delta_q + \epsilon^2\delta_q + \epsilon) \\ &- gf\nu_m^2 + g\epsilon\delta_q + \mu_p\nu_m^4\epsilon\delta_q + \epsilon^2\nu_m^2\delta_q + g\nu_m^2\epsilon\delta_q + \epsilon^2\delta_q + \mu_p\nu_m^2\epsilon\delta_q = 0.\end{aligned} \quad (2.14)$$

### 2.3.3 Analysis of the Dispersion Relation

Before turning to numerical analysis, we first utilize some analytical techniques to find the boundary of the region of maximum pattern formation, and to determine the dominant wavenumber. The dominant wavenumber is the spatial wavenumber that maximizes the temporal growth rate. We rewrite the dispersion relation (2.14) as

$$p_1 = \sigma^3 + a_2\sigma^2 + a_1\sigma + a_0, \quad (2.15)$$

where

$$\begin{aligned}a_2 &= \epsilon + \mu_p\nu_m^2 + \nu_m^2 + g + 1 + \epsilon\delta_q, \\ a_1 &= \epsilon\nu_m^2 + \epsilon\delta_q + \mu_p\nu_m^4 + \mu_p\nu_m^2\epsilon\delta_q + \mu_p\nu_m^2 + g\nu_m^2 + g + g\epsilon\delta_q + \nu_m^2\epsilon\delta_q\end{aligned}$$

$$
\begin{aligned}
&+ \quad \epsilon^2\delta_q + \epsilon, \\
a_0 \quad &= \quad -gf\nu_m^2 + g\epsilon\delta_q + \mu_p\nu_m^4\epsilon\delta_q + \epsilon^2\nu_m^2\delta_q + g\nu_m^2\epsilon\delta_q + \epsilon^2\delta_q + \mu_p\nu_m^2\epsilon\delta_q.
\end{aligned}
$$

Thus, $p_1$ is a function of $\sigma$.

We are interested in situations where pattern formation occurs, that is, where $\sigma_1 = \max_{\alpha\in\mathbb{C}}(\Re(\alpha)|p_1(\alpha) = 0)) > 0$. Using Descartes' rule of signs [SL54], we are able to determine regions in which positive real roots should occur. Descartes' rule of signs counts the number of sign changes of the coefficients of a polynomial to determine the maximum number of real positive roots. Furthermore, if there is a maximum of $n$ real positive roots, the number of allowable roots is $n, n-2, n-4, ...$ because complex roots must occur in pairs. Therefore, in order for a real positive root to occur, we must have $a_0 < 0$ (one sign change). This is equivalent to the condition,

$$
gf\nu_m^2 > g\epsilon\delta_q + \mu_p\nu_m^4\epsilon\delta_q + \epsilon^2\nu_m^2\delta_q + g\nu_m^2\epsilon\delta_q + \epsilon^2\delta_q + \mu_p\nu_m^2\epsilon\delta_q. \tag{2.16}
$$

Technically, Descartes' rule of signs limits us to a single positive real root, and either zero or two negative real roots. In the case where there are two negative real roots, we do not need to know anything about these negative real roots, as pattern formation occurs if a single root has a positive real part. When there are not two negative real roots, but $a_0 < 0$, we will argue that the two complex roots have a negative real part.

Assume our cubic has a positive real root $r_1$ ($r_1 > 0$), and a pair of complex roots $r_2 \pm r_3 i$. The expanded form of the polynomial is:

$$
\sigma^3 + \sigma^2(-r_1 - 2r_2) + \sigma(2r_1r_2 + r_2^2 + r_3^2) - r_1(r_2^2 + r_3^2). \tag{2.17}
$$

Since $a_2 > 0$ in (2.15), we must have $-r_1 - 2r_2 > 0$ in (2.17). Thus, since $r_1 > 0$ by assumption, we have $r_2 < 0$. Therefore, in the case where we have a single positive real root and two complex roots, our complex roots must have negative real parts.

In the case where $a_0 > 0$, Descartes' rule of signs indicates that there are no positive real roots and that the maximum number of negative real

roots is 3. Therefore, there is either 1 or 3 negative real roots for (2.15). Obviously, in the case of three negative real roots, no pattern formation can occur. There is the possibility of a single negative root, and a pair of complex roots with positive real parts. This case does not occur in the parameter space we explored in the numerical determination of the roots of (2.15) (in Section 2.3.4).

This means that our pattern formation analysis is restricted to the case where (2.15) has a single positive real root. We focus on this region when trying to determine the maximum region of pattern formation. Patterns will first form at wavelengths, $\nu_m$, and parameters chosen such that $\sigma_1$ first becomes positive. Therefore, we examine the behaviour of maximum $\sigma$ with respect to $\nu_m$ in (2.15). We know that the maximum pattern formation region with respect to the wavenumber, $\nu_m$, will occur when $p_2 = \frac{\partial p_1}{\partial(\nu_m^2)} = 0$. That is, if we take a derivative of $p_1$ with respect to the square of the wavenumber and set it to zero, we can determine the dominant wavenumber. The wavenumber at which pattern formation is maximum is called the dominant wavenumber. At this dominant wavenumber, $\frac{\partial \sigma}{\partial(\nu_m^2)} = 0$, thus we can reduce our polynomial (2.15) to order 2 by taking the derivative. In summary, the dominant wavenumber occurs when $\sigma_1 > 0$, $\sigma_2 = \max_{\alpha \in \mathbb{C}}(\Re(\alpha) | p_2(\alpha) = 0)) > 0$, and $\sigma_1 = \sigma_2$. The last condition must be satisfied since both $p_1 = 0$ and $p_2 = 0$ at the dominant wavenumber. Thus we have,

$$\begin{aligned} p_2 &= \frac{\partial a_2}{\partial \nu_m^2}\sigma^2 + \frac{\partial a_1}{\partial \nu_m^2}\sigma + \frac{\partial a_0}{\partial \nu_m^2}, \\ &= d_2\sigma^2 + d_1\sigma + d_0. \end{aligned}$$

where,

$$\begin{aligned} d_2 &= (\mu_p + 1), \\ d_1 &= (\epsilon + 2\mu_p\nu_m^2 + \mu_p\epsilon\delta_q + \mu_p + g + \epsilon\delta_q), \\ d_0 &= (-gf + 2\mu_p\nu_m^2\epsilon\delta_q + \epsilon^2\delta_q + g\epsilon\delta_q + \mu_p\epsilon\delta_q), \end{aligned}$$

Since $g > 0$, we have that $d_2 > 0$ and $d_1 > 0$. This means that there

is exactly one positive real root of $p_2$ if $d_0 < 0$. Therefore, $\sigma_1 > 0$ if and only if $a_0 < 0$, and $\sigma_2 > 0$ if and only if $d_0 < 0$. Using these conditions we can sketch the region of pattern formation (Figure 2.1). Additionally, we numerically calculate (using the method in Section 2.3.4) $\sigma_1$ and $\sigma_2$ and find the squared difference. If the squared difference is zero, this signifies a point of intersection between the two curves and a maximum value of $\sigma$ with respect to $\nu_m^2$. In short, the dominant wavenumber occurs at the intersection of $\sigma_1$ and $\sigma_2$, which is shown on the contour plot.

### 2.3.4 Numerical Analysis of the Dispersion Relation

Using a root-finding algorithm in Matlab, we calculated $\sigma_1$ while varying $\gamma$, the emergence rate (of flying MPB) at steady state, and $\nu_m$, the spatial wavenumber. The contour plot produced is shown in Figure 2.1. Additionally, we show the 2-dimensional plot of growth rate with respect to wavenumber. This curve shows the maximum growth rate with respect to emergence rate at each wavenumber. In our calculations we scaled the wavenumber, $\nu_m$, so that it would be the reciprocal of wavelength. The wavelength, $w_m$ can be calculated as,

$$w_m = \frac{2\pi}{\nu_m}. \tag{2.18}$$

The maximal eigenvalue of 8.04e-5 in the contour plot is dimensionless, and when redimensionalized becomes 0.0145 $\text{fh}^{-1}$, which is an appropriate time scale for pattern formation within a single summer (corresponding to 80 fh, or 2-4 weeks of the flight season). The maximal eigenvalue occured at the dominant wavenumber of 2.74 $\text{km}^{-1}$, with an emergence rate of 300 MPB/(ha·fh). Assuming an output of approximately 10,000 MPB/tree per flight season [PB09], this corresponds to approximately 2-3 source trees/ha. The resulting steady state density of nesting MPB is $Q^* \approx 20100$ MPB/ha. Using the conversion of 800 nesting MPB/tree [PB09], we find the resulting number of killed trees due to this attack is approximately 25. Therefore, this pattern of aggregation is important for the transition between incipient epidemic and epidemic densities of MPB. In an incipient epidemic [SW06],

the MPB population can form small clusters of attack rather than attacks occuring on large tracts of continuous forest (which will occur at epidemic densities). These source densities would describe the transition from incipient epidemic to epidemic densities.

There is great agreement between the analytical and numerical determinations of the dominant wavenumber and the region of pattern formation. The analytical method correctly identifies the region where there is a single positive root, and by Figure 2.1, this is exactly the same as the region where $\sigma_1 > 0$ (pattern formation occurs). Additionally, the wavenumber at which $\sigma_1 = \sigma_2$ in Figure 2.1 verifies the numerical calculation of the dominant wavenumber at 2.74 $\text{km}^{-1}$, which corresponds to a wavelength of 364 m. Thus, our analytical and numerical work yields the prediction that attack clusters during the transition between incipient epidemic and epidemic population levels will be approximately 364 m apart. This prediction is based on our model assumptions which include landscape homogeneity, chemotactic response of MPB due to pheromone (both attractive/repulsive), and a type three functional response describing the transition between flying and nesting MPB.

## 2.4 Data Analysis

The second component of this project was to compare spatial data of MPB attacks to the model predictions. We analyzed MPB attack data from the Sawtooth National Recreation Area (SNRA), located in the Rocky Mountains of central Idaho, to identify any characteristic distances between patches of beetle infestation. Data was provided by USDA Forest Service aerial detection survey (ADS) in and around the SNRA. Full details are provided in Crabb et al. [CPB12]. The data set extends over a period of 19 years, 1991-2009. The data are remarkably detailed, taken at a grid-scale of 30 m over a region of 275,776 ha. All 19 years include regions where MPB are at incipient epidemic densities; many of these years also have regions with epidemic densities of MPB. Thus, this data tracks the progression of an MPB epidemic as captured by dead (red top) trees. Trees develop a red

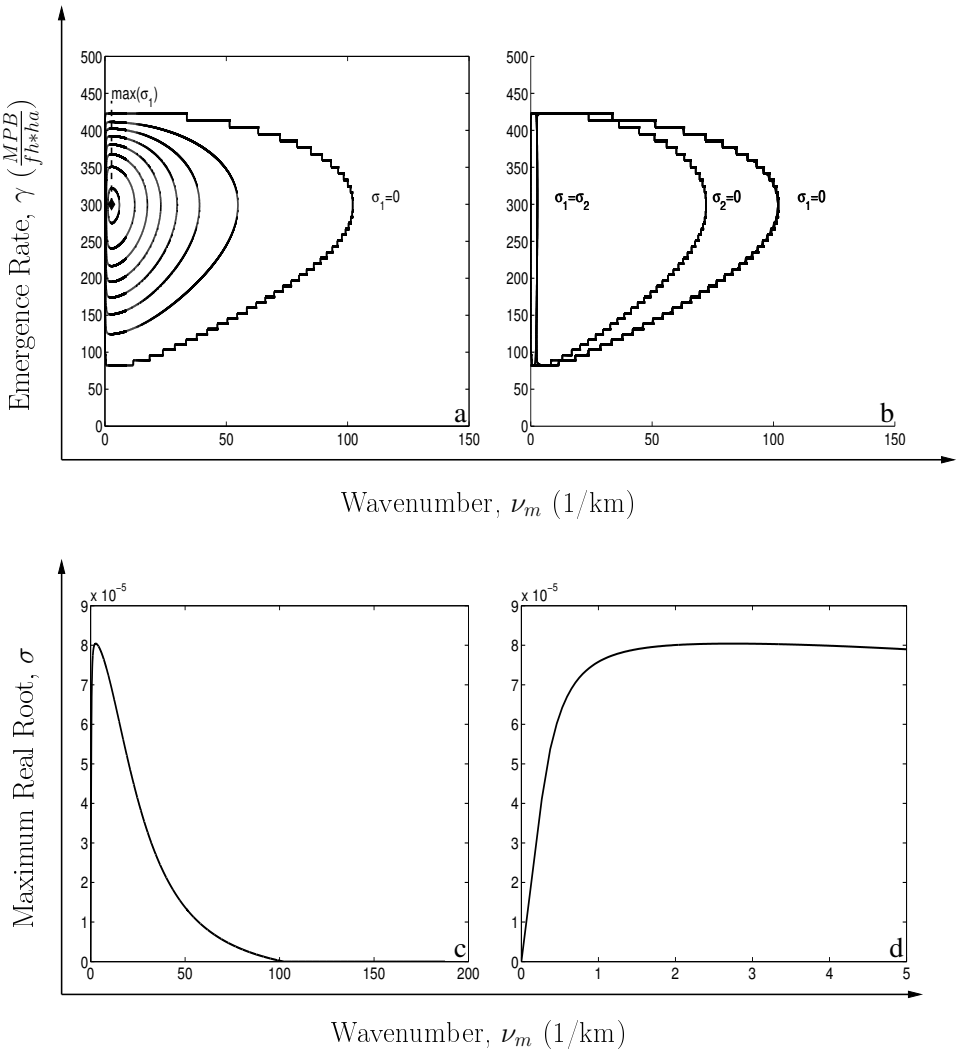


Figure 2.1: Numerical contour plot of the temporal growth rate, $\sigma_1$, against wavenumber and emergence rate of MPB (a). The maximum value of $\sigma_1$ is labeled with a diamond at $(2.74, 299)$. The surface is unimodal with a single maximum. The analytical contour plot of temporal growth rate against wavenumber and emergence rate of MPB is shown in (b). The contour plot in (b), uses the analysis of the dispersion relation to find the region of pattern formation ($\sigma_1 = 0$), and the dominant wavenumber ($\sigma_1 = \sigma_2$). The contour plot in (a), shows the region of pattern formation and the dominant wavenumber as determined numerically. The plot (c), is a horizontal slice of the surface in (a) at a fixed emergence rate, $\gamma = 299$ MPB/(fh·ha). A zoomed in portion of (c) is shown in (d) where the wavenumber varies from 0 to 5.

top the following summer after begin attacked as a result of beetle-induced mortality. The initial attacks at incipient epidemic levels resulted in small clusters of dead trees. During the 19 years, many of these populations had risen to epidemic levels and killed a more significant portion of the available pine trees over the landscape. The later years of this dataset capture the period after the epidemic where the MPB population density has decreased to lower levels. For the purposes of our analysis, the data was defined with ones given to grid cells (locations) of MPB attack, and zeroes given to locations with no MPB attack.

The data sets chosen for analysis in each year were from areas of incipient epidemic MPB population densities, consistent with the assumptions used in the linearization of the model. That is, we selected regions with small spots ($\leq$ 300 m in diameter) of MPB attack and at least 5 spots per region. Regions with large spots were characteristic of MPB at epidemic densities. For the size of these regions, we picked the largest region such that these two conditions were satisfied. The error in the computation of wavenumber decreased as the size of the chosen region increased because larger regions increased resolution in Fourier space. To calculate the distance between spots of MPB attack we used discrete fast Fourier transforms. Discrete Fourier transforms assumes that the data can be decomposed into a finite number of sine and cosine functions on a grid. The process returns the amplitude of these sine and cosine functions, the wavenumbers with the largest amplitude best describe the scale of aggregation of MPB attack in the data. The particular DFT used was Matlab's fft2, with which we calculated the radial wavenumber, $\nu_r$,

$$\nu_r = \sqrt{\nu_x^2 + \nu_y^2}, \tag{2.19}$$

where $\nu_x$ and $\nu_y$ are spatial wavenumbers of the data in the $x$ and $y$ directions. Since DFT returns the amplitude of both the sine and cosine components of the data we need to compute the power, which is the squared complex modulus of the amplitude. This factors both the sine and cosine amplitudes at each wavenumber into a single value, the power. An example

region and power spectral density is shown in the Appendix (Figure A.1).

We are interested mainly in the wavenumber at which the power is maximum. This is called the dominant wavenumber and is the most influential wavenumber represented in the data. To have error bounds we computed the upper ($\nu_u$) and lower ($\nu_l$) bounds for the dominant wavenumber, $\nu_d$, which were chosen such that:

$$\begin{aligned} \nu_l &= \{\min(\nu)|m(\nu) \geq 0.80m(\nu_d)\}, \\ \nu_u &= \{\max(\nu)|m(\nu) \geq 0.80m(\nu_d)\}, \end{aligned}$$

where $m(\nu)$ is the power at the wavenumber, $\nu$.

Since multiple regions were chosen in each year, the average dominant wavenumber in a given year was calculated as a weighted average based on the power:

$$\nu_d = \Sigma_i \left( \frac{m_i}{\Sigma_j m_j} \nu_i \right). \tag{2.20}$$

where $\nu_i$ is the dominant wavenumber for region $i$ and $m_i$ is the power at the maximum. Average upper and lower bounds for each year were calculated similarly.

The average dominant wavenumber in each year is displayed in Figure 2.2 over 1991-2009. The average dominant wavenumber varies between 1.5 and 5.5 km$^{-1}$. The dominant wavenumber appears to be higher in 1991-2000 than in the years 2001-2009. The mean dominant wavenumber is calculated to be 2.83 km$^{-1}$, which is very close to the model predicted dominant wavenumber of 2.74 km$^{-1}$. For more details and analysis from each year see Appendix A.1.

The frequency of each dominant wavenumber independent of year is given in Figure 2.3. The dominant wavenumber from the model, $\nu_{d,model}$, is validated by the data, as it is close to the center of the distribution of $\nu_d$. In fact, the majority of $\nu_d$ appearing is enclosed between the lower ($\nu_{l,model}$) and upper ($\nu_{u,model}$) bounds on the model dominant wavenumber.

A weighted histogram was also produced, where each count is scaled by the relative power at that $\nu_d$. This measure is important as it highlights the

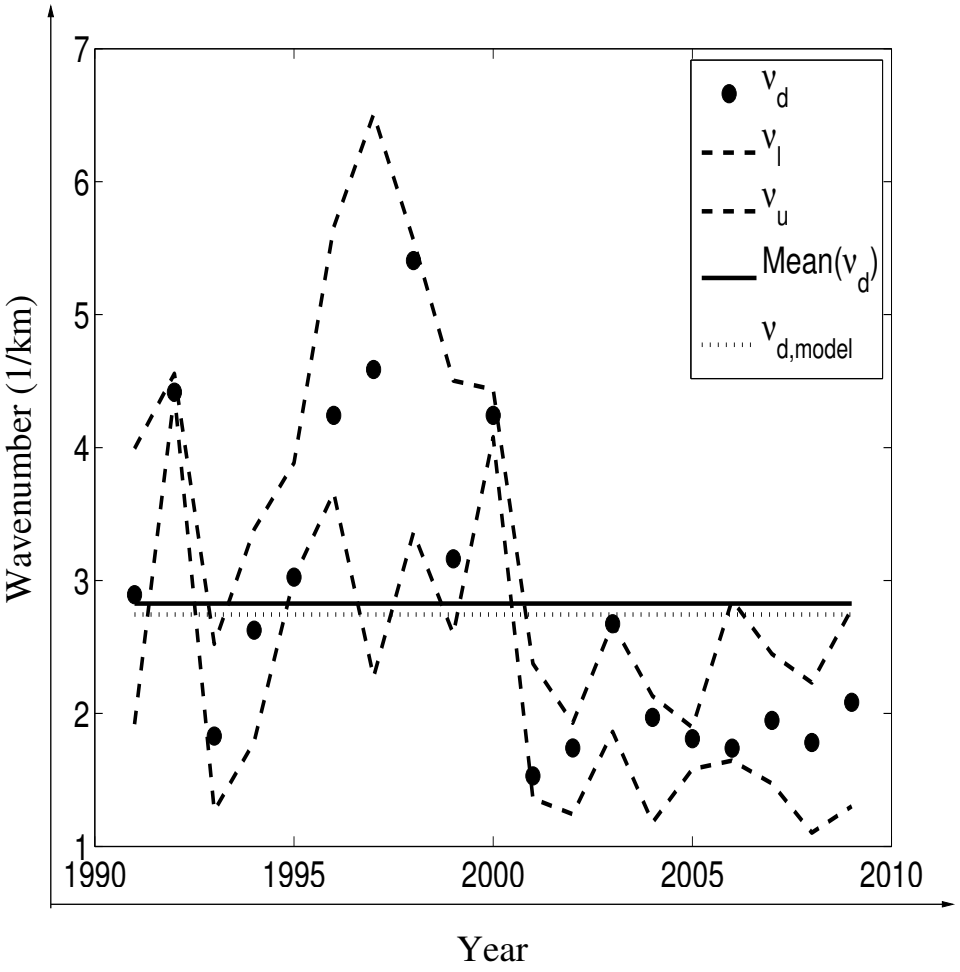


Figure 2.2: Average dominant wavenumber over years 1991-2009. $\nu_d$ refers to the average dominant wavenumber, $\nu_l$ and $\nu_u$ refer to the lower and upper bounds on $\nu_d$, Mean($\nu_d$) refers to the average of the dominant wavenumber over all years, and $\nu_{d,model}$ refers to the model predicted dominant wavenumber. This graph shows the trend in $\nu_d$ over the years 1991-2009. Points where $\nu_u$ and $\nu_l$ are near $\nu_d$ represent years in the data where the power spectral density shows a very large sharp peak at the given $\nu_d$.

wavenumbers which more strongly represent patterns in MPB attacks in the data. Similar to the first histogram, $\nu_{d,model}$ provided a good estimate of the center of the distribution of $\nu_d$ (data), and a large proportion the distribution of $\nu_d$ was effectively captured within the range between $\nu_{l,model}$ and $\nu_{u,model}$.

For the histogram, the upper and lower bounds for the model dominant wavenumber were chosen such that:

$$\begin{aligned} \nu_{l,model} &= \{\min(\nu)|\sigma_1(\nu) \geq 0.975\sigma_1(\nu_{d,model})\}, \\ \nu_{u,model} &= \{\max(\nu)|\sigma_1(\nu) \geq 0.975\sigma_1(\nu_{d,model})\}, \end{aligned}$$

where $\sigma_1(\nu)$ is the growth rate at the wavenumber, $\nu$.

We found an interesting trend when analyzing the data; As time progressed, the spots of MPB attack became larger and farther apart (results not shown). This trend in the spot pattern is intriguing and it would be valuable to investigate if this trend is characteristic of the progression of an MPB epidemic.

## 2.5 Management Implications

Here we consider management implications ensuing from our analysis. An important management goal is the disruption of the MPB aggregation, or pattern-formation process. Clearly this can be done by reducing the MPB population density, but what level of reduction is needed? To answer this question, we look for MPB population densities at which patterns do not occur. The regions of parameter space with and without patterns are shown in Figure 2.4.

Patterns do not form at any wavenumber for very large and very small MPB emergence rates. The very large population densities correspond to epidemic populations, which occur above $\gamma_{max}$=423 MPB/(ha·fh). This corresponds to approximately 4 source trees per hectare. At these densities the spot patterns disappear and are replaced with an area-wide infestation. We are interested in the low MPB population density below which infestation is

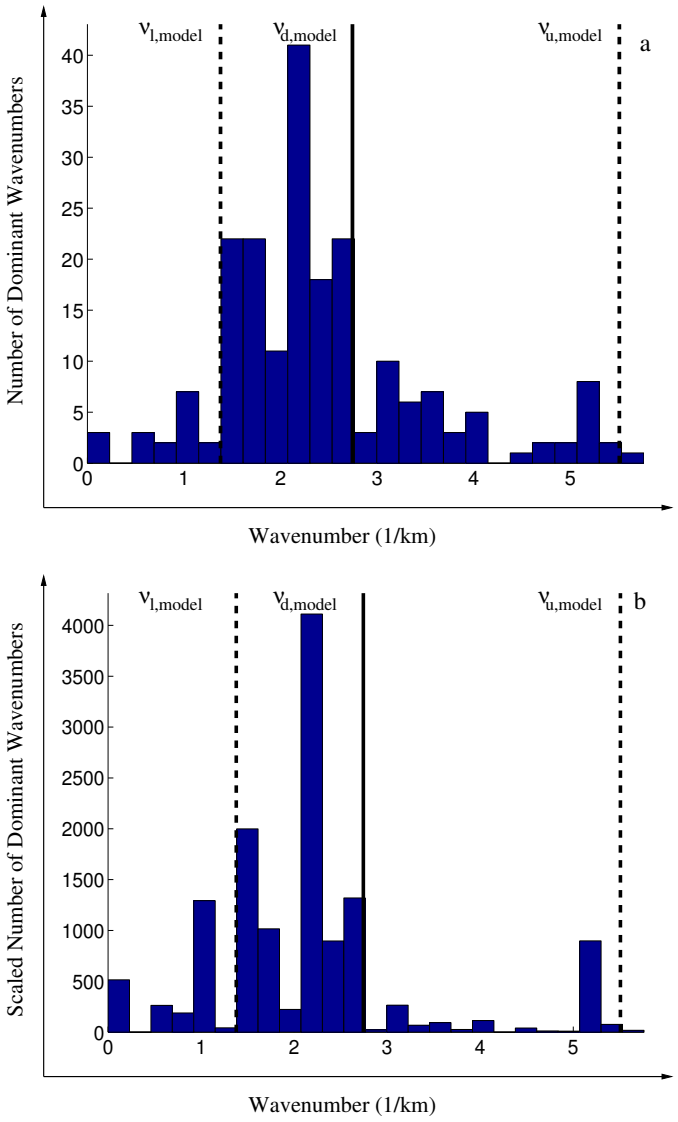


Figure 2.3: The histogram of dominant wavenumbers over all years (a) and the histogram weighted by the power at each dominant wavenumber over all years(b). The solid line is the model dominant wavenumber and the dotted lines are upper (5.5069 $km^{-1}$) and lower (1.3783 $km^{-1}$) bounds on the model dominant wavenumber.

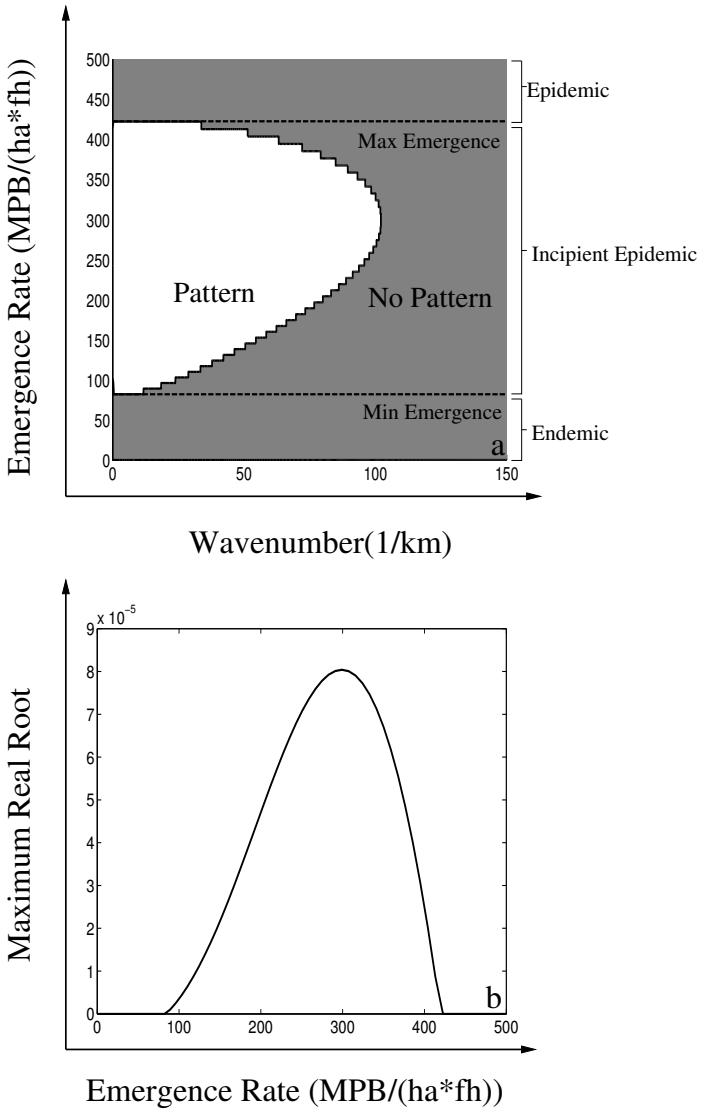


Figure 2.4: The contour plot (a) shows the region of pattern formation, and the range of population densities at which the MPB are displaying patterns consistent with endemic, incipient epidemic, and epidemic densities. The separation in between these densities are $\gamma_{max}$=423 MPB/(fh·ha) and $\gamma_{min}$=82 MPB/(fh·ha). The contour plot in (a) taken at a vertical cross-section at the dominant wavenumber $\nu_d = 2.74$, shows the temporal growth of patterns (maximum real root) against the emergence rate of MPB (shown in (b)).

endemic or absent. This level is $\gamma_{min}$= 82 MPB/(ha·fh), which corresponds to approximately 2 source trees per 3 ha. At this density, the pattern formation would not occur, and therefore the MPB would not be able to reproduce successfully due to low population densities. Thus, if control measures could reduce the impact to 2 source trees per 3 ha, our model predicts the MPB populations would decrease to endemic levels. The reductions in density to the MPB populations could be done through various management activities such as thinning, prescribed burning, or tree removal [SW06].

## 2.6 Discussion

Model pattern formation analysis predicts a dominant wavenumber of 2.74, or spots of MPB attack that are 364 m apart. Analysis of SNRA spot data indicates spots are 353 m apart on average, with a wavenumber of 2.83, only a 3% difference between the model predictions and field observations. Since our model was parameterized completely independently of the SNRA data, this correspondence between the model and data gives a strong validation of our model.

The model analysis revealed that clusters of MPB attack could be removed if the number of source trees per hectare can be reduced by management activities to 2 trees per 3 hectares. To accomplish this goal, it might be possible to use pheromone baits (repulsive and attractive) to disrupt the aggregation process. Our modelling approach could be used to determine whether or not judicious placement of pheromone baits could completely or partially hinder the formation of spot aggregates, and the number and placement of baits necessary to prevent the transition from incipient epidemic to epidemic.

Past forestry practises and fire suppression have given rise to homogeneous and even-age stands of lodgepole pine that have led to large outbreaks of MPB [SL00]. Our model could be used to determine what types of distributions of susceptible trees (and mixed tree forests) over a landscape would prevent pattern formation of MPB attack, and therefore stop a transition to epidemic densities. For this analysis, we would need to use a multi-year

model, as our current analysis will indicate transition emergence rates, but will not model the transition from endemic to epidemic densities. Our analysis in Chapter 4 tries to understand the density of source trees needed for transition from endemic to epidemic densities.

Our model assumes the habitat is homogeneous and therefore the wavelength between attacks formed by MPB predicted in our model is driven by the intrinsic biology of the MPB. This means that at incipient epidemic densities there can be development of aggregration pattern that is driven by the MPB movement dynamics and not heterogeneities in the landscape. A previous study by White and Powell [WP97] found that the patterns observed at endemic densities were driven by the landscape, while patterns observed at the epidemic densities are driven by the self-focusing dynamics of the MPB. Our study adds to this work by finding that the patterns at the incipient epidemic density (between the endemic and epidemic levels studied by White and Powell) can be explained by the MPB biology.

Our results are fairly robust to changes in parameter values. Parameter sensitivity analysis showed that our model wavelength prediction is most sensitive to increases in $\overline{\mu_p}$, the diffusion rate of MPB. This result is expected, intuitively, as diffusion is known to smooth patterns when pattern formation is driven by chemotaxis. All parameters were altered by 10% (while keeping all other parameters constant), and the most sensitive parameter, $\overline{\mu_p}$, only changed the wavelength prediction by at most 3.8%. These values can be seen in Appendix A.2. This means that our pattern formation analysis is relatively insensitive to parameter changes. Parameter sensitivity was measured as a ratio of standardized changes in wavenumber to standardized changes in parameter values [Hae05]. Future work needs to investigate the effects of varying multiple parameters simultaneously.

An important factor not included in our model is the effect of temperature, which has been shown to have a significant effect on MPB emergence and spread [HLZ$^+$08, GPLB04, PB09]. If temperature changes, through global warming [PL05], habitats that were previously unsuitable for MPB may become suitable. Additionally, temperature changes can increase the synchrony of emergence, which could increase the density of MPB attacks

and allow for spot formation. An interesting extension of our mathematical model would explore how the predicted wavelength changes as this factor is included. This could be done by making the emergence rate, $\gamma$, a function of temperature. This modification would add a new layer to the complexity of the pattern formation analysis, and may require numerical simulations to determine the expected wavelength between clusters in a given landscape.

The functional form of our nesting term is required for pattern formation, as smaller submodels with the same chemotaxis and diffusion terms will result in pattern formation. This is due to the local activation through MPB response to pheromone and the long-range inhibition of diffusion. Our specific sigmoidal nesting term is required, however, to obtain the correct wavelength and close correspondence with the data.

From an analytical standpoint, it would be interesting to complete the second-order perturbation analysis of these equations [Mur03, Tys96]. We only investigate spot aggregation patterns in the present work, but it may be that other patterns are possible. An understanding of the possible aggregation patterns would provide managers with an additional tool for gauging the MPB population level and risk of an epidemic.

A final interesting extension of our work would be to determine the time it takes for the MPB population to reach epidemic levels once the characteristic wavelength of pattern formation (364 m) has been established. In order to do this, the model would require a between-season component to describe the over-winter reproduction and development of MPB. This study is currently in progress by the Tyson lab.

Our modelling approach can be applied to other organisms that exhibit patchy spread [SKT95]. Examples include birds such as house finches [LP00], sparrows, and starlings [SKT95]. Additionally, there are insects who exhibit patchy spread, such as are rice weevils [SKT95], emerald ash borer, leaf-miner moth, pinewood nematode, corn rootworm [CMM$^+$10], and gypsy moth [PM10]. Some plants, such as cheat grass [LP00], also exhibit patchy spread. Note that the patchiness of the MPB spread is an inherent property of the chemotactic behaviour of the insects. The patchy spread exhibited by the other organisms may be due to other factors, such as patchy resources,

or could be influence by the same inherent mechanisms as the MPB and comparisons would be both interesting and instructive. Many of the populations mentioned are invasive species and so an understanding of their spatial invasion dynamics is vitally important, as invasive species can devastate populations of native flora and fauna [MSL$^+$00]. Additionally, once we understand how a species may successfully invade we may be use this knowledge to enhance survival of native species which are threatened by extinction.

# Chapter 3

# Edge Effects on Mountain Pine Beetle Movement

## 3.1 Introduction

Fragmentation of habitat can have diverse effects on ecological communities [FCC99], through edge behaviour and alterations in dispersal, mortality, and species interactions. Changes in movement behaviour as a result of fragmentation is well-documented [CDO07, FCC99, HC03, HC06, MAD10, Ova04, SW04, SB03] and can have important implications for survival of species and the outcomes of competition or predator-prey interactions [FCC99, GTLS]. For the purposes of this chapter, we define a landscape as a combination of focal habitat patches (where the individual may reproduce and/or find food) and matrix habitat (the habitat in which the individual cannot reproduce or find food). Matrix habitat is defined as high quality if the individual can disperse throughout this habitat with a low probability of death due to such pressures as predation. We define edges as boundaries between the focal habitat patch and the matrix habitat. The degree of habitat fragmentation effects depends heavily upon the size of individual focal and matrix habitat patches and the quality of the matrix habitat [HC03, HC06, ST09, ST12]. Fahrig [Fah07] predicted that populations are differentially affected by habitat fragmentation as a result of their varying movement rates and the original quality of their matrix habitat. For instance, populations with large movement probabilities, that result from high-quality matrix habitat, would be highly vulnerable to focal habitat loss or reductions in matrix quality. In contrast, a population with low

movement, as a result of low-quality matrix habitat, would be less affected by focal habitat loss or lower quality matrix habitat. This population would, however, exhibit a strong negative response to lower colonization (successful movement to a new focal habitat patch with successful establishment) probability.

One important potential change in movement behaviour is the willingness of a species to cross habitat boundaries/edges [CC82, Jon77, RH98, SC01, WSM04]. This is often referred to as the permeability of the boundary and describes the probability that the species will cross from the focal habitat patch to the matrix habitat. Intuitively, a boundary with high permeability has a high probability that the species will cross the edge, while a low probability of crossing an edge results from an edge with low permeability.

There are several characteristics of movement behaviour that can be altered by increased habitat fragmentation. Chapman et al. [CDO07] found that the dispersal paths of leaf beetles in matrix habitats had smaller turning angles and the movement event lasted longer than movement events in the focal habitat. The authors also found that if the boundaries were less permeable, colonization was dramatically reduced. Haynes and Cronin [HC03, HC06] found that populations of planthoppers have different movement speeds in brome grass and mud matrix habitats. Additionally, planthoppers developed different responses to the edges of the different types of matrix habitat. That is, the permeability of the edge was different between a focal habitat/brome grass matrix edge and a host habitat/mud matrix edge. Studies by Jones [Jon77] and Courtney and Courtney [CC82] found that movement and oviposition of butterflies results in clumped egg distribution at the edges of focal habitat patches.

The Mountain Pine Beetle (MPB) has been extensively studied due to the economic impact it has on the forestry industries in Western Canada and the United States [SW06, Hug02]. Nonetheless, the effect of habitat fragmentation on the spatial spread of MPB is not well understood [BAL93, Hug02, RWNW]. For MPB, susceptible habitat, where susceptible lodgepole pine trees for MPB attack and reproduction are found, are

defined as focal habitat. Theoretical work by Hughes [Hug02] predicted that habitat fragmentation can slow the spread of MPB if the focal habitat patch sizes are small enough. In contrast, empirical studies by Robertson et al. [RWNW] found that the spread of MPB over small scales increased with increasing habitat fragmentation. Understanding the spatial spread of MPB in response to habitat fragmentation is crucial as many current management strategies, such as prescribed burning and removal of susceptible stands of lodgepole pine, rely on the assumption that MPB spread can be slowed by the introduction of matrix habitat and reduction in the amount of focal habitat. Further studies by Reid [Rei09] found that decreased tortuosity in the flight path of MPB can reduce the time required to cross a matrix habitat between two good quality habitats. This result would imply that MPB will move more quickly in matrix habitat, which would violate the assumption underlying present management in that the introduction of matrix habitat will slow the spatial spread of MPB.

We want to understand how MPB dispersal in fragmented habitats is reflected in trap catches on the local (stand) scale. In particular, we are interested if the MPB distribution at the beginning of the attack period is more uniform over the landscape or localized to the emergence sites. Additionally, we want to understand the rates of diffusion of MPB in fragmented habitat. In this chapter we report on an experimental study and use theoretical work to help understand the effects of habitat fragmentation on the movement of MPB. The experimental study consists of trap catch data for MPB in different domains of fragmented habitat. Specifically, we record pheromone trap catches on either side of the edge of a fragmented habitat for different combinations of clearcut, thinned, and dense forest regions in Section 3.2. To help understand the results of this experiment with relation to MPB movement we develop a spatially explicit reaction-diffusion model with chemotaxis for MPB in Section 3.3. Simulations of this model are run in Section 3.4, using the numerical scheme outlined in Section 3.5. Section 3.6 outlines our simulation results and Section 3.7 ties the empirical and theoretical results of our study together. Discussion and Future work is reserved for section 3.8.

## 3.2 Experimental

Biological experiments were conducted by Mary Reid in Parson, British Columbia over 2007 and 2008. Two fragmented stands were chosen with clearcut harvested regions, and two fragmented stands with thinned harvested regions were also selected. The dense stands had approximately 2000 stems/ha, while thinned stands had only 1000 stems/ha of susceptible lodgepole pine trees. Statistical analysis of the trap catches across the different fragmented regions were performed to understand the effect of harvested regions on the dispersal of MPB. Examining the MPB catches in the bait traps in each landscape, Dr. Reid found the following experimental results: a statistically significant difference was found between the clearcut and dense region, but no significant difference was found between the thinned and dense region. Comparing across studies Dr. Reid found that the clearcut and thinned bait trap catches were not significantly different. Finally, in a given habitat (harvested or unharvested) the 20 m and 90 m traps did not differ significantly in terms of the MPB trap catches. Further details of the experiment can be found in Strohm et al. [SRT].

## 3.3 Mathematical Model

To mathematically analyze MPB movement across habitat edges, we needed a spatially explicit model which describes the interaction between MPB, lodgepole pine trees, MPB pheromones, and pheromone baits. Our model is based on previous theoretical work [WP97] examining MPB dispersal. This model is a continuous set of Partial Differential Equations (PDEs) describing the period of flight, emergence, and attack. Our five variables are $P$ - the density of flying MPB, $Q$- the density of nesting MPB, $J$ - the density of pre-adult MPB (beetles not yet emerged from the bole of the tree), $A$ - the concentration of beetle pheromone, and $C$ - the concentration of tree kairomones. In addition, $S$ - is a measure of the relative density of

lodgepole pine trees. The model equations are:

$$\frac{\partial P}{\partial t} = \overbrace{\mu_p \nabla^2 P}^{diffusion} - \overbrace{\nabla\left[\left(\nu_c \nabla C + \nu_a \frac{b_0 - A}{b_0 + A/b_1}\nabla A\right) P\right]}^{chemotaxis} - \overbrace{\delta_p P}^{death} - \overbrace{g(P,C)S}^{nesting} + \overbrace{\gamma J}^{emergence}, \tag{3.1a}$$

$$\frac{\partial Q}{\partial t} = \overbrace{-\delta_q Q}^{death} + \overbrace{g(P,C)S}^{new\ nesters}, \tag{3.1b}$$

$$\frac{\partial C}{\partial t} = \overbrace{\mu_c \nabla^2 C}^{diffusion} + \overbrace{a_2 S}^{synthesis} - \overbrace{\delta_c C}^{degradation} + \overbrace{\alpha}^{baiting}, \tag{3.1c}$$

$$\frac{\partial A}{\partial t} = \overbrace{\mu_a \nabla^2 A}^{diffusion} + \overbrace{a_1 Q}^{synthesis} - \overbrace{\delta_a A}^{degradation}, \tag{3.1d}$$

$$\frac{\partial J}{\partial t} = \overbrace{-\gamma J}^{emergence}. \tag{3.1e}$$

where,

$$g(P,C) = \overbrace{\lambda P}^{landing} \overbrace{\frac{P^2}{P^2 + (k_p)^2}}^{mass\ attack}.$$

All parameters are defined and given specified values in Table 3.1.

This model describes MPB emergence and dispersal during a single flight period, that is, over a single summer season. Note that we are not trying to model the population spread across multiple years.

A submodel derived from (3.1) has recently been used to elucidate the spacing observed between MPB attack locations in a single year (Chapter 2). These attack locations appear as spots in the data. The model was shown to reproduce the correct spatial frequency of attacks present in Aireal Detection Survey data from the Sawtooth National Recreation Area (Chapter 2). This work provides some validation of the submodel and the parameter values used. For this chapter, we build on our earlier work by adding several new

components to the submodel, ariving at (3.1).

The most important departure from the original submodel is the addition of a spatially-heterogeneous landscape. In our previous work (Chapter 2), we were looking for the pattern of MPB attack on a spatially homogeneous landscape. Here we are interested in studying the effects of habitat edges on MPB dispersal, and so we include heterogeneity in the distribution of trees, $S(x)$. As a result, the interaction between MPB and tree-produced kairomone becomes important necessitating the addition of (3.1c). The kairomone, $C$, diffuses, is synthesized by susceptible trees, and degrades over time. We also add a baiting term, $\alpha$, that simulates the production of pheromone by traps. We included this term in the kairomone equation and not in the pheromone equation to differentiate it from the pheromone naturally produced by the MPB. Kairomone, also appears in (3.1a), as flying MPB have a chemotactic attraction to kairomone and will be attracted up the gradient of $C$ [WP97].

The indicator of susceptible tree density, $S(x)$, varies between 0 (no susceptible trees) and 1 (landscape is entirely susceptible). Next, we add the variable $J(x,t)$, for the density of emerging MPB at any point in time and space during the summer. Most emergence occurs over a brief time period during the flight season, and can extend over longer times under appropriate climactic conditions [SW06]. We are interested in both scenarios, so we allow the emergence rate, $\gamma(t)$, to vary with time. The timing of emergence is crucial to the successful attack of MPB [GPLB04] and so we expect temporal variations to be important in the behaviour of the model. For the simulations shown in this chapter we chose $\gamma(t)$ such that 99.9% of MPB emerge within the first 20 flight hours of the season. We simulated other choices of $\gamma(t)$ and discuss the results in Section 3.8.

The selection of parameter values is informed by previous theoretical and empirical work [BPBL00, RB83]. We chose the parameters $a_2$ and $\alpha$ based on the results of numerical simulations of the model in order to simulate the correct biological behaviour. A detailed discussion of parameter values for MPB dispersal can be found in Strohm et al. (Chapter 2.3). The values used in this study are listed in Table 3.1.

Table 3.1: Table of parameter values for the dimensional model (3.1).

| Parameter | Description | Units | Value |
|---|---|---|---|
| $\mu_p$ | diffusion of flying MPB | $\frac{ha}{fh}$ | 1 |
| $\mu_c$ | diffusion of host volatiles (kairomones) | $\frac{ha}{fh}$ | 0.648 |
| $\mu_a$ | diffusion of beetle pheromones | $\frac{ha}{fh}$ | 0.648 |
| $\nu_c$ | kairomone attractiveness | $\frac{ha^2}{\mu g * fh}$ | 0.8 |
| $\nu_a$ | beetle pheromone attractiveness | $\frac{ha^2}{\mu g * fh}$ | 5.7 |
| $b_0$ | concentration of pheromones at which dissipation occurs | $\frac{\mu g}{ha}$ | 5.4 |
| $b_1$ | concentration at which pheromone is saturated | $n/a$ | 1 |
| $\lambda$ | random landing rate of flying MPB | $\frac{ha}{trees * fh}$ | 0.16 |
| $k_p$ | flying beetle density required for 50 percent success of mass attack | $\frac{mpb}{ha}$ | 250000 |
| $\delta_p$ | death rate of flying MPB | $fh^{-1}$ | 0.014 |
| $\delta_q$ | death rate of nesting MPB | $fh^{-1}$ | 0.001 |
| $\delta_c$ | degradation of tree kairomones | $fh^{-1}$ | 180 |
| $\delta_a$ | degradation of beetle pheromone | $fh^{-1}$ | 180 |
| $\gamma(t)$ | emergence rate of pre-adult beetles | $fh^{-1}$ | 0.345 |
| $a_1$ | rate of pheromone increase due to nesting MPB | $\frac{\mu g}{fh * mpb}$ | 0.02 |
| $a_2$ | rate of kairomone increase due to susceptible trees | $\frac{\mu g}{fh * trees}$ | 0.02 |
| $\alpha$ | rate of kairomonne production by traps | $\frac{\mu g}{ha * fh}$ | 1458 |

### 3.3.1 Non-dimensionalization of Model

We non-dimensionalize the model for ease of mathematical analysis. We choose the following non-dimensionalizations for our variables:

$$\begin{aligned}
\overline{Q} &= \frac{a_1}{b_0\delta_a}Q, \quad \overline{P} = \frac{a_1}{b_0\delta_a}P, \quad \overline{C} = \frac{\nu_c}{\mu_c}C, \\
\overline{S} &= \frac{\lambda}{\delta_p}S, \quad \overline{A} = \frac{1}{b_0}A, \quad \overline{J} = \frac{a_1}{b_0\delta_a}J, \\
\overline{t} &= \delta_a t, \quad (\overline{x},\overline{y}) = \sqrt{\frac{\delta_a}{\mu_a}}(x,y).
\end{aligned}$$

Many of the scalings chosen reflect dynamics of the MPB pheromone. $Q$ and $A$ are scaled such that they represent density of MPB and concentration of MPB pheromone required to alter the MPB response to pheromone from attractive to repulsive. $P$ and $J$ are scaled by the same parameter combination as $Q$ since they all represent densities of MPB. The tree kairomone, $C$, is scaled by the ratio of diffusive movement of kairomone to the attractiveness of kairomone to MPB. The susceptible tree density, $S$, is scaled by the ratio of the average time until natural death of flying MPB divided against the average time before flying MPB randomly land on a susceptible tree. Time and space are scaled by the average time and distance that the pheromone can spread before degradation.

Using these variable scalings we obtain the model equations,

$$\begin{aligned}
\frac{\partial\overline{P}}{\partial\overline{t}} =& \frac{\mu_p}{\mu_a}\overline{\nabla}^2\overline{P} - \frac{\mu_c}{\mu_a}\overline{\nabla}(\overline{P\nabla C}) - \frac{\nu_a b_0}{\mu_a}\overline{\nabla}\left(\frac{1-\overline{A}}{1+\overline{A}/b_1}\overline{P\nabla A}\right) \\
&- \frac{\delta_p}{\delta_a}\overline{P} - \frac{\delta_p}{\delta_a}\frac{\overline{P}^3}{\overline{P}^2+(\frac{k_p a_1}{b_0\delta_a})^2}\overline{S} + \frac{\gamma}{\delta_a}\overline{J},
\end{aligned} \tag{3.2a}$$

$$\frac{\partial\overline{Q}}{\partial\overline{t}} = -\frac{\delta_q}{\delta_a}\overline{Q} + \frac{\delta_p}{\delta_a}\frac{\overline{P}^3}{\overline{P}^2+(\frac{k_p a_1}{b_0\delta_a})^2}\overline{S}, \tag{3.2b}$$

$$\frac{\partial\overline{C}}{\partial\overline{t}} = \frac{\mu_c}{\mu_a}\overline{\nabla}^2\overline{C} + \frac{\delta_p a_2\nu_c}{\delta_a\lambda\mu_c}\overline{S} - \frac{\delta_c}{\delta_a}\overline{C} + \frac{\nu_c}{\delta_a\mu_c}\alpha, \tag{3.2c}$$

$$\frac{\partial \overline{A}}{\partial \overline{t}} = \overline{\nabla}^2 \overline{A} + \overline{Q} - \overline{A}, \tag{3.2d}$$

$$\frac{\partial \overline{J}}{\partial \overline{t}} = -\frac{\gamma}{\delta_a} \overline{J}. \tag{3.2e}$$

Some of the parameter values shown in Table 3.1 differ by orders of magnitude, and so processes in the model act over fast and slow time scales [PMW98]. We can explicitly highlight these different timescales by defining a scaling parameter. We choose as our parameter the ratio of average time before degradation of pheromone and the average time prior to death flying MPB,

$$\epsilon = \frac{\delta_p}{\delta_a}.$$

Using this scaling parameter, we define the dimensionless parameters

$$\begin{aligned}
\overline{\mu_p} &= \frac{\mu_p}{\mu_a}, \quad \overline{\nu_a} = \frac{\nu_a b_0}{\mu_a}, \quad \overline{k_p} = \frac{k_p a_1}{b_0 \delta_a}, \\
\overline{\mu_c} &= \frac{\mu_c}{\mu_a}, \quad \epsilon\overline{\lambda} = \frac{\epsilon a_2 \nu_c}{\lambda \mu_c}, \quad \overline{\alpha} = \frac{\nu_c}{\delta_a \mu_c}\alpha, \\
\overline{\delta_c} &= \frac{\delta_c}{\delta_a}, \quad \epsilon\overline{\gamma} = \frac{\gamma}{\delta_a}, \quad \epsilon\overline{\delta_q} = \frac{\delta_q}{\delta_a}.
\end{aligned}$$

The values of the non-dimensional parameters can be found in Table 3.2. Substituting these non-dimensional parameters into (3.2) we arrive at the non-dimensional model (3.3). equations:

$$\begin{aligned}
\frac{\partial P}{\partial t} =& \mu_p \nabla^2 P - \mu_c \nabla (P \nabla C) - \nu_a \nabla \left( \frac{1-A}{1+A/b_1} P \nabla A \right) \\
& - \epsilon P - \epsilon \frac{P^3}{P^2 + k_p^2} S + \epsilon \gamma J,
\end{aligned} \tag{3.3a}$$

$$\frac{\partial Q}{\partial t} = -\epsilon \delta_q Q + \epsilon \frac{P^3}{P^2 + k_p^2} S, \tag{3.3b}$$

$$\frac{\partial C}{\partial t} = \mu_c \nabla^2 C + \epsilon \lambda S - \delta_c C + \alpha, \tag{3.3c}$$

Table 3.2: Table of parameter values for the non-dimensional model (3.3).

| Parameter | Value |
|---|---|
| $\epsilon$ | 0.0000778 |
| $\overline{\mu_p}$ | 1.54 |
| $\overline{\mu_c}$ | 1 |
| $\overline{\nu_a}$ | 47.5 |
| $\overline{\lambda}$ | 0.154 |
| $\overline{k_p}$ | 5.14 |
| $\overline{\delta_q}$ | 0.0714 |
| $\overline{\delta_c}$ | 1 |
| $\overline{\gamma}$ | 24.6 |
| $\overline{\alpha}$ | 10 |

$$\frac{\partial A}{\partial t} = \nabla^2 A + Q - A, \tag{3.3d}$$

$$\frac{\partial J}{\partial t} = -\epsilon\gamma J. \tag{3.3e}$$

Note that we have dropped the overbars on the variables and equations for convenience.

## 3.4 Simulation Setup

The goal of the model is to help illuminate the results of the baiting experiment performed in Section 3.2.

The simulation was set up (Figure 3.1 according to the landscapes and trap locations defined in the experimental portion of our study. We simulate a two-dimensional landscape that is heterogeneous and changes with a piece-wise constant manner. For $x < 0$, the landscape is unharvested and populated with a uniform density of susceptible trees. We define this unharvested region as the dense region. For $x > 0$ the landscape is harvested and populated with susceptible trees at a thinned density, or with no trees at all (clearcut). We examined MPB movement behaviour in these two types of landscapes with pheromone traps placed at -90, -20, 20, and 90 m from the boundary between the dense and harvested regions.

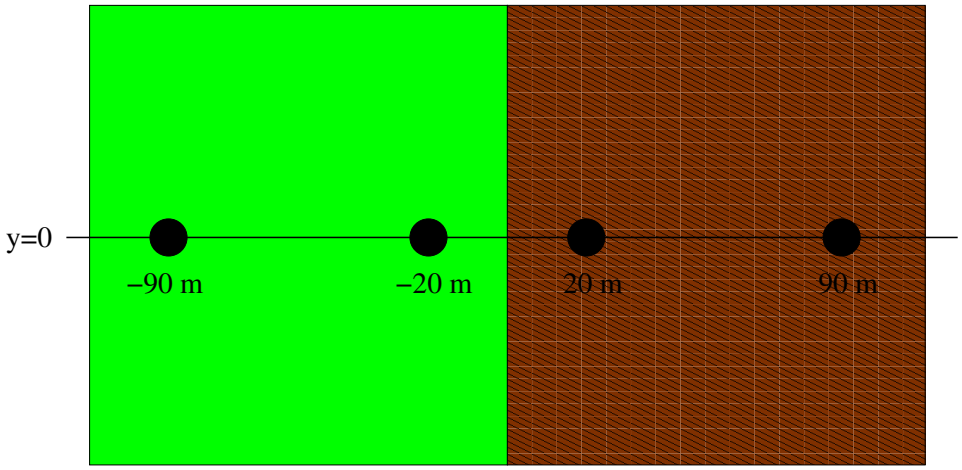


Figure 3.1: This plot shows a heterogeneous habitat with 4 bait sites. The light region (left) is uniformly dense suitable habitat and the dark region (right) is either a clearcut or a thinned habitat. The bait sites are at $\pm 20, \pm 90$ and are marked by circles.

Several MPB parameters were varied across the simulations: MPB emergence distribution, diffusion rate, and finally MPB population density. Two emergence distributions were investigated; (1) uniform emergence and (2) emergence only in the dense region. The uniform case arises from the hypothesis that flying MPB are first distributed fairly uniformly over the domain after emergence, before beginning the process of focussing on target trees (personal communication, Jim Powell). The other initial condition arises from the alternative hypothesis that beetles remain close to their source trees after emergence and so will initially only be found in the dense region. Different diffusion rates were simulated as there is evidence that MPB may move more quickly in the harvested region due to the reduced density of trees and therefore less tortuous flight paths [Rei09]. Finally, a range of population densities was simulated to understand how the baseline MPB population density affects MPB bait trap catches.

At a given time and position, the bait trap catches were calculated by integrating the flying MPB and nesting MPB density in a 6 m radius around the bait site. We then assumed that $\frac{1}{10}$ of flying MPB are caught in the trap, while all of nesting MPB are caught in the trap. Since we are interested in trap catches over the summer, we averaged the trap catches over time. This will give us an expected qualitative population densities of MPB in each trap. We simulated a very synchronous emergence and bait trap catches were taken over the period before the MPB population decreased dramatically due to death and lack of new emerging MPB. The complex ecology of MPB makes it difficult to assess the MPB population size in each trap, so our method provides a qualitative understanding of the trap catches.

The simulation landscape was chosen to have a size of 100 m in the y-direction and 2.82 km in the x-direction (Figure 3.1). Other than the traps at the center of the vertical landscape, the rest of the landscape is uniform with respect to $y$. The domain was chosen very large in the x-direction to avoid the effects of boundary conditions on the bait trap catches. The boundary conditions used for this simulation were chosen as zero-flux (reflecting) boundary conditions, so no MPB were lost at the boundary. We assume that the simulation is embedded in a large domain that is periodic

in y, so we need only simulate a single strip.

## 3.5 Numerical Method for Simulations

The MPB equations (3.3) are a set of Reaction-Diffusion-Advection equations. There are optimal schemes for separate Advection, Diffusion and Reaction equations, but finding a scheme that can solve all three simultaneously is difficult [LeV07]. Problems that can arise include finding an appropriate timestep size for stability and grid-scale oscillations in the solutions [Tys96]. Therefore, we use the technique of Strang Splitting so that we can use separate schemes for each type of equation and join them together using this fractional step method. Note that second-order accuracy in solutions is obtained, assuming each individual scheme is second-order accurate [LeV07]. We rewrite the system of equations as

$$u_t = D(u) + A(u) + R(u), \tag{3.4}$$

where $D(u)$ is the diffusion step, $A(u)$ is the advection step, and $R(u)$ is the reaction step. The splitting technique involves taking a half-step of advection, then a half-step of diffusion, followed by a full-step of reaction. After this it proceeds in the the reverse order, with a half-step of diffusion, and then a final half-step of advection. Thus, there is a full-step of diffusion, reaction and advection over the splitting technique. Mathematically, we write

$$u^{n+1} = A\left(\frac{\Delta t}{2}\right) D\left(\frac{\Delta t}{2}\right) R(\Delta t) D\left(\frac{\Delta t}{2}\right) A\left(\frac{\Delta t}{2}\right) u^n. \tag{3.5}$$

The method of Strang splitting, and the specific order of the diffusion, advection, and reaction steps in (3.5) follows work by Tyson et al [TSL00] and was chosen for its accuracy and stability for PDE systems with chemotaxis. The advection step is solved using a software package called CLAWPACK (Conservation LAWs PACKage) [LeV97]. This software uses wave propagation methods to solve multidimensional hyperbolic systems of partial differential equations. The algorithm solves the Riemann problem for the

waves, which requires computation of the flux-difference splitting between each cell. Finally, flux limiters are used to obtain second-order accuracy and maintain high resolution.

The diffusion step is solved using an ADI (Alternating Direction Implicit Method, (3.6)) in space and a TR-BDF2 (Trapezoidal, Backwards Differentiation Formula of order 2, (3.7)) method in time. The TR-BDF2 method was used instead of a standard second-order Crank-Nicholson Method since grid-scale oscillations have been found to occur in similar problems [TSL00]. The reason for the grid-scale oscillations was that the Crank-Nicholson method is only A-stable, whiled the TR-BDF2 method is both A-stable and L-stable [LeV07]. Finally, the reaction step is solved by using the standard fourth-order Runge-Kutta method, (3.8). The combination of these methods for diffusion, advection and reaction using Strang Splitting (3.5) has been used successfully to solve other reaction-diffusion chemotaxis equations [Tys96].

The ADI method uses equations [LeV07],

$$U^*_{ij} = U^n_{ij} + \frac{k}{2}(D^2_y U^n_{ij} + D^2_x U^*_{ij}), \tag{3.6a}$$

$$U^{n+1}_{ij} = U^*_{ij} + \frac{k}{2}(D^2_x U^*_{ij} + D^2_y U^{n+1}_{ij}). \tag{3.6b}$$

The TR-BDF2 obeys the equations [LeV07],

$$U^* = U^n + \frac{k}{4}(f(U^n) + f(U^*)), \tag{3.7a}$$

$$U^{n+1} = \frac{1}{3}(4U^* - U^n + kf(U^{n+1})). \tag{3.7b}$$

The Fourth-Order Runge-Kutta Equations are [LeV07],

$$Y_1 = U^n, \tag{3.8a}$$

$$Y_2 = U^n + \frac{1}{2}kf(Y_1, t_n), \tag{3.8b}$$

$$Y_3 = U^n + \frac{1}{2}kf\left(Y_2, t_n + \frac{k}{2}\right), \tag{3.8c}$$

$$Y_4 = U^n + kf\left(Y_3, t_n + \frac{k}{2}\right), \tag{3.8d}$$

$$\begin{aligned} U^{n+1} =& U^n + \frac{k}{6}(f(Y_1, t_n) + 2f\left(Y_2, t_n + \frac{k}{2}\right) + 2f\left(Y_3, t_n + \frac{k}{2}\right) \\ &+ f(Y_4, t_n + k)), \end{aligned} \tag{3.8e}$$

In (3.6), (3.7), and (3.8), $k$ represents the time step, $D_x^2$ and $D_y^2$, is the second derivative in space in the $x$ and $y$ direction, $i$ and $j$ are the $x$ and $y$ coordinates, $f$ is the function such that $u'(t) = f(u(t), t)$, and $t_n$ is the current simulation time.

Simulations were run in Fortran on the SARAHS cluster at UBC, Okanagan Campus.

To test the method used to solve the reaction step of the PDEs, we simulated the system using an explicit and implicit method. The implicit method, a Backwards Euler Method, and the explicit method, a fourth-order Runge Kutta routine, converged to the same solution. Therefore, we use the explicit method to enhance the speed of computations.

After consultation with Dr. Randy LeVeque, the author of Clawpack, we decided to check convergence of the solution using grid and time scale-tests on initial stages of pattern formation. It was recommended to use full problem instead of a subset of the reaction, advection, and diffusion pieces of the equation, because many problems only arise when all portions of equation are put together. The

The convergence to the correct solution in nesting and flying MPB for decreasing space (and time) step sizes is displayed in Figure 3.2. We chose our space step, $h$ to decrease with the time step, $k$, according to the equation $k = 4h$ [LeV07]. The log-log plot of the absolute value of the error with decreasing step size is shown in Figure 3.3. It can be seen that the error in the simulation decreases as step size decreases and that the convergence to the solution occurs for small space step sizes.

To numerically compute the error we run the simulation over a short period of time with the initial pattern formation occuring. Since we do not have the true solution set of our equations (3.3) we used the method of

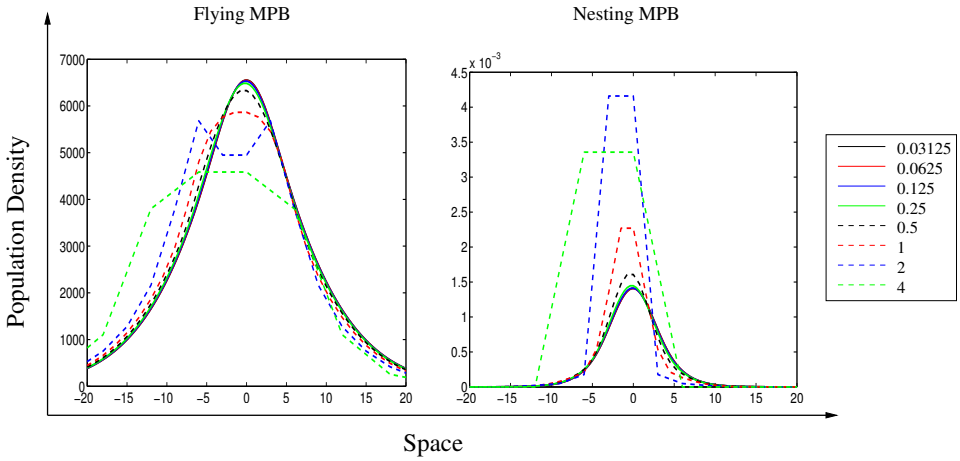


Figure 3.2: The graphs illustrate the convergence of solutions of flying (left) and nesting (right) MPB for decreasing space step sizes, $h$. The different space step sizes are shown in the legend.

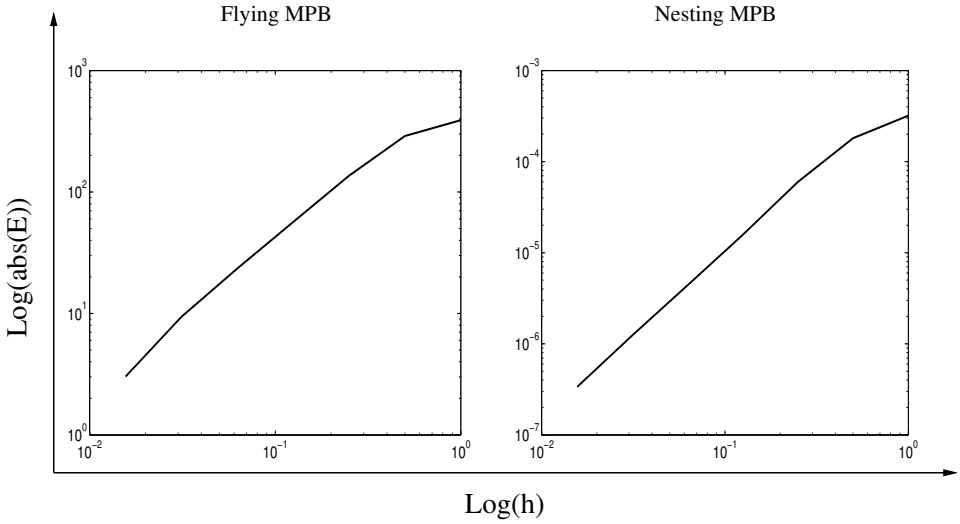


Figure 3.3: Log-log error plots of the absolute value of the error against space step size, $h$, for flying (left) and nesting (right) MPB.

Table 3.3: Order of accuracy for nesting, $q$, and flying, $p$, MPB solutions with decreasing space step size, $h$. $\log_2(R)$ is the order of accuracy for a given space step size.

| Variable | $\log_2(R(4))$ | $\log_2(R(2))$ | $\log_2(R(1))$ |
|---|---|---|---|
| $q$ | 0.8207 | 1.5933 | 1.9301 |
| $p$ | 0.4353 | 1.0831 | 1.2671 |
| Variable | $\log_2(R(0.5))$ | $\log_2(R(0.25))$ | $\log_2(R(0.125))$ |
| $q$ | 1.8407 | 1.8220 | 1.8824 |
| $p$ | 1.2716 | 1.3210 | 1.6342 |
| Variable | $m$ | | |
| $q$ | 1.6482 | | |
| $p$ | 1.1687 | | |

computing errors for numerical solutions (3.9) [LeV07]. That is, for small step sizes in space and time we assume that

$$E(h) = Ch^m + o(h^m), \tag{3.9a}$$

$$E(h) \approx Ch^m, \text{ as h} \to 0, \tag{3.9b}$$

$$E\left(\frac{h}{2}\right) \approx C\left(\frac{h}{2}\right)^m, \tag{3.9c}$$

$$R(h) = \frac{E(h)}{E(h/2)} = 2^m, \tag{3.9d}$$

$$m \approx \log_2(R(h)). \tag{3.9e}$$

where, $E(h)$ is the error at space step size $h$, $C$ is the error constant, $R$ is a ratio of errors, and $m$ is the order of accuracy.

This allows us to produce Table 3.3, which numerically summarizes the order of accuracy in our solutions (for flying and nesting MPB) as we decrease the space step size, $h$.

Based on the order of accuracy from Table 3.3, we find that our numerical simulations are above order 1.5 accuracy for nesting MPB density, and greater than order 1 accuracy for flying MPB density. These two quantities have the non-linear and chemotaxis portions of the code and thus are the most important variables to calculate error and ensure accuracy of the solutions.

## 3.6 Model Results

For our simulations, we used emergence population densities, $J_0$, varying between 31,250 MPB/ha and 250,000 MPB/ha. Assuming that a single source tree can produce on the order of 10,000 MPB per flight season [PB09], these densities correspond to between 3 and 25 source trees per ha. Diffusion rates ranging from 1 to 2 ha/fh were considered, consistent with the estimation in Powell et al. [BPBL00], and will be used to test the hypothesis of faster diffusion in the harvested region.

All variables were initially set to zero, except for $J$, which gives the initial density of MPB emerging from trees and becoming flying MPB. We ran simulations of our mathematical model (3.3) with various initial population densities and diffusion rates. We tracked the spatial dynamics of flying ($P$) and nesting ($Q$) MPB along a linear transect ($y = 0$, position of bait traps, Figure 3.1) at small and large intial densities of MPB for four cases: clearcut and thinned harvested region with dense forest initial conditions (Figures 3.4 and 3.5, respectively), and clearcut and thinned harvested region with uniform initial conditions (Figures 3.8 and 3.9, respectively).

When MPB emerged only in the dense forest, the MPB had similar dynamics in both clearcut (Figure 3.4) and thinned (Figure 3.5) harvested regions. Both figures have, in general, higher densities of MPB in the forested region than in the harvested region. This difference is due to the fact that no MPB emerged from this region, they only emerged from the unharvested region. This diffusion of MPB into the harvested region creates a decreasing population density curve from the unharvested (left) to harvested (right) region. Therefore, we expect the number of MPB to decrease from left to right (-90 m, -20 m, 20 m, 90 m). In general, this hypothesis is upheld by the simulation results, with evident spikes in both the nesting and flying MPB at the location of the bait traps. At high densities, another dynamic emerges, where there is sufficient MPB to begin a successful attack. In this simulation the MPB attack and nest to the left of the trap at -90 m. This successful attack pulls other MPB toward it and thus we see the change in the slope of the flying MPB profile in the plots at 4.8 and 6.4 flight hours

(fh). The last plot at 8 fh, shows the progression of the successful attack reaching the -90 m trap, and MPB are beginning to attack near this trap at a high density. This pulls MPB not already nesting or caught in traps from surrounding regions of -90 m towards that trap, lowering catches in nearby traps.

The major difference between Figures 3.4 and 3.5 is the right hand ($x > 0$) tail in the distribution of nesting MPB. In the clearcut (Figure 3.4), the population of nesting MPB is essentially zero, while it is small but positive and decaying with $x$ in the thinned region (Figure 3.5). Compare the second and fourth columns of Figure 3.4 against Figure 3.5. The positive density of nesting MPB comes from nesting MPB who have diffused into the harvested region from the unharvested region.

The bait trap catches corresponding to the MPB distributions in Figures 3.4 and 3.5 are shown in Figure 3.6. There is essentially no difference between the left and right graphs. This is because the number of MPB who diffuse from the unharvested region to the harvested region is small enough that nesting in the thinned region does not cause a significant increase in the density of MPB trapped at that point.

The bait trap catches in both cases are ordered, with the number of trapped MPB decreasing from the -90 m to the 90 m trap along the $y = 0$ transect. This makes sense since diffusion pulls MPB away from the sources in the unharvested region and into the harvested region. This creates a declining density from left to right along the $y = 0$ transect. It is interesting to note that the attracting region for the -20 m and 20 m bait traps overlap (Figure 3.7) and so it is possible that these two traps could interfere with each other and disrupt the ordering of the trap catches expected from diffusion alone. We do not observe this, however, and so the trap catch pattern is dominated by the effects of diffusion.

As the density of MPB increases from left to right in each plot in Figure 3.6, there are two changes to the graph. First, since a larger density of MPB are emerging, more make it to the trap at 90 m (in the harvested region). Consequently, the difference between the trap catches at 20 m and 90 m decreases. The second major change is that there is a major aggregation

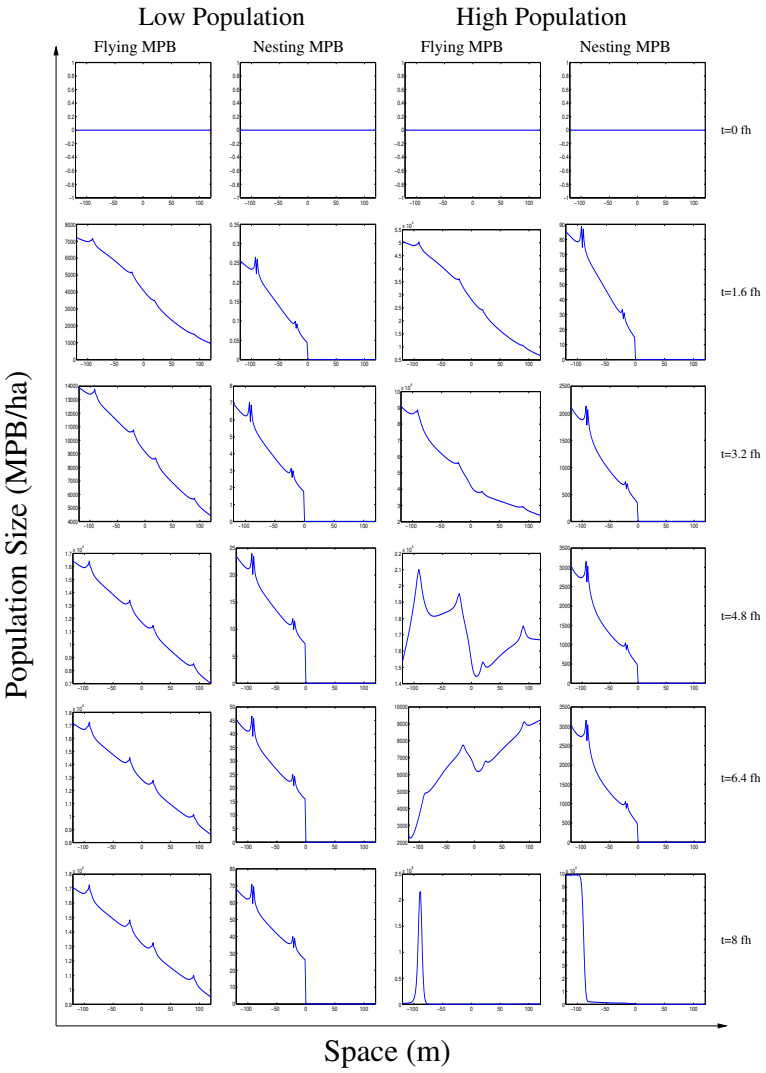


Figure 3.4: Spatial population densities of flying and nesting MPB in a landscape that has a clearcut harvested region and dense forest intial conditions. The spatial plots are shown over increasing time simulation in MPB flight hours (fh). The two columns on the left depict the MPB at a low initial population density ($J = 31,250$ MPB/ha, approximately 3 source trees per ha) and the two right columns illustrate high initial population densities ($J = 218,700$ MPB/ha, approximately 22 source trees per ha). The simulations shown assume diffusion is 1 ha/fh.

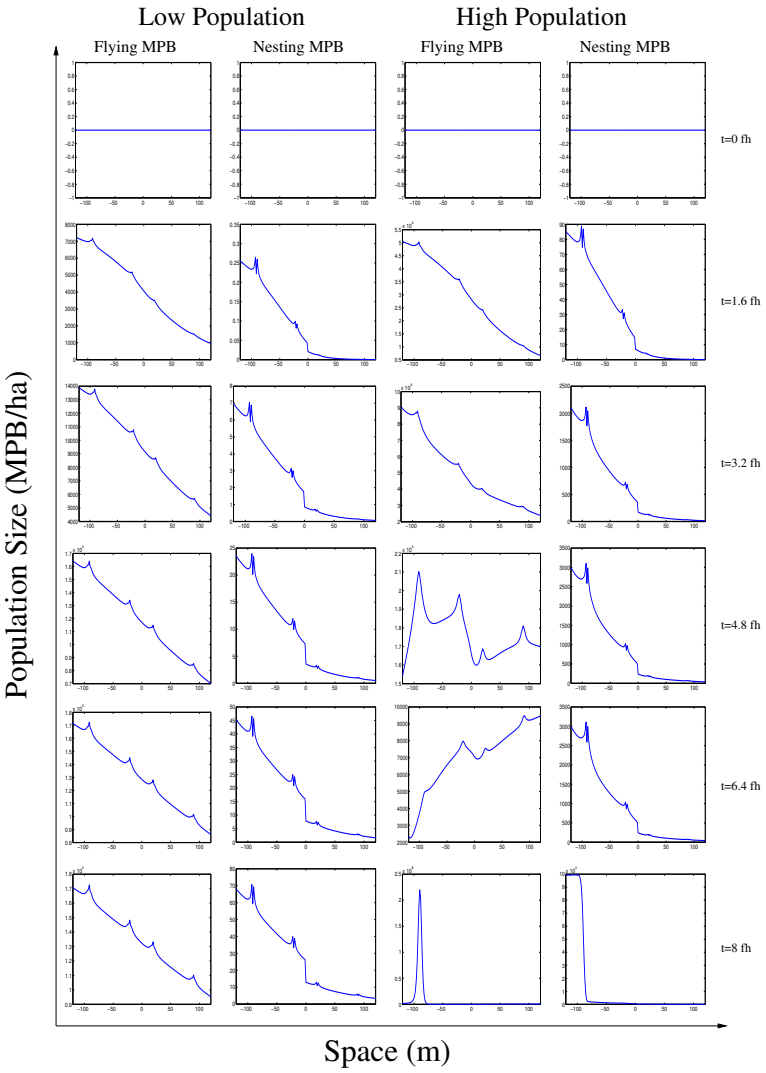


Figure 3.5: Spatial population densities of flying and nesting MPB in a landscape that has a thinned harvested region and dense forest intial conditions. The spatial plots are shown over increasing time simulation in MPB flight hours (fh). The two columns on the left depict the MPB at a low initial population density ($J = 31,250$ MPB/ha, approximately 3 source trees per ha) and the two right columns illustrate high initial population densities ($J = 218,700$ MPB/ha, approximately 22 source trees per ha). The simulations shown assume diffusion is 1 ha/fh.

event left of the -90 m trap at high densities of MPB. This is shown in the distribution of flying and nesting MPB at $t = 8$ fh for high MPB population densities in Figures 3.4 and 3.5. The large density of nesting MPB draws in nearby flying MPB populations and there is a large increase in the flying and nesting MPB near the -90 m trap. This major aggregation event is due to the self-focusing nature of the MPB biology [WP97]. Once a high enough density of flying MPB begin to nest, the nesting MPB produce pheromone, which draws more flying MPB towards that site. Once the site has reached a critical density, the pheromone becomes repulsive and approaching MPB nest instead in nearby trees. This process is the cause of the major increase in the trap catches at -90 m for densities of MPB above $1.8 \times 10^5$ per ha.

It is unclear whether the MPB in a given landscape are largely from local sources, or if a significant proportion of beetles drift in from elsewhere via long-distance dispersal. In the first case, we expect MPB to emerge only in the unharvested region (dense forest ICs); this was the case simulated in Figures 3.4 and 3.5. In the second case, we expect the initial distribution of MPB to be more uniform, assuming that MPB arrived/emerged in a uniform manner in both the dense forested region (unharvested) and the harvested region. The resulting spatial population densities of flying and nesting MPB over time at a high and low population density are displayed in Figures 3.8 and 3.9. Another mechansim which could give rise to a more uniform emergence density is if there is a sexual maturation time involved before MPB begin to attack susceptible trees and become responsive to chemical signals [HFSL06].

In this scenario, instead of the strongly sloped MPB density profile seen in Figures 3.4 and 3.5, the flying MPB have a uniform density, with spikes at the bait locations. If there are trees to nest in at these locations, these bait traps will also act as the initial positions of MPB aggregation on the susceptible landscape. The spikes in nesting MPB density are evident in Figures 3.8 and 3.9. At low densities, the nesting MPB change the flying MPB density as expected. In the clearcut case (Figure 3.8 the nesting MPB produce pheromone which attracts more flying MPB and thus the density of flying MPB in the unharvested region is always larger than in

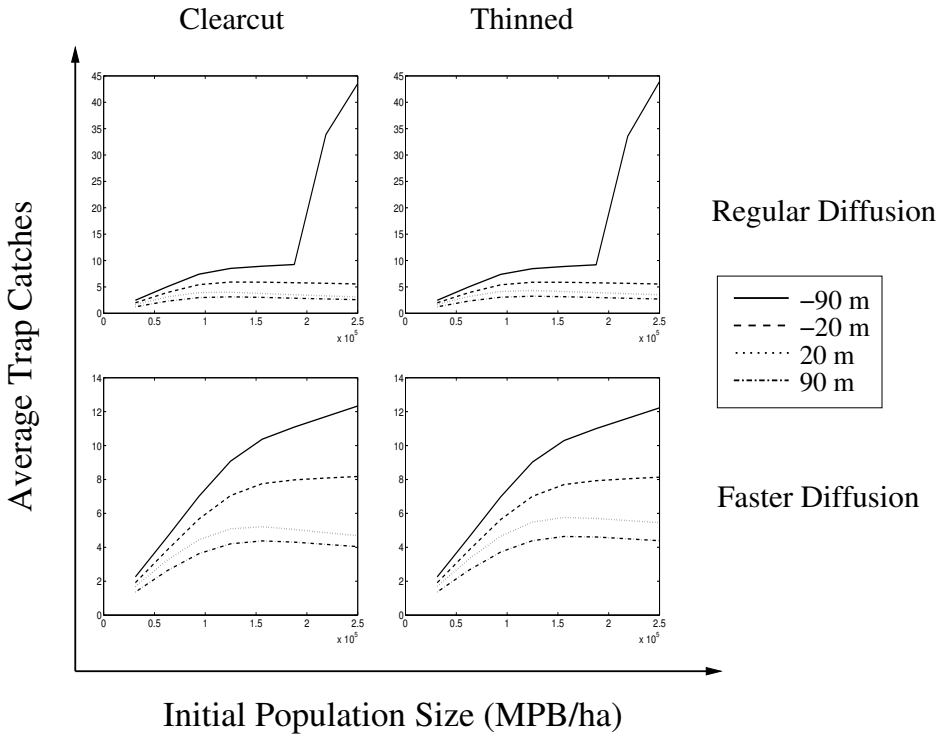


Figure 3.6: Average trap catches in the bait sites at $\pm 20, \pm 90$ m with an initial condition of MPB in dense forested region only. The bait trap catches are shown for heterogeneous landscapes with the harvested region either clearcut or thinned. The bottom two plots show the trap catches expected if MPB diffuse faster in harvested regions.

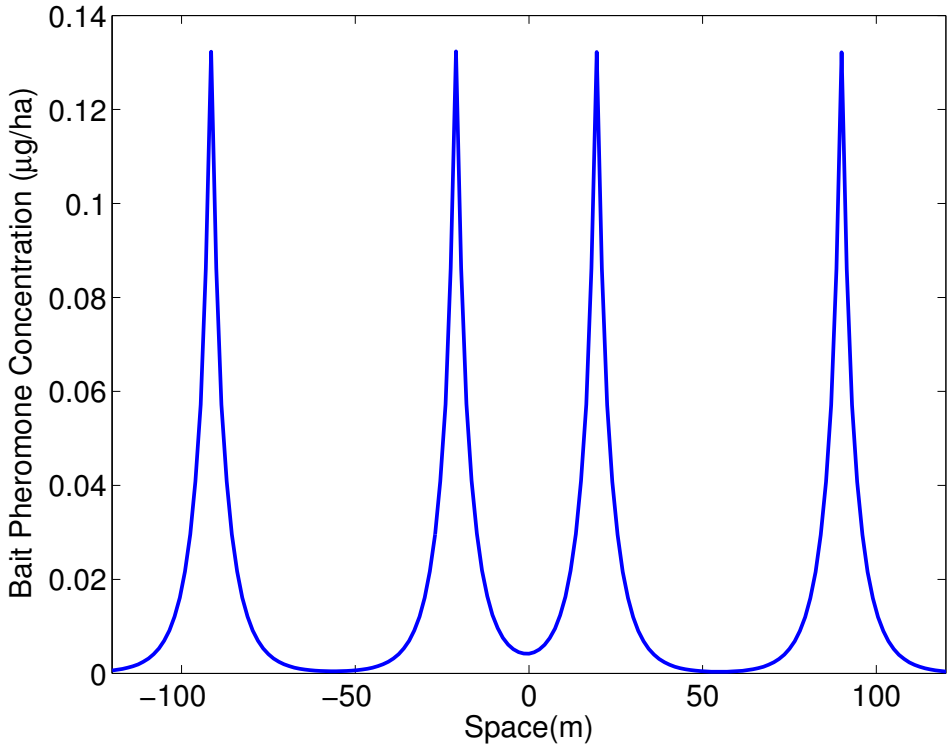


Figure 3.7: This graph represents the bait pheromone profile at the beginning of a simulation. It can be seen that the baits are at ± 90 and ± 20 m. The profiles at ± 20 m overlap, therefore sharing an attraction region. The simulations shown assume that the diffusion rate is 1 ha/fh.

the harvested region. In the thinned case (Figure 3.9) the MPB are able to nest in the harvested region, so the difference in MPB between the two regions is smaller. The smaller density of susceptible trees in the harvested region results in a slower nesting rate, and thus more MPB are found in the unharvested region.

At higher densities, the thinned and clearcut results are similar for the first 3.2 flight hours. First the nesting occurs exclusively (clearcut) or mainly (thinned) in the unharvested region. Notice that the density of MPB at the -20 m site is larger than the density of MPB at the -90 m site. This behaviour is due to the nature of the MPB attraction to pheromone. Since the landscape changes at 0, the change in MPB pheromone concentration sharply decreases at this point. Since the MPB respond to the gradient of MPB pheromone (chemotaxis term), and this gradient is largest at the border between the harvested and unharvested region, the attraction to the unharvested region is maximum near this point. Figure 3.10 shows the MPB pheromone profile (and the resulting chemotactic attraction). Therefore, since the emergence is uniform, MPB will begin to nest in greater numbers at the -20 m site versus the -90 m site. Once the nesting at the -20 m site begins, the self-focusing behaviour of the MPB strongly affects the spatial dynamics of the population. At the initial aggregation site, nesting beetles release pheromone, increasing the gradient there and attracting more flying MPB. This sets up a positive feedback cycle that intensifies the initial aggregation. Once enough MPB have nested and increased the pheromone to a critical level the pheromone becomes repulsive and signals for MPB nest in nearby trees. The nesting density of MPB then broadens to a larger spatial region of attack.

Once repulsion of MPB has broadened the spatial region of attack (high density, 4.8 fh) the shape of the nesting MPB curve is determined by the type of harvesting (thinned or clearcut). If the spatial region is clearcut (Figure 3.8), MPB cannot nest there, so there is a build-up of MPB at the border between the harvested and unharvested regions. At this point the MPB pheromone gradient is very steep, and thus very attractive, so there is a build-up of MPB at the border of the harvested and unharvested region.

This leads to a very sharp peak of nesting and flying MPB density near this point. To the left of this peak there is a bump in the uniform nesting MPB density at the intial site of attraction. This is due to the larger density of MPB needed to produce the pheromone required before the pheromone signal became repulsive. For nearby trees, there is already a large concentration of pheromone present, so it takes a lower density of nesting MPB to produce the needed pheromone for the pheromone to become repulsive. It can be seen there is also a small increase at -90 m, due to the increased attractiveness of the bait site from bait pheromone.

If the region is thinned (Figure 3.9), the spatial dynamics are a little different. Similar to the clearcut region, the flying MPB build up on the edges of the nesting MPB curve and there are peaks in the nesting MPB density at the bait sites due to steep pheromone gradients there. The largest peak of nesting MPB occurs at the initial bait site of -20 m (3.2 fh, high density). The behaviour that differentiates the thinned case from the clearcut one is that the nesting MPB density spreads into the harvested region (since there are trees to nest in). There is an interesting spike at the border between the harvested and unharvested region (0 m). This is due to the difference in kairomone production and the difference in nesting rate across the boundary between the two regions.

We calculated bait trap catches based on integration of these curves, the results are shown in Figure 3.11. Differences between thinned and clearcut are more significant if MPB emergence occurs uniformly (Figure 3.11) instead of only in the dense forest (Figure 3.6). The uniform emergence ensures a higher density of MPB in the harvested regions. This results in a larger proportion to be caught in the traps of the thinned harvested region. Finally, the traps at $\pm$ 90 and $\pm$ 20 m display more differences with uniform initial conditions than dense initial conditions.

An interesting note is that the trap at 20 m actually has less MPB than the trap at 90 m (clearcut). This is due to the MPB pheromone at the -20 m trap attracting MPB flying near the 20 m trap (see Figure 3.10). This result is due to the overlap in MPB pheromone from the traps at $\pm$20 m.

The same process also explains how the trap in the thinned region, at

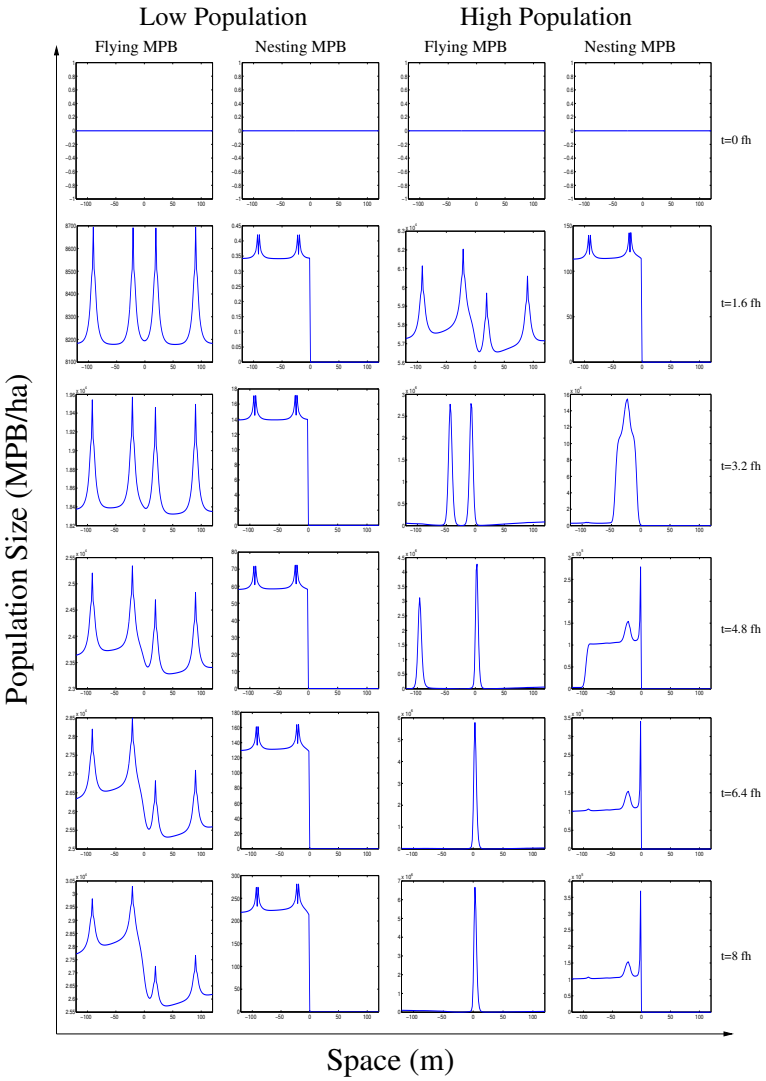


Figure 3.8: Spatial population densities of flying and nesting MPB in a landscape that has a clearcut harvested region and uniform intial conditions. The spatial plots are shown over increasing time simulation in MPB flight hours (fh). The two columns on the left depict the MPB at a low initial population density ($J = 31,250$ MPB/ha, approximately 3 source trees per ha) and the two right columns illustrate high initial population densities ($J = 218,700$ MPB/ha, approximately 22 source trees per ha). The simulations shown assume diffusion is 1 ha/fh.

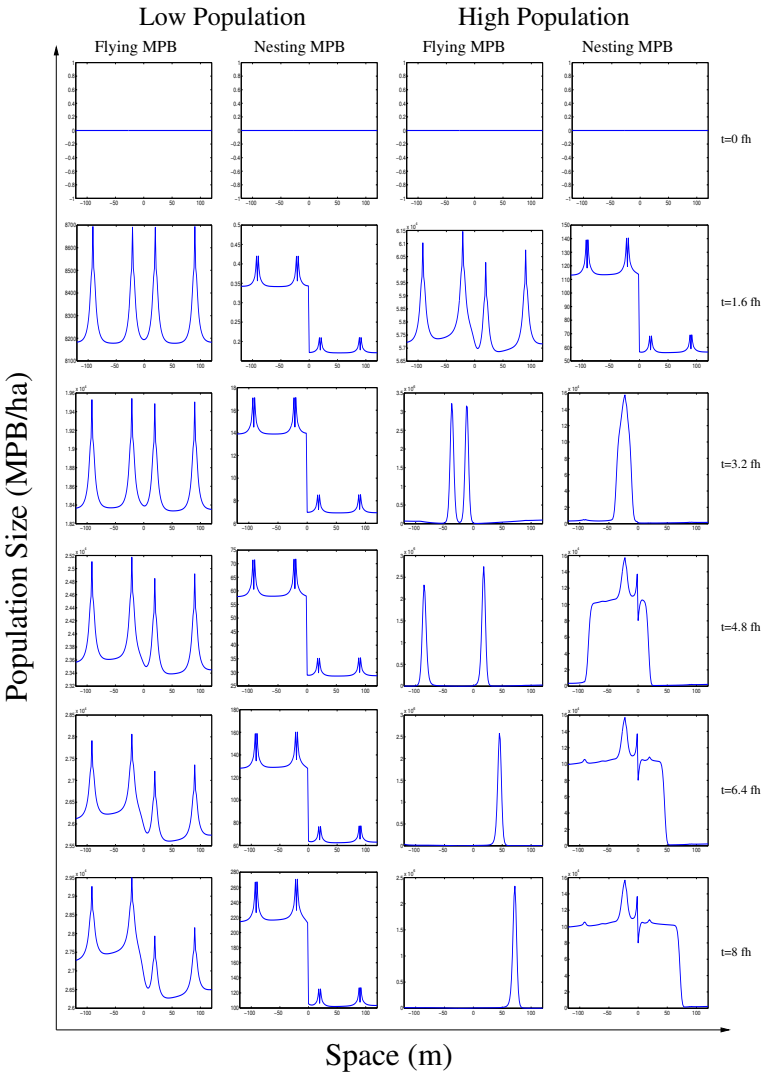


Figure 3.9: Spatial population densities of flying and nesting MPB in a landscape that has a thinned harvested region and uniform intial conditions. The spatial plots are shown over increasing time simulation in MPB flight hours (fh). The two columns on the left depict the MPB at a low initial population density ($J = 31,250$ MPB/ha, approximately 3 source trees per ha) and the two right columns illustrate high initial population densities ($J = 218,700$ MPB/ha, approximately 22 source trees per ha). The simulations shown assume diffusion is 1 ha/fh.

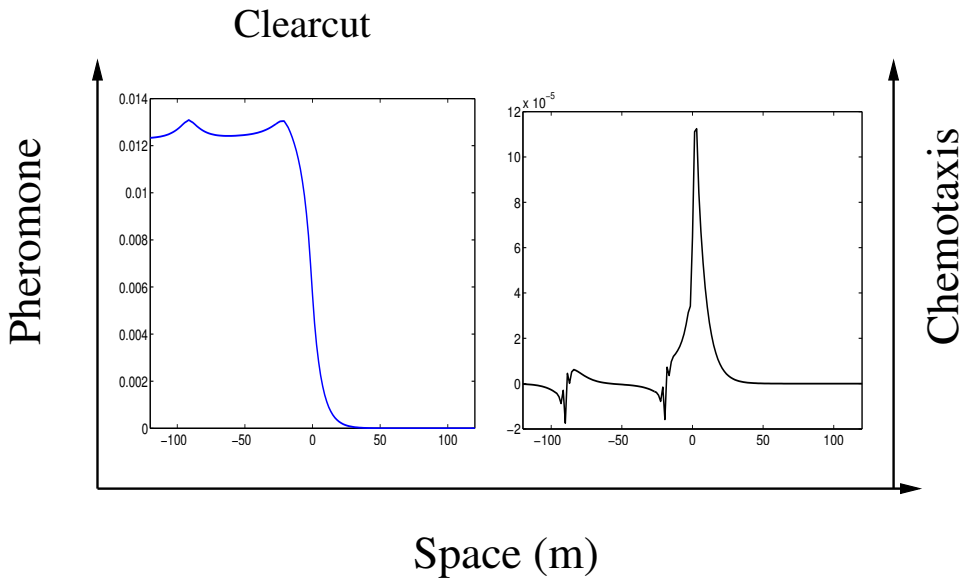


Figure 3.10: This graph represents the MPB pheromone profile (left) and resulting chemotactic response (right) near the beginning of the simulation before significant nesting occurs. It can be seen that the pheromone profile across the border between the unharvested and harvested edges has a steep gradient which causes significant attraction (large chemotactic response) to the unharvested region. This specific simulation is at a high density ($J = 218,700$ MPB/ha, approximately 22 source trees per ha) for the uniform initial conditions with a clearcut harvested region. The simulations shown assume diffusion is 1 ha/fh. Pheromone concentration is in $\mu g/ha$ and chemotactic response has units $1/fh$.

20 m, has more MPB than the trap at -90 m for larger initial densities of MPB. The initial MPB aggregation occurs at -20 m and the excess MPB near this trap may spillover to the 20 m trap. In Figure 3.9 (at 4.8 fh) it is evident that the right peak of flying MPB density (the one progressing through the harvested region) is larger than the peak in the unharvested region. This is due to the greater attraction of MPB in the harvested region because of a sharper gradient in the MPB pheromone profile. Additionally, the pheromone profile at -90 m is largely smooth. The main reason that the MPB pheromone concentration is lower in the harvested region is the lower density of susceptible trees. This results in a lower density of nesting MPB and thus a lower concentration of pheromone.

We tested the effect of faster movement by increasing the diffusion by a factor of 2. This is represented in the plots labeled fast diffusion in Figures 3.6 and 3.11. The increase in diffusion will have two main effects. First, if MPB are initially only in the dense forested region (Figure 3.6), the faster diffusion allows more MPB to travel into the harvested region and MPB to move through the harvested region more quickly. This changes the rate at which the MPB approach the pheromone traps. The second effect of the faster diffusion is that it smooths out the sharp peaks of flying MPB. MPB will still be attracted to pheromone, but the peaks that form will not be as sharp or large. This is evident in either initial condition, as shown in Figures 3.6 and 3.11.

In Figure 3.6, the faster diffusion increased the trap catches in the $\pm$ 20 m and 90 m traps, and decreased the trap catches at the -90 m trap. This makes sense as the higher diffusion rate allowed a larger density of MPB to move into the harvested region. The trap catch decreasing at -90 m is due to a two-fold effect. First, the diffusion smooths the peak of MPB that forms at this site and second, the faster diffusion of MPB into the harvested region decreases the number of MPB present in the unharvested region. Finally, the higher number of MPB in the trap at -20 m is due to the smoothing and diffusion of MPB away from the trap at -90 m.

The effect of faster diffusion with uniform emergence of MPB (Figure 3.11), is mainly a decrease in the trap at -20 m. This also changes the

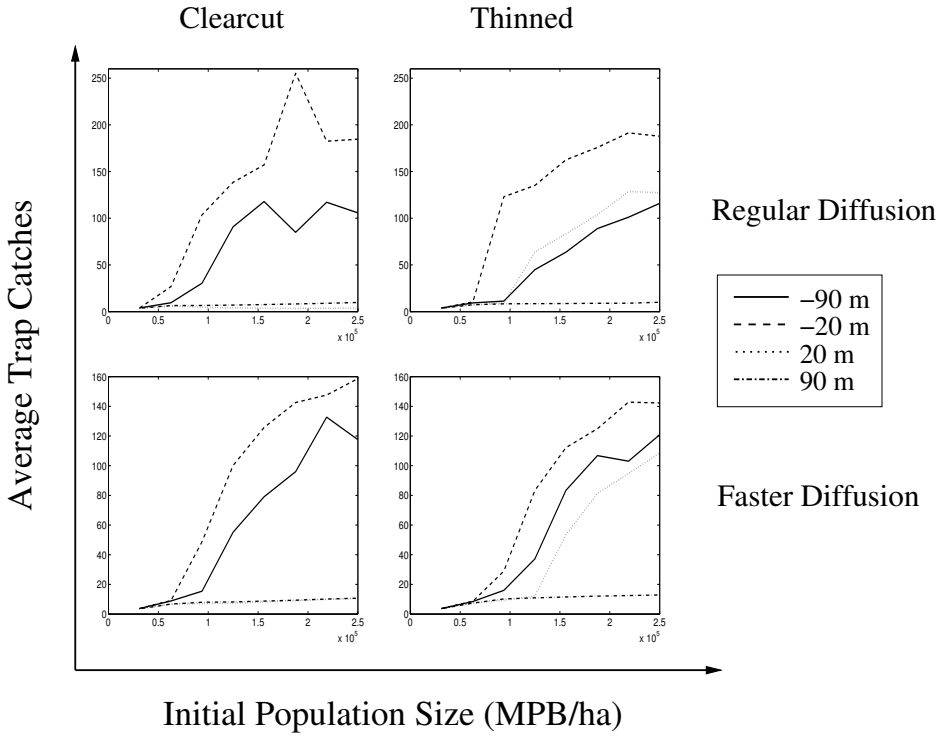


Figure 3.11: Average trap catches in the bait sites at $\pm 20, \pm 90$ m with an initial condition of MPB at a uniform density over the domain. The bait trap catches are shown for heterogeneous landscapes with the harvested region either clearcut or thinned. Additionally, the diffusion rate is changed to see the effect of increased movement rate in harvested regions. Note that the peaks in trap catches differ between the regular and faster diffusion cases.

trap catches at 20 m. The smoother pheromone peak at -20 m results in a smaller attraction and consequently a lower density of MPB. In the case with a thinned harvested region, this means there are fewer MPB which will find the nearby trap at 20 m. If the harvested region is clearcut, the lower attraction of pheromone at -20 m (when compared to the regular diffusion case) results in less MPB moving from the 20 m trap to the -20 m trap. Thus, there is a slight increase in the MPB density at 20 m if the harvested region is clearcut. The final consequence of a lower number of MPB at -20 m is an increase in the trap catches of MPB at -90 m.

## 3.7 Connections Between Theoretical and Empirical Results

We did not have enough information in the field study to discern the initial population sizes and whether the initial distribution of MPB was uniform or not. We therefore discuss the comparison between our simulation results and data first under the assumption of uniform initial conditions and second under the assumption of dense forest initial conditions.

Using uniform initial conditions, we find there is a more significant difference between the clearcut and dense region than there is between the thinned and dense region (Figure /reffig:uniformic). This is consistent with our experimental results which show a statistically significant difference between the clearcut and dense region but not between the thinned and dense region. In general, the difference between the harvested and unharvested regions is smaller at lower population sizes but increases as MPB population size increases. An exception to this trend is the trap catches at 20 m.

Empirical results found no statistically significant difference between the two types of harvested regions, thinned and clearcut. This is consistent with our simulation results for the 90 m trap and for the 20 m trap for low population densities.

The final empirical result is that pairs of traps in the harvested and unharvested region were not significantly different. Our simulation results

in the harvested region agree with the empirical results. That is, traps in the harvested region were not significantly different for low population sizes. In contrast to the empirical results, however, only at the lowest population size are the simulation predictions of the bait trap catches the same in the unharvested region.

Under the assumption that MPB are initially only present in the dense forested region, we find that there are only small differences between all trap catches. Only at very high densities do the simulation results predict any difference between the harvested and unharvested traps. Thus, these simulation results agree with the experimental results that the difference between traps is not significant at different locations within the harvested or unharvested region. Additionally, the simulation results agree that no significant difference will be found between the traps between the clearcut and thinned region, as well as no significant difference across the traps in the thinned and dense regions. In contrast to the experimental results, however, our simulation results predicts no significant difference between the clearcut and dense region.

Under either initial condition, a faster diffusion of MPB resulted in a decreased difference between all traps. The simulations shown were done with the diffusion increased by a factor of 2. Other simulations were performed with the diffusion increased by a factor of 5 and 10 (results not shown). As expected, trap catches became even closer as diffusion increased. Currently, our model simulation results predict that the pairs of traps in the harvested or unharvested region will only be similar for low population sizes, under uniform initial conditions. If we assume diffusion is increased, our simulation results become closer to the experimental results, since the differences between pairs of traps in each region decrease.

To test the effect of the pheromone response function chosen [WP97, HFSL06] we ran the simulations with the effects of MPB pheromone neglected (results not shown). That is, the pheromone from the bait traps still worked as usual, but the pheromone produced by the MPB had no attractive or repulsive effect on the MPB. This led to the prediction of increased MPB numbers in the harvested region, and smaller differences between pairs of

traps in each region when compared to the standard pheromone response used in this study.

If population levels increased beyond the results shown in Section 3.6 (results not shown), it was found that the repulsive nature of the pheromone led to increased densities in the harvested zone. Thus the repulsive nature of the pheromone becomes increasingly important at higher densities of MPB.

## 3.8 Discussion

Our experimental results indicate that differences in MPB trap catches were not statistically significant between the dense forested region and thinned forested region as well as the pairs of traps in either the harvested (thinned or clearcut) or unharvested (dense forest) landscape. Finally, the difference in MPB trap catches between the different types of harvested region was not statistically significant.

Our simulation results most closely agreed to experimental results when the initial distribution of MPB on the landscape was uniform. This result supports the hypothesis that MPB were fairly uniformly spread over the harvested and unharvested landscape at the start of the summer. This distribution could be due to the free-flight behaviour of the MPB [Hug02], or could be due to external sources of MPB blanketing the landscape [dCA12]. Furthermore, for the clearcut and the dense forested region to show statistically significant differences between trap catches, the population of MPB must be sufficiently large. That is, the experimental results show a statistically significant difference between the clearcut and dense region, and thus, according to our simulations, the population of MPB must be sufficiently large before this difference becomes apparent.

In contrast, the simulation results where MPB emerged only from the unharvested region did not agree well with the experimental results. The dense forest initial conditions lead to smaller trap catches in the harvested region then was observed in the experimental trap catches. Additionally, we expected initial aggregation at the trap sites, which did not occur due to the diffusive spread of the MPB population in the unharvested region into

the harvested one.

The experimental results illustrated very little difference between traps at 20 and 90 m from the edge of the habitat in both the harvested and unharvested regions. Our simulation results become closer to this experimental result as we assume that diffusion increases over the landscape. Faster diffusion means smaller catches at each trap, but the trap catches at 20 and 90 m from the edge also become more similar. This result supports the hypothesis that MPB may move faster in harvested regions due, possibly, to less tortuous paths [Rei09]. Higher diffusion rates in matrix habitat has been observed in studies of other insects such as leaf beetles and planthoppers [CDO07, HC03, HC06].

As the density of attacking MPB increases, pheromone interactions become more important. In the current chapter we assume that pheromone can be both attractive and repulsive [WP97], and this combination allows for the spreading of MPB attack from an initial aggregation. Strictly attractive pheromone responses were suggested by Hughes [Hug02], but in our model this would lead to uncharacteristic densities of MPB in a single aggregation at the initial site.

In our study, we also made the assumption that MPB had a very synchronous emergence. If this is not the case, the density of MPB needs to be significantly higher to nucleate a successful initial aggregation. In this scenario, we would expect much lower trap catches than were reported in the simulation results in Section 3.6 due to lower densities of nesting MPB, and consequently lower densities of flying MPB attracted to the sites with nesting MPB.

In the simulation results with uniform initial conditions, we found that the pheromone produced by traps was very important in determing the initial aggregation position of MPB. After this point, however, we found that the pheromone produced by MPB had a much larger impact. That is, at higher densities of MPB the pheromone produced by MPB was much more effective in determining the behaviour of MPB than the trap pheromone. This supports the conclusion that natural sources of pheromone can largely affect the timing and trap catches of MPB, as predicted by Bentz [Ben06].

Our model does not include any explicit boundary behaviour at the interfaces between regions, but several empirical [CC82, Jon77, RH98, SC01, WSM04] and theoretical studies [ML, GTLS] have shown that this may be an important factor. Another direction for future study is to consider spatially explicit diffusion, changing in each patch. Variations in spread rate have been found to be important in other theoretical studies [ML].

The difficulties in determining the movement behaviour of MPB is well-known, especially under habitat fragmentation [BAL93] and when using trap catches to provide information about MPB densities [Ben06]. Our study links mathematical and experimental studies to create a powerful approach to elucidate MPB spatial dynamics. Through our combined approach we provide evidence that MPB move faster in harvested landscapes, and that MPB emergence and movement behaviour leads to a more uniform density of MPB prior to attacks on susceptible trees.

The results of our study gives new insight into several areas. It has been hypothesized that MPB movement may be faster in harvested landscapes [Rei09, BPBL00]; our study provides significant support to this hypothesis. Additionally, understanding the dispersal of MPB in fragmented landscapes is crucial to inform management decisions, as MPB moving differently in matrix habitat will change the optimal strategy for control of the insect. In addition, the results of our simulation helps us understand the movement behaviour of MPB prior to attack. The fairly uniform initial distribution of MPB is very important, as it allows us to understand the spatial distribution of MPB prior to attack, and will allow further study to target the best way to control MPB spread.

# Chapter 4

# Impacts of Management on Mountain Pine Beetle Movement

## 4.1 Introduction

The economic and widespread impact of the MPB has led to extensive management efforts, through direct and indirect control [SW06]. Direct control mechanisms have focussed on harvesting newly attacked (green attack) trees to prevent the spread of the MPB before they can emerge from the tree. Additionally, semiochemicals, both attractive and repulsive to the beetle, have been used to help prevent spread and to direct MPB movement towards specific stands. This allows for a more targeted management of the beetle. A direct control mechanism which has been tested in the past is prescribed burning of beetle infested areas of the landscape. The problem with this control technique is that the beetle can survive unless the fire is a high-intensity one. Since high-intensity fires are dangerous and very difficult to control, prescribed burning is no longer used as a method of direct control. The most common indirect control method has been prescribed burning and harvesting of susceptible lodgepole pine tree stands which have not yet been attacked by the MPB. This control method is used to decrease the density of susceptible host trees.

In the past two decades, MPB populations rose to epidemic levels and have had devastating effects on forests in both British Columbia [SW06] and Alberta [TR08]. In particular, Banff National Park (NP) has been affected

by the MPB since 1997 [TR08]. Management efforts in Banff have focussed on prescribed burning and baiting and felling of green attack trees. Baiting of the trees focusses the attack of nearby MPB, allowing Parks Canada personnel to do intensive land surveys around the baited area to fell and burn trees recently attacked by the MPB. Prior to the initiation of MPB control efforts, Banff NP was divided into two areas, one with management and one without. The resulting data can help elucidate the effectiveness of control efforts. An initial study found that the management activity limited the long-distance spread of the MPB, but did not reduce the area of lodgepole pine affected [TR08]. However, this conclusion was confounded by differences between the two zones: the management zone had a larger area of dense, susceptible lodgepole pine than the control area. There is need for a mathematical model to test competing hypotheses to explain the empirical results. This model could also be used to test the effectiveness of management activities *in silico*, without long-term consequences to the landscape.

The effect of prescribed burning on MPB depends critically on the intensity of the fire. High-intensity fires can reduce brood density and reproduction [SLSH01], reduce the attractiveness to MPB [SLSH01, Mur77, SG89, ER04], reduce susceptibility of the forest to MPB attack, and reduce traversability of the landscape to MPB [BLB$^+$06]. As mentioned earlier, however, high-intensity fires can be difficult to control and can result in major damage to the site (such as soil damage) [SG89]. Suprisingly, lower intensity fires that only moderately burn trees, may actually increase the attractiveness of these sites to MPB [SLSH01, SG89]. In addition, there may be increased competition with other insects such as Pine Engravers (personal communication, Jane Park), and possibly increased [MKW03] or decreased [Rei07] resin production.

The pattern of attack of the MPB is intrinsically determined at epidemic and incipient epidemic densities [WP97] (Chapter 2) and is determined by the susceptible landscape at endemic densities. Similarily, at low densities of MPB, stressed, partially burned trees on the edge of a prescribed burn are preferentially attacked [ER04]. At high densities of MPB, the same pattern

is not observed, and burned and unburned trees are equally likely to be attacked.

Previous modelling efforts have investigated beetle dynamics over a single season, but few models have looked at beetle populations across multiple years. Of those that have looked at multiple-year dynamics, there are no models of which we are aware that explicitly model both population dynamics and dispersal, including the interactions between beetles, beetle pheromones, tree kairomones, and the forest landscape. These interactions are extremely important as they will determine the spread dynamics of MPB over the landscape.

In this chapter, we build a multi-year spatially explicit model (Section 4.2) to test the effectiveness of the management strategies of baiting and tree-removal (Section 4.3.1) and prescribed burning (Section 4.3.2). Using our model, we find that baiting and tree-removal is always more successful at reducing MPB density and forest impact at high initial MPB population densities but may lead to greater forest impact and greater MPB population growth at low initial levels of MPB. We predict that tree removal without baiting can be more successful than combined baiting and tree removal if the searched area is optimal (high MPB density). Finally, our analysis indicates that prescribed burning is more effective than unmanaged controls, and can be more effective than clearcutting given assumptions about the reproductive output and attractiveness of burned trees.

In Section 4.4 we present indicators of MPB population densities on the landscape that emerge from simulations of our model in the absence of control strategies. First, we discuss the number of source trees in a cluster needed for MPB to initiate an epidemic (and conversely the threshold required to reduce to endemic population densities). Second, we discuss the distance needed between source trees for MPB to successfully mass-attack the susceptible landscape. Finally, we discuss the width of trees removed needed for a clearcut to be successful in reducing MPB spread and reproduction.

## 4.2 Mathematical Model

Our model consists of a discrete set of difference equations for the overwintering period (September-June) and a continuous set of reaction-diffusion-chemotaxis equations for the beetle flight, emergence, and attack period (July-August). Existing theoretical and empirical work [RB83, PMW98] informed the selection of parameter values, and the choice of structure for each term in the equations.

We assume that the continuous set of Partial Differential Equations (PDEs) describing the period of flight, emergence, and attack incorporates five variables. These variables are $P$ - the density of flying MPB, $Q$- the density of nesting MPB, $J$ - the density of pre-adult MPB (beetles not yet emerged from the bole of the tree), $A$ - the concentration of beetle pheromone, and $C$ - the concentration of tree kairomones. The set of discrete equations describing the overwintering period incorporates only two variables, $S_t$ - the density of susceptible trees and $L_t$ - the density of overwintering pre-adult beetles. The equations for the summer dispersal are

$$\frac{\partial P}{\partial t} = \overbrace{\mu_p \nabla^2 P}^{diffusion} - \overbrace{\nabla\left[\left(\nu_c \nabla C + \nu_a \frac{b_0 - A}{b_0 + A/b_1}\nabla A\right) P\right]}^{chemotaxis} - \overbrace{\delta_p P}^{death} - \overbrace{g(P,C)S_t}^{nesting} + \overbrace{\gamma(t)J}^{emergence}, \tag{4.1a}$$

$$\frac{\partial Q}{\partial t} = \overbrace{-\delta_q Q}^{death} + \overbrace{g(P,C)S_t}^{new\ nesters}, \tag{4.1b}$$

$$\frac{\partial C}{\partial t} = \overbrace{\mu_c \nabla^2 C}^{diffusion} + \overbrace{a_2 S_t}^{synthesis} - \overbrace{\delta_c C}^{degradation} + \overbrace{\alpha}^{baiting}, \tag{4.1c}$$

$$\frac{\partial A}{\partial t} = \overbrace{\mu_a \nabla^2 A}^{diffusion} + \overbrace{a_1 Q}^{synthesis} - \overbrace{\delta_a A}^{degradation}, \tag{4.1d}$$

$$\frac{\partial J}{\partial t} = \overbrace{-\gamma(t)J}^{emergence}, \tag{4.1e}$$

and the equations for the overwintering stage are

$$L_{t+1} = r_1 Q \left( e^{-r_2\left(\frac{r_3 Q-1}{r_4}\right)^{r_5}} - e^{-r_6\left(\frac{r_3 Q-1}{r_4}\right)^{r_7}} \right), \tag{4.2a}$$

$$S_{t+1} = S_t(1 - \eta \frac{L_{t+1}^2}{L_{t+1}^2 + k_j^2}), \tag{4.2b}$$

where,

$$g(P,C) \quad = \quad \overbrace{\lambda P}^{landing} \overbrace{\frac{P^2}{P^2 + (k_p)^2}}^{mass\ attack}.$$

The functional form of (4.2a) incorporates both competition of larvae for resources and tree defences against MPB. At low densities of nesting MPB, the MPB will not survive as tree defences will overcome the small nesting brood. At high densities of MPB, competition becomes a factor and survival of larvae is decreased due to scarce resources. The maximum reproduction and survival of larvae occurs at medium densities of MPB, large enough to overcome tree defences, but not too large as to compete within the host tree.

The model we choose, represented by the system of equations in (4.1) and (4.2), is fairly complex. We feel this complexity is necessary to incorporate the interactions between MPB, their pheromones, and lodgepole pine trees for a multi-year model. A simpler model may be able to understand parts of this system, but in order to understand the system as a whole, this level of complexity is required. We assume that the initial conditions at the beginning of each summer are $P(\vec{x}, 0) = Q(\vec{x}, 0) = C(\vec{x}, 0) = A(\vec{x}, 0) = 0$ and $J(\vec{x}, 0) = L_t(\vec{x})$. That is, the density of pre-adult beetles in the summer is determined entirely by the density of pre-adult beetles produced from the larvae that survive the previous winter. The model parameters are discussed below.

### 4.2.1 Estimation of parameters

Many of the parameters for the continuous portion of the model (4.1) were estimated by Powell et al [PLB96, BPBL00] by projecting a spatial partial diffential equation model onto the local (single-tree) scale and then utilizing historical MPB data. Most of the parameters for the discrete portion of the model (4.1) are estimated from a study by Raffa and Berryman [RB83].

The remaining unknown parameters are $\gamma$, $k_p$, $k_j$, $r_3$, and $r_4$. We chose the rate of emergence parameter, $\gamma$, such that 99.9% of the emerging MPB leave the host tree after approximately 20 beetle flight hours. This time corresponds to approximately half the beetle flight period. All other parameters were chosen based on the data provided by Raffa and Berryman [RB83]. The parameter $k_p$ is the density of flying MPB required for 50% nesting beetle success. Assuming each female beetle makes a single gallery, we estimate the density of flying MPB required for a 50 percent success of mass attack to be 40 beetles / $m^2$ [RB83]. Since our model uses ha instead of $m^2$ we must multiply this quantity by a conversion factor:

$$B_h = B_m \frac{SA}{TA}, \tag{4.3}$$

where $B_h$ is the number of beetles per hectare, $B_m$ is the number of beetles per $m^2$, $SA$ is the surface area of the tree attacked, and $TA$ is the area within which a beetle is considered to be "attacking" a tree. In the discrete equations (4.2), $r_3$ is defined as the area within the tree that the beetle is attacking and $r_4$ is defined as the surface area of the tree attacked. Thus, $r_3 = TA$ and $r_4 = SA$.

We estimate the surface area as $SA = \pi dh$, where the tree diameter, $d$, can range from 0.1874 m to 0.3456 m and the height $h$ is taken to be 7.5 m [RB83]. Therefore, $SA$ can range from 4.42-8.14 $m^2$. We assume that each tree is centred in a 10 $m^2$ attractive zone. Any beetle flying in that zone will be attracted to and join the attack on the central tree. Thus, $TA = 10 m^2 = 10^{-3}$ ha, which makes $k_p = 176,800 - 325,600$ beetles/ha. We initially assume the intermediate value of $k_p$=250,000.

The parameter $k_j$ is the density of surviving MPB, $L_t$, required for 50% tree mortality to occur. We approximate that the density of pre-adult beetles required for this to occur is 5 beetles/tree. Therefore, using the same estimate of $TA = 10\text{m}^2$, we find $k_j$ is approximately 5000 pre-adult beetles/ha. We choose this small value for $k_j$ since a non-zero density of surviving MPB, $L_t$, is a signal for tree death. In the model, tree resistance to MPB occurs in the summer nesting term (4.1) and in the discrete equation for $L_t$ (4.2).

The dimensional model (4.1) and (4.2) parameter values can be found in Table 4.1 while the non-dimensional model (4.4) can be found in Table 4.2.

### 4.2.2 Non-dimensionalization

We non-dimensionalize the model for ease of mathematical analysis. We choose the following non-dimensionalizations for our variables:

$$\begin{aligned}
\overline{Q} &= \frac{a_1}{b_0\delta_a}Q, \quad \overline{P} = \frac{a_1}{b_0\delta_a}P, \quad \overline{C} = \frac{\nu_c}{\mu_c}C, \\
\overline{S_t} &= \frac{\lambda}{\delta_p}S_t, \quad \overline{A} = \frac{1}{b_0}A, \quad \overline{J} = \frac{a_1}{b_0\delta_a}J, \\
\bar{t} &= \delta_a t, \quad (\overline{x}, \overline{y}) = \sqrt{\frac{\delta_a}{\mu_a}}(x, y).
\end{aligned}$$

By examination of the parameter values in Table 4.1 it can be seen that many parameters differ by orders of magnitude. To identify parameters which are small (act over slow time scales) and large (act over fast time scales) we choose a scaling parameter, $\epsilon$,

$$\epsilon = \frac{\delta_p}{\delta_a}.$$

Using this scaling parameter, we define the dimensionless parameters

$$\begin{aligned}
\overline{\mu_p} &= \frac{\mu_p}{\mu_a}, \quad \overline{\nu_a} = \frac{\nu_a b_0}{\mu_a}, \quad \overline{k_p} = \frac{k_p a_1}{b_0\delta_a}, \\
\overline{\mu_c} &= \frac{\mu_c}{\mu_a}, \quad \epsilon\overline{\lambda} = \frac{\epsilon a_2 \nu_c}{\lambda\mu_c}, \quad \overline{\alpha} = \frac{\nu_c}{\delta_a\mu_c}\alpha,
\end{aligned}$$

Table 4.1: Table of parameter (Par) values for the dimensional model (4.1) and (4.2).

| Par | Description | Units | Value |
|---|---|---|---|
| $\mu_p$ | diffusion of flying MPB | $\frac{ha}{fh}$ | 1 |
| $\mu_c$ | diffusion of host volatiles (kairomones) | $\frac{ha}{fh}$ | 0.648 |
| $\mu_a$ | diffusion of beetle pheromones | $\frac{ha}{fh}$ | 0.648 |
| $\nu_c$ | kairomone attractiveness | $\frac{ha^2}{\mu g * fh}$ | 0.8 |
| $\nu_a$ | beetle pheromone attractiveness | $\frac{ha^2}{\mu g * fh}$ | 5.7 |
| $b_0$ | pheromone dissipation concentration | $\frac{\mu g}{ha}$ | 5.4 |
| $b_1$ | concentration at which pheromone is saturated | $n/a$ | 1 |
| $\lambda$ | random landing rate of flying MPB | $\frac{ha}{trees * fh}$ | 0.16 |
| $k_p$ | flying beetle density required for 50 percent success of mass attack | $\frac{mpb}{ha}$ | 250000 |
| $\delta_p$ | death rate of flying MPB | $fh^{-1}$ | 0.014 |
| $\delta_q$ | death rate of nesting MPB | $fh^{-1}$ | 0.001 |
| $\delta_c$ | degradation of tree kairomones | $fh^{-1}$ | 180 |
| $\delta_a$ | degradation of beetle pheromone | $fh^{-1}$ | 180 |
| $\gamma(t)$ | emergence rate of pre-adult beetles | $fh^{-1}$ | 0.345 |
| $a_1$ | rate of pheromone increase due to nesting MPB | $\frac{\mu g}{fh * mpb}$ | 0.02 |
| $a_2$ | rate of kairomone increase due to susceptible trees | $\frac{\mu g}{fh * trees}$ | 0.02 |
| $r_1$ | production of pre-adult beetles (pupae) from nesting MPB | $n/a$ | 26.3 |
| $r_2$ | density dependent effects of nesting MPB | $\left(\frac{m^2}{mpb}\right)^{r_5}$ | 0.0015 |
| $r_3$ | area surrounding tree where MPB are attacking tree | $ha$ | 0.001 |
| $r_4$ | surface area of tree attacked | $m^2$ | 6 |
| $r_5$ | constant of MPB competition | $n/a$ | 1.5 |
| $r_6$ | success of tree defenses | $\left(\frac{m^2}{mpb}\right)^{r_7}$ | 0.0026 |
| $r_7$ | cooperative effects of MPB | $n/a$ | 1.6 |
| $\eta$ | maximum success of pre-adult beetles | $n/a$ | 1 |
| $k_j$ | pre-adult beetle density required for 50 percent success in overtaking tree | $\frac{mpb}{ha}$ | 5000 |
| $\alpha$ | rate of kairomonne production by traps | $\frac{\mu g}{ha * fh}$ | 1458 |

Table 4.2: Table of parameter values for the non-dimensional model (4.4).

| Parameter | Value |
|---|---|
| $\epsilon$ | 0.0000778 |
| $\overline{\mu_p}$ | 1.54 |
| $\overline{\mu_c}$ | 1 |
| $\overline{\nu_a}$ | 47.5 |
| $\overline{\lambda}$ | 0.154 |
| $\overline{k_p}$ | 5.14 |
| $\overline{\delta_q}$ | 0.0714 |
| $\overline{\delta_c}$ | 1 |
| $\overline{\gamma}$ | 24.6 |
| $\overline{r_3}$ | 48.6 |
| $\overline{k_j}$ | 0.103 |
| $\overline{\alpha}$ | 10 |

$$\overline{\delta_c} = \frac{\delta_c}{\delta_a}, \quad \epsilon\overline{\gamma} = \frac{\gamma}{\delta_a}, \quad \epsilon\overline{\delta_q} = \frac{\delta_q}{\delta_a}.$$

Next, my define scaling factors for the terms in my set of discrete equations,

$$\begin{aligned} S_{t+1} &= \frac{\delta_p}{\lambda}\overline{S_{t+1}}, \quad L_{t+1} = \frac{b_0\delta_a}{a_1}\overline{L_{t+1}}, \\ \overline{r_3} &= \frac{b_0\delta_a}{a_1}r_3, \quad \overline{k_j} = \frac{a_1}{b_0\delta_a}k_j. \end{aligned}$$

Substituting these values into (3.2) we arrive at the non-dimensional model (4.4). The number of parameters was reduced from 25 to 19 during the non-dimensionalization process.

Summer Dispersal:

$$\begin{aligned} \frac{\partial\overline{P}}{\partial\overline{t}} =& \overline{\mu_p}\overline{\nabla}^2\overline{P} - \overline{\mu_c}\overline{\nabla}(\overline{P\nabla C}) - \overline{\nu_a}\overline{\nabla}\left(\frac{1-\overline{A}}{1+\overline{A}/b_1}\overline{P\nabla A}\right) \\ & - \epsilon\overline{P} - \epsilon\frac{\overline{P}^3}{\overline{P}^2+\overline{k_p}^2}\overline{S_t} + \epsilon\overline{\gamma}\overline{J}, \end{aligned} \tag{4.4a}$$

$$\frac{\partial \overline{Q}}{\partial \overline{t}} = -\epsilon\overline{\delta_q Q} + \epsilon\frac{\overline{P}^3}{\overline{P}^2 + \overline{k_p}^2}\overline{S_t}, \tag{4.4b}$$

$$\frac{\partial \overline{C}}{\partial \overline{t}} = \overline{\mu_c}\overline{\nabla}^2\overline{C} + \epsilon\overline{\lambda S_t} - \overline{\delta_c C} + \overline{\alpha}, \tag{4.4c}$$

$$\frac{\partial \overline{A}}{\partial \overline{t}} = \overline{\nabla}^2\overline{A} + \overline{Q} - \overline{A}, \tag{4.4d}$$

$$\frac{\partial \overline{J}}{\partial \overline{t}} = -\epsilon\overline{\gamma}\overline{J}. \tag{4.4e}$$

Overwintering:

$$\overline{L_{t+1}} = r_1\overline{Q}\left(e^{-r_2\left(\frac{\overline{r_3 Q}-1}{r_4}\right)^{r_5}} - e^{-r_6\left(\frac{\overline{r_3 Q}-1}{r_4}\right)^{r_7}}\right), \tag{4.4f}$$

$$\overline{S_{t+1}} = \overline{S_t}(1 - \eta\frac{\overline{L_{t+1}}^2}{\overline{L_{t+1}}^2 + \overline{k_j}^2}). \tag{4.4g}$$

Our mathematical model was simulated using Fortran with the numerical scheme as described in Chapter 3.

## 4.3 Effects of Management

Our study is motivated by questions regarding the impacts of MPB management activities, with specific focus on the management activities carried out in Banff National Park in Alberta, Canada. We carried out several different studies to investigate the effects of baiting and tree removal (Section 4.3.1), and clearcutting and prescribed burning (Section 4.3.2). Our study of baiting and tree removal focuses on simulations with three (Section 4.3.1) and five source trees (Section 4.3.1). Other source tree densities were tested, though the results displayed are sufficient to explain the trends for baiting and tree removal.

### 4.3.1 Baiting and Tree Removal

An initial study of the effects of pheromone baiting and tree removal found unexpected differences in MPB attack between the management and

monitoring zones in Banff. It was found that the impact (area of trees consumed) of the beetles in the two zones was the same, though management did slow the spatial spread of the beetle [TR08]. Figure 4.1 shows an illustration of both patterns of attack. In both cases, beetles emerged from a source at the centre of the grid, and the number of grid cells attacked by MPB is the same. The main difference between the two zones is the distance of beetle spread (distance from the attacked cells to the centre of the grid). A confounding factor in the study was that the management area contained susceptible habitat of higher quality (higher MPB reproductive success) than the monitoring zone. The results also led us to ask if there might be a situation in which it would be better to only do removal of green-attack trees without the baiting component. Indeed, while Parks Canada used the baiting and tree removal (in Banff), elsewhere in the province the Alberta Environmental and Sustainable Resource Development (ESRD) used solely tree removal with no baiting component. The motivation for using pheromone baiting is that it concentrates the MPB attack to a known local area, so that the management knows where to search, whereas without pheromone baiting the attacked trees are harder to find.

**Three source tree simulations**

To elucidate the effects of tree baiting and removal we set up a 1-dimensional simulation with three source trees that were attacked in the previous year. Neighbouring source trees are placed a constant distance $d_s$, apart from the central source tree. This landscape is depicted in Figure 4.2. The simulation included a single bait location, which produced pheromone during the first year of study. At the end of the summer dispersal season, once MPB had settled inside new hosts, a search radius, $r_{search}$, around the bait trap was searched. A proportion, $p$, of MPB and susceptible trees were removed from this search radius based on the search success. The removal of trees and MPB occured only if the MPB density reached a threshold. Below this threshold, it was assumed that the tree could successfully defend the low density of MPB and thus the tree was not attacked at sufficiently high

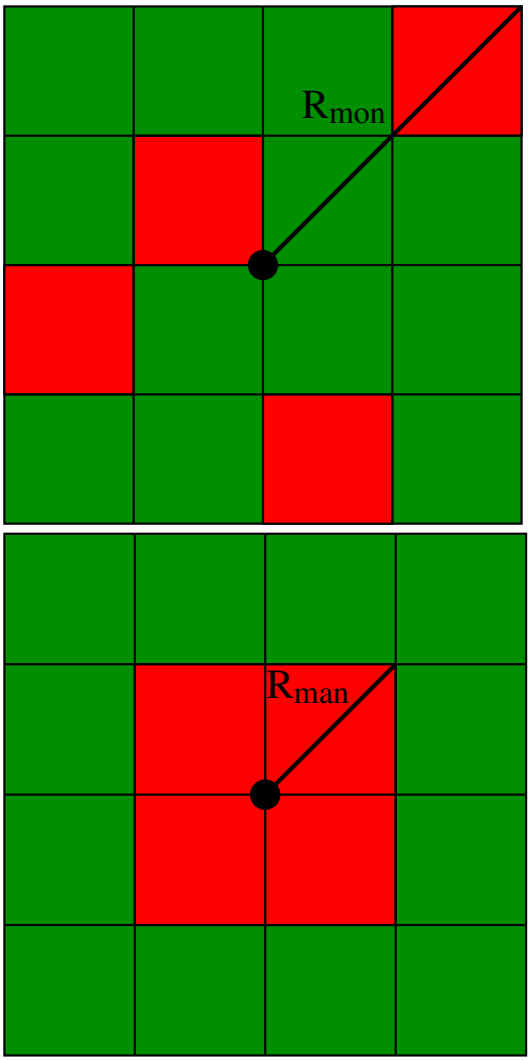


Figure 4.1: Simple grid representations of the monitoring (top) and management (bottom) zones. Areas consumed by the beetles are shown in red, while areas of unattacked forest are shown in green. $R$ is the radius from the central emergence region to the farthest attacked stand; with the subscripts "man" referring to the management zone and "mon" referring to the monitoring zone.

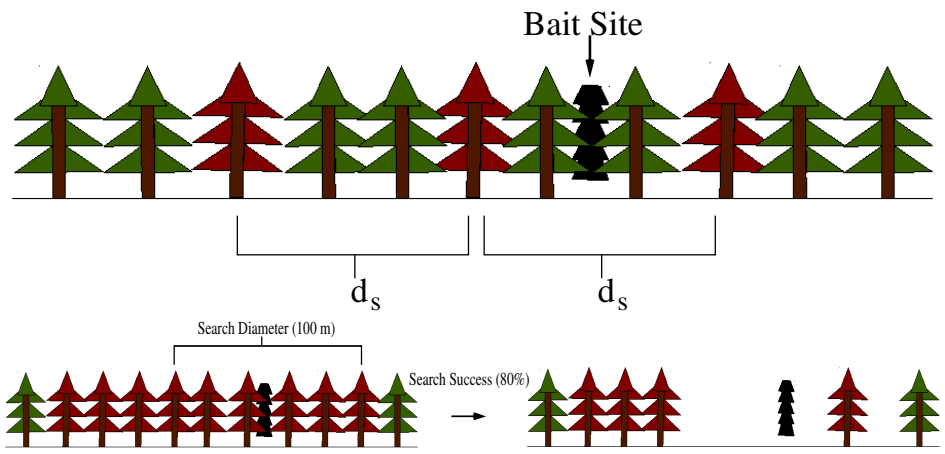


Figure 4.2: Simulation initial conditions are shown in the top figure. There are three source trees, separated by distance, $d_s$, with a bait site to the right of the center source tree. Once the summer dispersal season is over, trees that are attacked are shown in red. Management searches a radius around the bait site (in this example 50 m) and removes attacked trees and MPB with some success rate (80% in picture).

densities and consequently, was not removed.

The simulation was run for two years, starting with emergence and dispersal in the first summer, and with baiting and/or tree removal only occuring in the first summer and fall. We need only to simulate two years, as this is sufficient to illustrate the effects of management. Simulations over 3 or more years did not yield novel results which the 2 year process could not explain. We investigated three separate management scenarios: no management (monitoring/control), baiting only, and baiting with tree removal. Running the control case was important for determining the effects of the management activity, and baiting only was investigated to determine the effects of removal after baiting. These three types of management led to the results shown in Figures 4.3 and 4.4.

The density of nesting MPB at the end of each summer dispersal period in years 1 and 2 is shown in Figure 4.3. Within each plot, results are shown for three inter-source tree distances, $d_s$. The control case (no management)

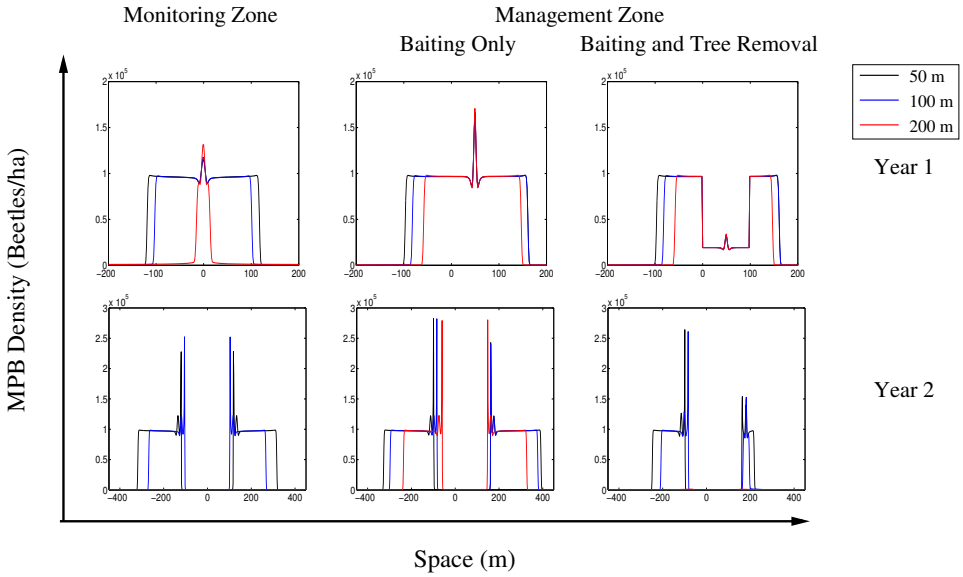


Figure 4.3: Plots of nesting MPB density over space at the end of each year for two years. Simulations are shown in the monitoring zone (no management, left), and with the management activities of baiting only (middle), and combined baiting and tree removal (right). Three distances, $d$, between source trees are shown; 50, 100, and 200 m. The top panel shows nesting MPB densities at the end of the first summer, while the bottom panel shows nesting MPB densities at the end of the second summer.

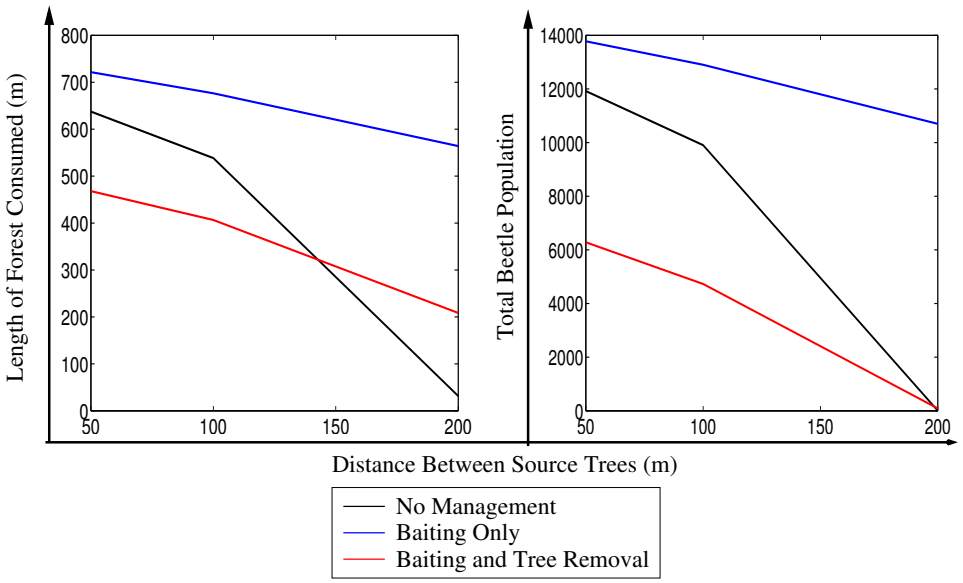


Figure 4.4: Length of forest consumed (left) and MPB population size (right) are shown for different distances between source trees. The three curves represent the impact of MPB with no managment (black), baiting only (blue), and combined baiting with tree removal (red). Simulations were run for two years to obtain these densities and length of forest impact.

is shown in the left panel. As $d_s$ is increased, it is harder for MPB to aggregate in sufficient numbers to launch a mass-attack on the trees. Note that spreading source trees farther apart also simulates lower landscape-level population densities of MPB. In the case where source trees are too far apart, the MPB will successfully nest in the first year, but will not produce enough offspring for successful mass attack and nesting in the second year. Thus, there is an MPB population density below (or $d_s$ above) which the beetle population dies out. This situation does not occur however, for baiting only (middle panel, Figure 4.3) for the $d_s$ simulated. There is still some minimum population threshold for the baiting only case, but it is not reached for the $d_s$ simulated. Baiting focusses MPB aggregation on the bait site, increasing the success of MPB at the initial aggregation stage. Consequently, the spread and impact of a given MPB population is increased in the presence of baiting. The effect of tree removal combined with baiting are shown in Figure 4.3 (right panel). The combined approach is effective at reducing the population of MPB below the levels seen with monitoring only.

A summary of the impact and extent of the MPB infestation after two years is shown in Figure 4.4. These plots show the total MPB population and total susceptible landscape affected by the end of the second year. Not suprisingly, baiting only is the worst management option, as it improves the success of initial MPB aggregation, and so the length of forest consumed and population size of MPB at the end of the second year is largest. Baiting in combination with tree removal yields the lowest population of nesting MPB remaining. This result gives support to baiting with removal as a management tool for reducing the density of MPB. In contrast, the initial success of the MPB aggregation with baiting allows the MPB population to successfully attack a larger portion of the landscape than it would have attacked in the control case. The impact of MPB on the landscape is thus higher with baiting and tree removal when the initial MPB source trees are positioned far apart (akin to a low MPB population density).

These simulations were run assuming a constant search radius of 50 m and a search success of 80%. We then repeated the numerical experiment with a search radius ranging from 25-150 m, and search success ranging

from 0.2-1.0. A search success of 1.0 represents the case where all green-attack trees in the search area are successfully found and removed. Our results are displayed in Figure 4.5. As search success or search radius increases, the density of nesting MPB after the second year decreases. These are both intuitive results. In addition we can use our simulations to determine whether it is better to search in a small area with high success or in a large area with low success. According to our results, it appears that increasing search radius is more important than increasing search success. In our graphs, when we increased the search radius to 100 m or more, only the lowest search success (0.2) had MPB after the second year. We suggest that increasing search radius is more important than increasing search success since increasing search radius will dilute the overall density of MPB emerging the following year. If the MPB population is sufficiently reduced and spread out over an area, it is more difficult for the MPB population to successfully aggregate and mass attack susceptible trees.

**Five source tree simulations**

To examine the effect of adding more source trees to the landscape, we increased the number of source trees in our simulation from three to five. For our five tree simulations, we simulated four management activities. Baiting with tree removal, baiting only, tree removal only, and control (no management). Tree removal uses the same conditions (search area, search success, and removal threshold) as combined baiting and tree removal, but has no baiting component during the flight period. We had 5 initial source trees equally spaced over the susceptible landscape, and increased the inter-source tree distance, $d_s$. As we increase $d_s$ we find that the length of forest consumed and the total population of nesting MPB in the second year decreases, which is consistent with our three-tree simulations. We display the 5-tree results in Figure 4.6.

In these simulations we additionally vary the initial population density in the source trees to test the effect of initial population size. We find that the results are very different as we change the source tree MPB densities.

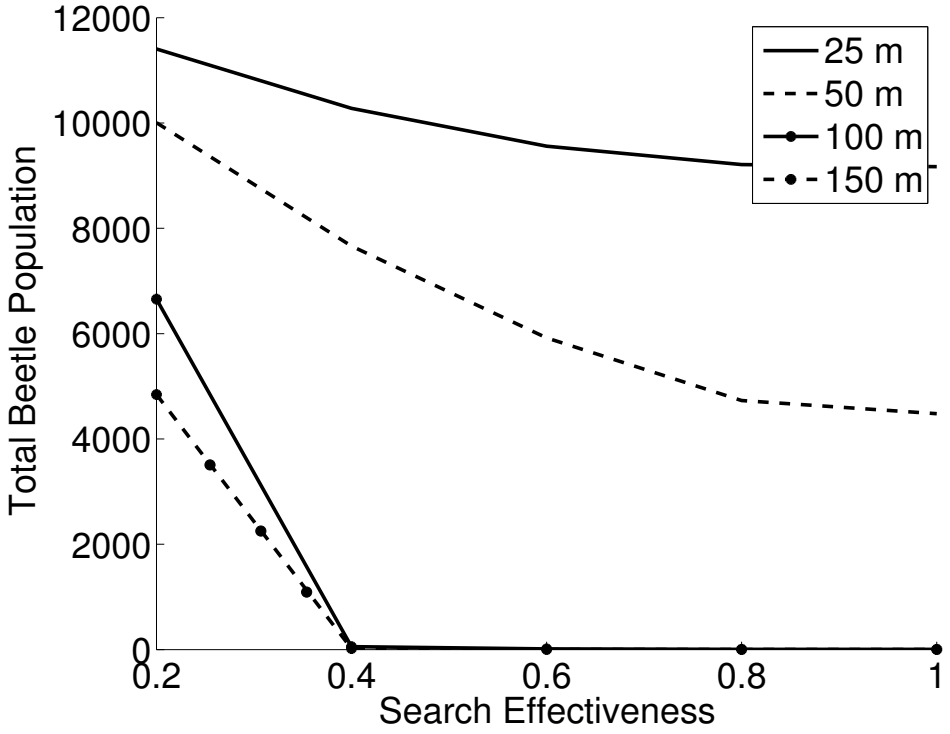


Figure 4.5: MPB population sizes with varying search width and search effectiveness. Search widths shown in this simulation are 25, 50, 100, and 150 m. Search effectiveness values were 0.2, 0.4, 0.6, 0.8, and 1.0. A search effectiveness of 1.0 designates that 100% of the attacked trees in the neighbourhood of the bait tree are found and removed

At high densities, the relative impact of each management activity does not change with variations in $d_s$ tested. For both length of forest consumed and total MPB population after the second year, the best management activity is tree removal only, followed by baiting and tree removal, then control, and finally baiting only. For all inter-source tree distances, $d_s$, tested, there were always MPB remaining after the second year. If we assume however, that the source trees had an even smaller initial population density, we find that populations will not survive to the end of the second year for some distances between source trees, and the trends in MPB population size and the length of forest consumed are different.

From the point of view of MPB population size after the second year, the management strategies rank (in ascending population size) as tree removal only, baiting and tree removal, monitoring only, then baiting only for low distances between source trees (Figure 4.6, top panel). As the spatial difference between source trees increases, there is a switch and more MPB may result after utilizing baiting and tree removal approach than with monitoring only. The same trend that is observed in length of forest consumed.

The result that monitoring alone will produce a lower number of MPB and a smaller length of forest consumed than baiting and tree removal at low initial MPB densities (source trees spaced far apart) is due to the enhanced initial aggregation and increased success of MPB due to the baiting component of management. These results are consistent with the three tree simulations: Baiting and tree removal is a successful management strategy unless MPB population density is low.

If the same simulations are run with management efforts occuring in both years (Figure 4.7), and compared with the single year of management scenarios (Figure 4.6) the results are intuitively expected. Tree removal only over both years reduces the impact of MPB even further, regardless of spacing between source trees, whereas the effects of a second year of baiting and tree removal are dependent on the source tree spacing. If the source trees are close together (MPB density is high), baiting and tree removal over consecutive years reduces the impact of MPB (length of forest consumed and MPB population survived) below that experienced with a single year of

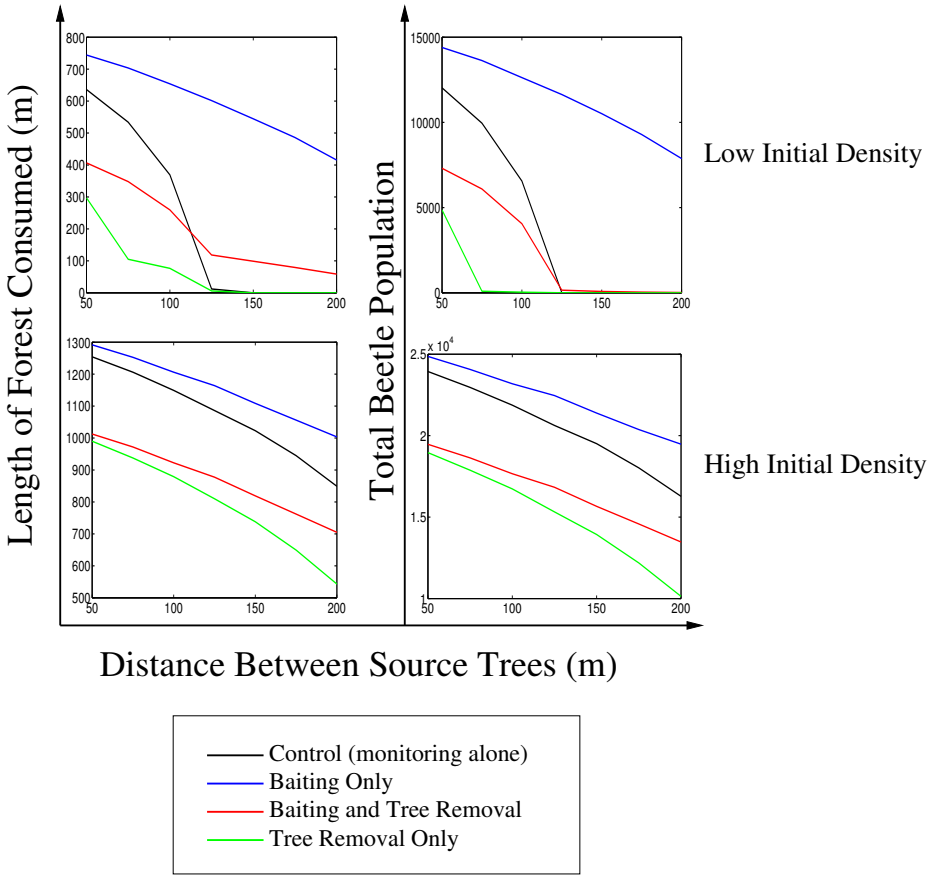


Figure 4.6: Length of forest consumed (left) and total MPB population (right) with different management types as the distance between source trees is increased. The simulation results are shown after a two year simulation initiated with 5 source trees. The four management types tested are control (no management), baiting only, tree removal only, and combined baiting and tree removal.

management. As expected, when the population density is low/source trees are far apart, baiting and tree removal over multiple years increases the impact of MPB when compared to a single year of management activities. Thus, larger MPB densities and larger forest consumption will result from consecutive management activities of baiting and tree removal, if performed at low MPB densities. Comparing the results of baiting only, we find that consecutive baiting will increase the impact of MPB when source trees are farther apart. The difference between single-year and consecutive baiting only at small source tree distances is not significant.

**Management implications: Baiting and Tree Removal**

At a first glance our results indicate that tree removal only is a better strategy than baiting combined with tree removal. This is conditional on removing MPB in the correct location. In the simulations we assumed that the tree removal only occured in the same spot as the tree removal in the baiting only case. That is, we removed trees in an area which was rich in MPB and therefore had a large impact on the spread of MPB. If we had searched in the wrong area, and removed a smaller proportion of the MPB on the landscape, then the predicted output would be the same as in the control case. Therefore, the success of tree removal only as a strategy may vary between the curve for tree removal only and the control curve based on the choice of search location. The advantage of baiting is that the MPB are drawn to a known site, and attacked trees are easier to find.

The danger of using baiting is that if the MPB population is low or source trees are spread far apart, baiting will allow the MPB to aggregate and survive where they would not have naturally been able to do so. In this case, baiting will increase the impact of MPB on the susceptible landscape. This effect of baiting was not well understood in past studies.

The motivation for this study came fron the differences observed in MPB spread between the management and monitoring zones. The management zone had the same area affected as the monitoring zone, but the long-distance spread was lower. Based on the results of our simulations, we

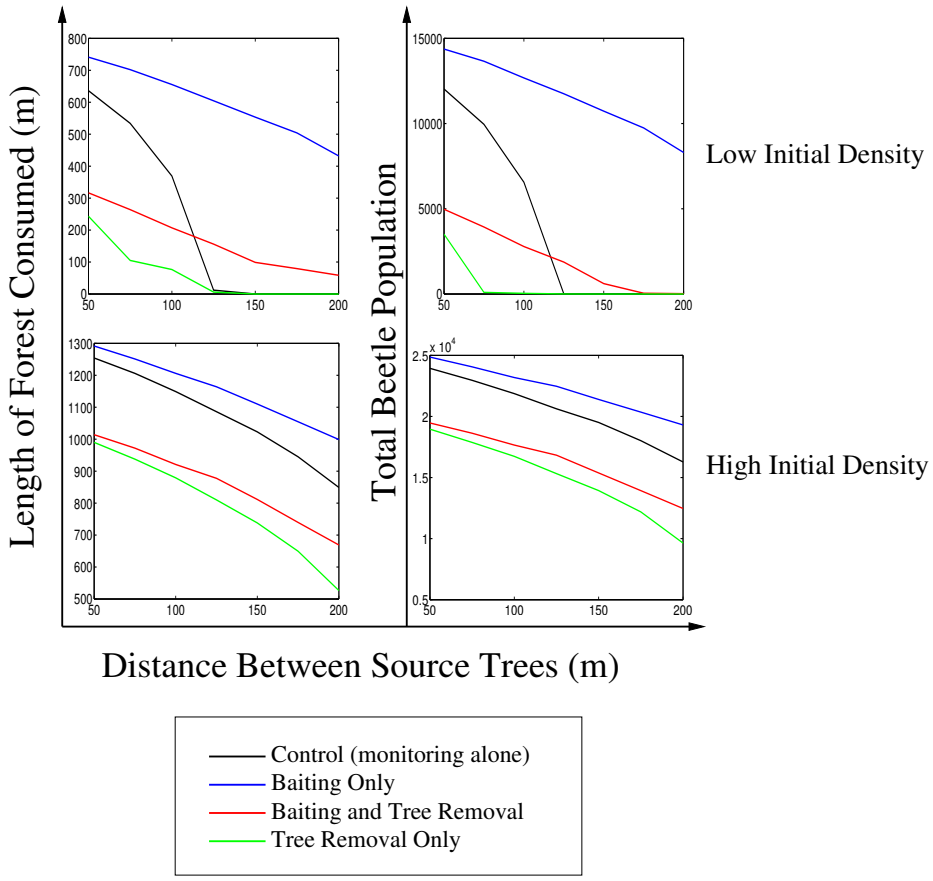


Figure 4.7: Length of forest consumed (left) and total MPB population (right) with different management types as the distance between source trees is increased. The simulation results are shown after a two year simulation where management occurs over both years, with 5 source trees initially. The four management types tested are control (no management), baiting only, tree removal only, and combined baiting and tree removal.

believe this could have occured because of the interaction of attraction to bait site, removal of trees, and increased MPB aggregation success. First, the baiting in each year concentrates the MPB movement, thus increasing the density and success of MPB in attacking susceptible trees on the landscape. After removal of green-attack trees, any MPB missed would produce the following year's MPB population. These new MPB would be at a lower density than in the monitoring zone (due to removal) and would be attracted to the new pheromone baits, both of which would reduce long-distance spread. The local impact in the management zone, however, would be larger since baiting increases the success of MPB in attacking susceptible trees. Thus, this yearly pattern of bait and removal over the landscape would result in a more concentrated spread (less long-distance spread) of MPB, which was exactly the difference observed between the management and monitoring zones in Banff National Park.

### 4.3.2 Prescribed Burning

The next management activity we tested was prescribed burning. In high-intensity fires, prescribed burning reduces the amount of susceptible lodgepole pine available for the MPB and introduces unsuitable habitat between patches of susceptible landscape. Low-intensity fires have been hypothesized to introduce more competition for reproduction, and trees in these areas may be more attractive to MPB (*Mary Reid, personal communication*). More competition through reproduction may occur through other species attacking and reproducing within the same host tree, such as pine engravers. This can occur since partially damaged trees may become suitable hosts for these other forest pests due to the damage induced by the fire. The reason that trees may be more attractive to MPB is not yet fully understood. In this section we investigate how these two factors change the spread of MPB over the landscape.

We simulated four cases: Control (No change between unburned and partially damaged trees), higher attraction to partially damaged trees (attractive), lower reproduction in partially damaged trees (low growth), and

a combination of lower reproduction and higher attractiveness of partially damaged trees (attractive low growth). We chose a symmetric 1-dimensional landscape that was burned (scorched) in the centre, then partially burned (damaged) outside of that, and finally was surrounded by undamaged susceptible landscape. There were therefore 5 patches, all of the same size, in the order undamaged, partially damaged, scorched, partially damaged, undamaged. Each patch was chosen to be 100 m across, and the simulation setup is displayed in Figure 4.8.

Studies of real landscapes do not yet provide sufficient information for us to select a single initial condition as most realistic. Therefore, we simulate three initial MPB distributions, with MPB emerging from focal habitat, damaged habitat, or matrix habitat. The MPB will emerge in: (1) The left undamaged patch (0-100 m), (2) the left partially damaged patch (100-200 m), and (3) the scorched patch (200-300 m). We use initial distributions of MPB on the only one side (left) of the landscape to test scenarios of MPB invading a landscape, and examining how MPB movement will respond to fragemented habitat that has been burned or clearcut. We chose MPB to start in each type of landscape (scorched, partially damaged, and undamaged) to examine the nesting and movement behaviour under our four different assumptions. We also test initial densities of MPB between 31,250 MPB/ha and 250,000 MPB/ha. This corresponds to the output of approximately 3-25 source trees per hectare, assuming 10,000 MPB/tree per flight season [PB09].

A summary of the fraction of susceptible forest consumed (m) against the source tree density (per ha) is shown in Figure 4.9. More detailed outputs of the density of nesting MPB at the end of each year for the three initial conditions and different assumptions on the attraction and reproduction of partially damaged trees is found in Appendix B in Figures B.1, B.2, and B.3 .

A number of patterns emerge from the output of Figure 4.9. The initial MPB density is very important, as the proportion of trees in the landscape killed by MPB increases at different rates with initial population size. In all four assumptions on growth and attractiveness, the fastest increase in

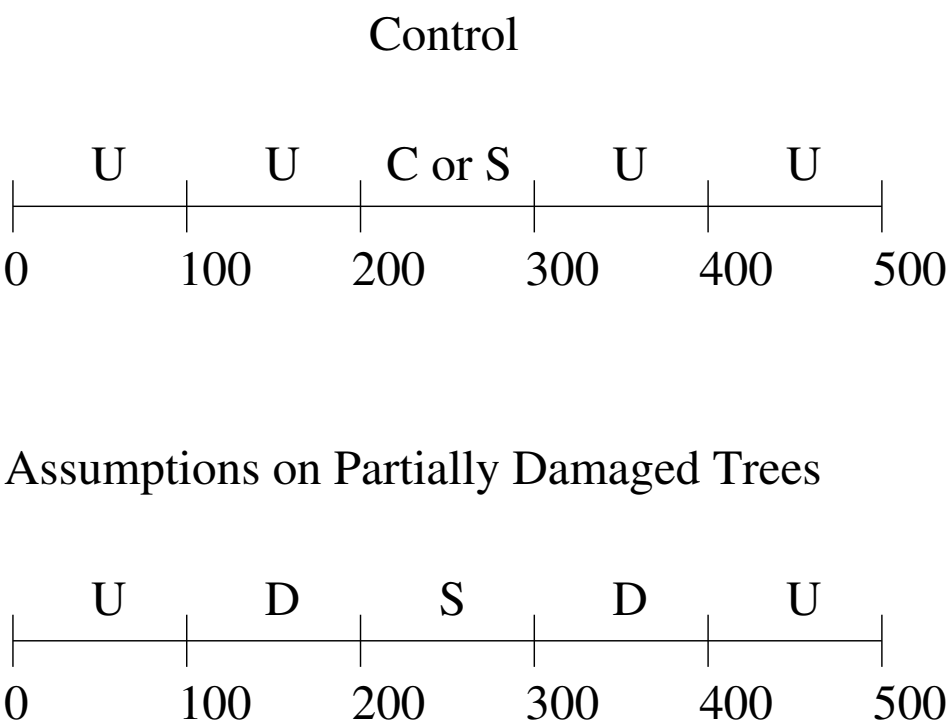


Figure 4.8: Simulation setup for prescribed burn. "U" represents undamaged stands, "D" represents partially damaged stands, "C" represents clearcut stands, and "S" denotes scorched stands. In the control situation (top), no additional assumptions are made upon the partially damaged stands, so they act as essentially the same as undamaged stands. Since there is no partially burned trees the centre can be thought of as essentially a clearcut region in an undamaged forest (or a scorched region with no difference between "D" and "U" from the MPB perspective). When additional assumptions on the growth or attractiveness of partially damaged trees are made (bottom), the undamaged stands differ from partially damaged stands, thus the stands around the scorched region, "S", have been designated as partially damaged, "D". Each type of stand is chosen to be 100 m, with a total domain size of 500 m.

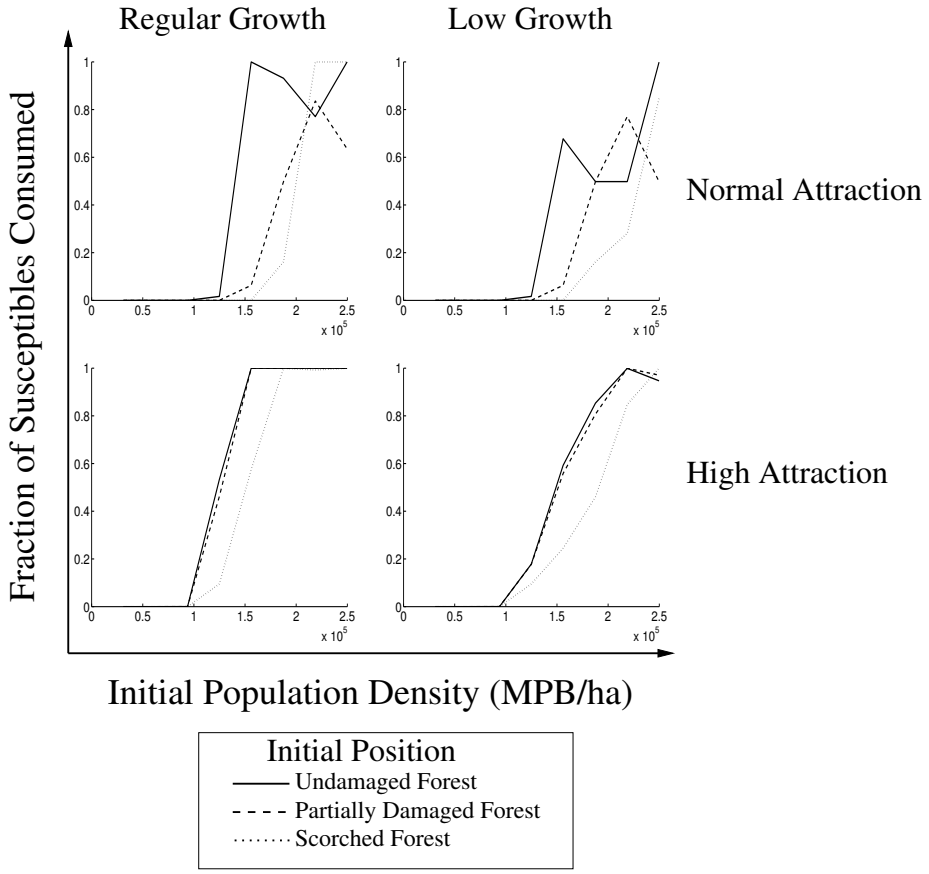


Figure 4.9: Fraction of susceptible trees attacked in regions that have been burned by a prescribed fire. The values vary with the initial source tree density during emergence in the first year. Simulations were run for three years. MPB emergence either occured in the left undamaged forest, in the partially damaged region, or in the scorched region. 2 different parameters were varied in the simulation, attractiveness and growth of partially burned trees. The simulations were run with normal or low reproduction and normal or high attractiveness in partially burned trees.

proportion of susceptible landscape killed occured when the MPB emerged from the undamaged forest only. This is due to fact that susceptible trees are very easy to locate if MPB begin in the undamaged forest only. This rate was reduced if the MPB emerged in the damaged forest only, and was minimum if the MPB were initially distributed in the scorched forest only. At first glance, this result is suprising since in the control case there is no difference between the MPB growth or attractiveness in the damaged and undamaged forest, and thus both patches could be thought of as undamaged forest, as displayed in Figure 4.8. The reason that MPB emerging from the undamaged forest lead to a higher proportion of landscape killed is due to the progression of MPB population spread. In the control case, if the MPB emerge from the undamaged region, they first nest in this region. In the subsequent year, they nest in the partially damaged region, and then in the third year they may successfully cross the gap of scorched forest to nest in the right damaged and undamaged landscapes. Note that this trend depends upon the population size, as low initial populations may not successfully survive to year 2 or 3 and high initial population sizes may cross the scorched forest in year 2. If, on the other hand, the MPB in the control case, emerge from the damaged region, they first nest in this region. The next year, spread occurs primarily to the left into the undamaged region, instead of spreading across the scorched region to the damaged and undamaged forests on the right. This leftward spread makes it more difficult for the MPB to spread across the scorched region in the subsequent year, as the distance to cross now includes the damaged region that was consumed in the first year. So the total dispersal distance becomes 200 m instead of 100 m. It is for this reason that at lower population densities, MPB beginning in the left undamaged forest will be more successful in killing susceptible trees in the right damaged and undamaged forests than the same population beginning in the damaged forest. The final case of the scorched region initial condition is intuitively last since the MPB must disperse from the scorched region to the damaged region before nesting in the first year. This dispersal process results in additional mortality of MPB in the first year, when compared to the other initial conditions. This trend in proportion of trees killed is similar

for the other assumptions on reproduction and attraction in the damaged forest.

The second pattern we observe is a decrease in the proportion of forest consumed at higher densities of MPB in some cases. The reason for this decrease is limitation of host trees. As the MPB population spreads between the first and second year the number of susceptible trees available in the second year is reduced by the length of forest consumed in year 1. At high MPB population densities, the MPB consumes a large portion of forest in the first year and in the second year, has less susceptible landscape (to the left of the scorched region) for reproduction. Since the susceptible landscape is smaller, total reproduction of MPB is reduced and there is a lower total impact over the three year period. In other words, higher initial densities of MPB are less successful in crossing the scorched area because the reproductive success in the first year creates strong resource limits in the second year. The property of area limitation is conditional on the size of the scorched region and the size of each patch. If the scorched region was smaller (larger) we would expect smaller (larger) area limitation effects on the spread of MPB.

When considering the case of lower growth we observe the intuitive result that the proportion of susceptible trees consumed is smaller than in the control case, with all three initial conditions. If MPB emerge initially in the undamaged region, the lower reproductive success prior to crossing the scorched area, leads to a lower overall impact on the susceptible landscape. Similarily, if MPB emerge from the scorched region, the spread in the second year is heavily affected by the decreased reproductive success in the first year. In contrast, the MPB emerging from the partially damaged region are not as significantly affected as the other two initial conditions. This is because the largest limitation on the spread of MPB, with this initial condition, is the spread in the third year. The reproduction prior to this major dispersal event (between years 2 and 3) occurs in the undamaged forest, so the effects of the assumption of lower growth in the partially damaged forest do not affect the MPB impact with this initial condition as significantly as the MPB impact with the other two initial conditions.

The assumption of higher attractiveness changes the simulations in two important ways. First, the MPB starting in the undamaged forest are attracted to the damaged area, so as the attractiveness of the damaged area increases, the initial conditions of starting in the damaged or undamaged areas become essentially the same. The second major difference is that the higher attractiveness enhances the success of the MPB in crossing the scorched area. Thus, all initial conditions show increased mortality of susceptible trees on the landscape. That is, MPB populations of smaller size are able to persist, and have a larger impact on the susceptible landscape. Additionally, there is no longer a decrease in the proportion of susceptible trees consumed at high MPB densities. Since the scorched area is not as difficult to cross, MPB in this simulation cross the scorched region earlier (in the second year), and thus are not subject to a limiting susceptible tree density. These patterns were not observed in simulations with medium, rather than high, attraction to the partially damaged forest. Therefore, the results in Figure 4.9 are critically dependent on the degree of attraction of the damaged region.

Finally, the combination of high attractiveness and lower reproduction in damaged trees leads to curves of proportion of susceptibles consumed that are intermediate between the curves with high attraction (and normal growth) and low growth (with normal attraction). We predicted that increased attractiveness to the partially damaged area (which yield lower growth) may reduce the susceptible fraction of trees consumed in comparison to the control case. This is true when the MPB emerge initially from the undamaged area. For the other two initial conditions, however, the higher attractiveness of the damaged region (causing populations to successfully cross the scorched area) was a larger factor than the lower reproduction in these regions. Therefore, the fraction of susceptibles consumed when MPB emerge from the scorched or damaged region was larger with high attractiveness and lower growth than in the control case. In addition, the combination of lower growth with high attractiveness allowed for smaller area limitation effects (than in the control case), as the scorched area was easier to cross.

Therefore, in terms of the success of the MPB population, there is a

trade-off between the damaged trees being more attractive and having a lower growth rate. The lower growth rate decreased the MPB population in the following year, but the higher attractiveness allows the beetles to spread further across patches of scorched timber to reach partially burned stands. The balance point is obviously dependent upon the magnitude of increased attractiveness and decreased reproduction. Additionally, if the size of all of the patches is increased, the results will differ slightly because the MPB density required to cross the gap (scorched area) will also increase.

**Management Implications: Prescribed Burning**

Our simulations indicate that lower reproduction of MPB in damaged trees always results in smaller spread MPB and decreased damage to susceptible trees. Additionally, scorched regions of the forest are both unsuitable for reproduction, and a barrier to the spread of MPB due to dispersal limitation and limitation of susceptible host density. Therefore, if MPB do indeed have a lower reproduction in damaged trees, our simulations would support the use of prescribed burning as a management activity.

The control simulations assume that there is no difference between the damaged and undamaged stands. In this case, the scorched area acts the same as a clearcut introduced in the center of a two-patch system (Figure 4.8). As a result, we can compare simulations of clearcutting to prescribed burning by comparing simulations of the control scenario to the other three scenarios.

From Figure 4.9, we can see that if damaged stands have lower MPB reproduction, prescribed burning reduces the impact of MPB more than clearcutting the area equivalent to the scorched area. In contrast, if the damaged trees are more attractive to beetles, the scorched area becomes easier to cross. Therefore, if the damaged area is highly attractive, it may be a better strategy to remove trees through clearcutting instead of using a prescribed burn.

In the case where the damaged region is both attractive and has lower reproduction, the results will be dependent on the magnitude of decreased

reproduction and increased attractiveness. Our results are critically dependent on assuming the partially damaged trees are highly attractive. If the partially damaged trees only have a medium level of attractiveness, no significant changes from the normal levels of attractiveness are observed. We therefore conclude that, if damaged trees are both attractive and have lower reproductive output, and the level attractiveness is not too high, the best management strategy will always be to burn a central patch rather than clearcut the equivalent area to reduce MPB impact.

## 4.4 Characteristics of MPB spread

### 4.4.1 Interaction Between Source Trees

MPB from different source trees interact, so we considered how far away source trees needed to be for MPB from separate source trees to influence one another. We simulated the interaction between source trees using a periodic environment with three source trees, all equidistant from each other. The source tree densities were chosen such that MPB populations would not persist with only a single source tree because of the need to overcome host defences. Thus, the interaction between MPB from different source trees was crucial to the survival and reproduction of the population. We found that if the distance between MPB source trees was greater than or equal to 325 m, the MPB population would not persist (Figure 4.10).

### 4.4.2 Clearcut Length

We were interested in what width of clearcut would be needed for MPB to be unsuccessful in crossing the region. We inserted a clearcut in the middle of the domain and observed the subsequent spread of the MPB population. We compared the source tree density (per hectare) against the clearcut distance needed to prevent MPB spread across the clearcut in one year, as shown in Figure 4.11. The clearcut distance needed increases approximately linearly as the source tree density increases. At 25 source trees per hectare, the minimum clearcut length is 1 km.

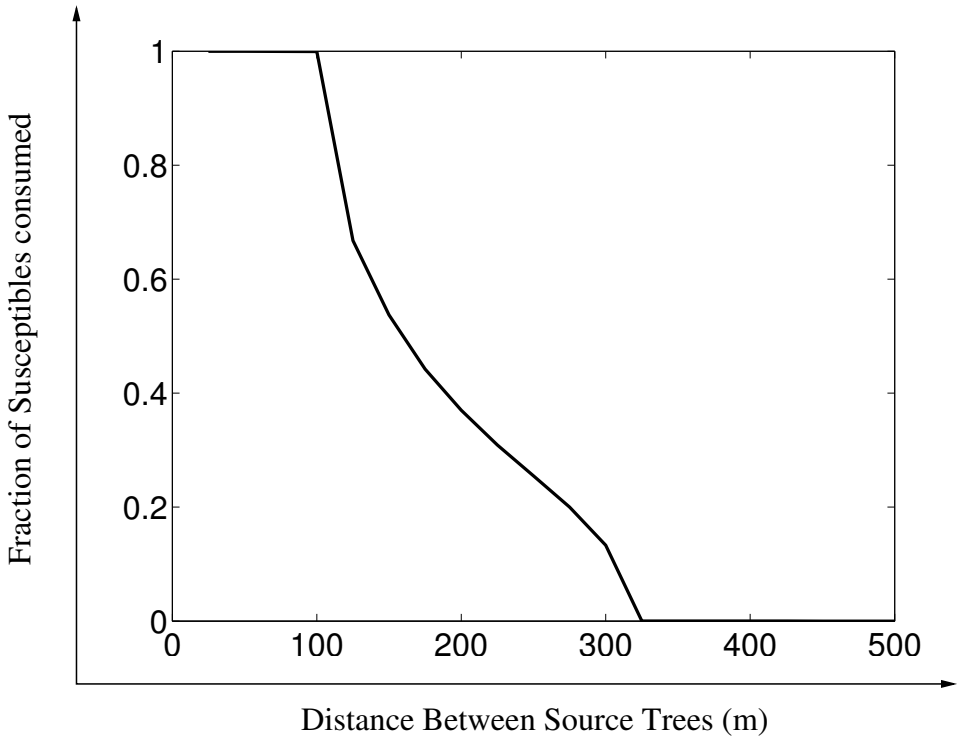


Figure 4.10: Fraction of susceptibles consumed after one year with varying distances between source trees. Trees equidistant over the periodic domain, which is equivalent to an infinite domain with source trees spaced at the distance specified on the $x$-axis.


Figure 4.11: Clearcut distance needed for MPB populations to not successfully cross gap. Densities of source trees is varied between 3 and 25 source trees per hectare.

### 4.4.3 Source Tree Mapping

Using our multi-year model, we simulated source tree density per hectare needed in a cluster of attack for the MPB to overcome the Allee threshold. That is, at low densities, MPB are not able to mass-attack trees, and therefore do not have successful reproduction. At higher densities, the MPB population is able to overcome the Allee threshold, and can grow to epidemic levels [HP08].

To find the Allee threshold, we considered a single group of source trees and simulated subsequent MPB emergence and attack. We mapped the initial source tree density from one year to the next. We considered a domain consisting of uniform susceptible trees and had MPB emerging at the centre of the domain. We ran simulations over a four year period and produced a year-to-year mapping of source tree densities in Figure 4.12. This plot shows that to overcome the Allee effect, there must be approximately 2.3 source trees per hectare. Above this threshold, the source trees grow in density from year to year, while below the threshold the source tree density decreases to 0. Thus, we can predict the source tree threshold at which the MPB population will transition from endemic to epidemic levels. MPB populations may persist at levels below the Allee threshold predicted because of stochastic factors which are not captured by our model framework.

## 4.5 Discussion

With our multi-year spatially explicit mathematical model, we studied the effectiveness of both direct and indirect management strategies. The direct management strategies we investigated were the application of tree removal with and without a trap baiting component. The indirect management strategies considered were clearcutting and prescribed burning.

The direct management strategy of baiting and tree removal was found to always decrease the MPB population density if the initial MPB population density is sufficiently large. At low initial MPB densities, the baiting component increases the success of initial aggregation, leading to a higher density

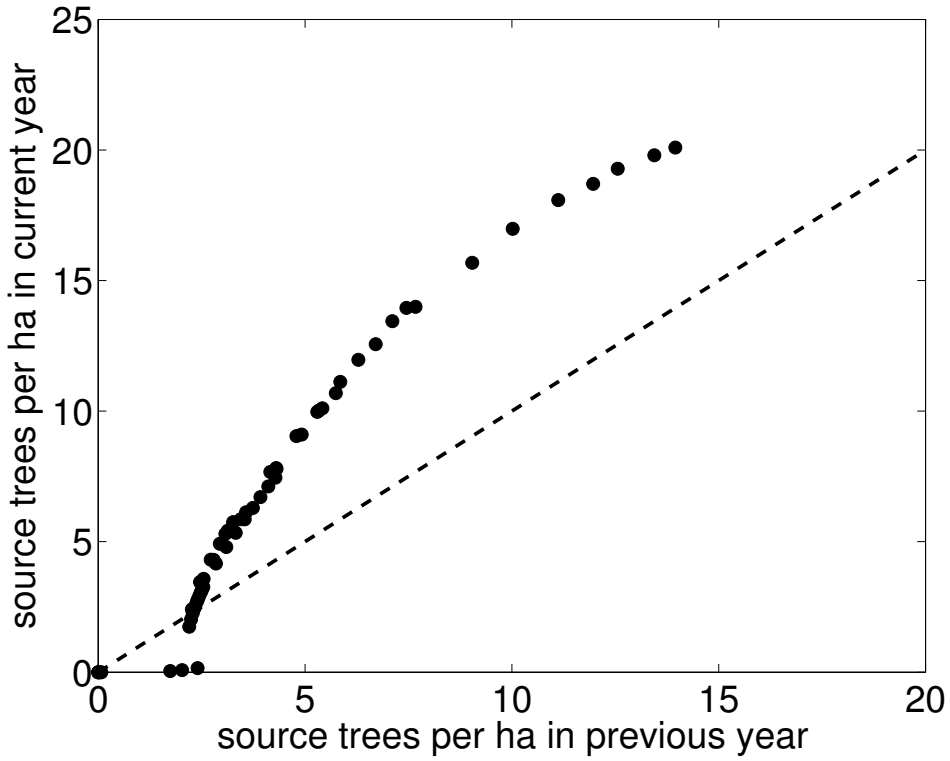


Figure 4.12: Number of source trees per hectare mapped from one year to the next. The identity line indicates points where the source trees mapped from one year to the next are constant. The simulation was run for 4 years to obtain these mapping results.

of nesting MPB and a larger impact on the susceptible landscape. Depending on the success rate in detection (and removal) of attacked trees, the baiting component of this management strategy allows populations of MPB which would otherwise not survive and reproduce to successfully continue spreading in subsequent years. These results suggest that caution should be used in the application of baiting at very low densities of emerging MPB, or when initial source trees are far apart.

We propose that the baiting and tree removal process is what led to the unexpected differences between the patterns of MPB attack in the management and monitoring zones in Banff National Park [TR08]. The management and monitoring zones had equal areas of susceptible landscape killed, but MPB spread in the management zone was less. The mechanism of baiting would have concentrated the MPB attack, thereby reducing long-distance spread, but also leading to higher MPB attack success rates in the local region of the bait. The tree removal component of this strategy likely reduced local MPB population densities each year enough to reduce long-distance spread, but not enough to reverse the epidemic. Thus, this difference in the two zones could be largely attributed to the mechanisms associated with baiting and tree removal. This observation is consistent with the results of Gray and Borden [GB89], who found that baiting and tree removal does slow the spread of MPB, but has the side-effect of concentrating the population.

When comparing the success of tree removal with and without the baiting component, the results depends critically on the success rate of finding high-densities of MPB-attacked trees. In particular, without baiting, the success rate depends on both the choice of search area and the proportion of attacked trees detected in that area. If the tree removal occurs in a region with high attack densities, then tree removal without baiting will always lead to lower MPB population densities and smaller areas of impacted landscape. Green-attack trees can be very difficult to find, however, even if the attack area is generally known (*Mary Reid, personal communication*). There is thus a trade-off between the increased success rate in locating green-attack trees when baiting is used, and the simultaneous increased reproductive success

of the MPB. The threshold MPB density at which the benefits of baiting as a management strategy outweigh the drawbacks depends also on our ability to anticipate the location of MPB attacks when baiting is not used.

When management activities are sustained over multiple years the ultimate effect depends on the initial density of MPB. If the density is high, baiting and tree removal is a more successful strategy when sustained over multiple years. If MPB density is low, baiting and tree removal over multiple years ultimately significantly increases the impact of MPB. Baiting only over multiple years always increases the impact of MPB, whereas tree removal only over multiple years always decreases the impact of MPB.

Direct management strategies employed in the past have met with limited success in supressing the MPB population (See Safranyik and Wilson [SW06] and accompanying references). This was hypothesized to be due to three problems. First, detection of early MPB attack locations and assessment of population growth is difficult. Our simulation results highlight that management strategies are most effective when early MPB locations are known, and that assessment of population size is important for choice of an appropriate management strategy. The second problem is that management efforts were not applied over multiple years. Our simulations show that significant results can be achieved only if management activities continue over multiple years. The final issue with past management strategies is that often only a portion of the affected area was targeted. According to our simulations, the success of baiting and tree removal is very dependent upon the search width, and targeting an area with a radius of 100 m or more of the affected trees is critical. A case study of successful suppression of MPB occured in Banff in the 1940's when all three of these shortcomings were addressed [HM45].

Using the indirect method of clearcutting or burning a portion of the landscape to create a population gap will consistently reduce the spread and population density of MPB. Prescribed burning can be used to create an intensely scorched region in which MPB cannot nest, with a surrounding region of partially burned trees. Which method is optimal depends upon the attraction level of MPB and the reproductive success in trees that have been

partially burned. Further work could be done to investigate how introducing repulsive and attractive pheromones will change these results.

If partially damaged trees lead to lower reproduction but have equal attractiveness to MPB when compared to undamaged trees, than creating a forest gap using prescribed burning is more effective than clearcutting in reducing the population density and impact of MPB. If partially damaged trees are more attractive and have equal reproduction for MPB when compared to undamaged trees, then the MPB population density can be increased by burning, compared to the clearcutting case. This result is due to the increase aggregation successs in partially damaged regions, and the increase in dispersal success of beetles across gaps of scorched trees. If partially damaged trees are both more attractive and have lower reproduction for MPB, the overall result will depend on the relative magnitudes of attractiveness and reproduction. If attractiveness is sufficiently low, burning the region will always result in a lower impact (smaller MPB population density and smaller length of forest consumed) than if the equivalent scorched region had been clearcut.

One counterintuitive result arising from our simulations shows that if undamaged forest is limiting, it is possible for MPB to become cornered there. Consequently, a lower initial population of MPB can spread across a clearcut or scorched region with higher success than a larger initial population of MPB. This pattern results when MPB do not cross the gap and consume too much of the susceptible habitat on one side of the gap. The following year, the population is only able to reproduce in the remaining amount of habitat on the one side. This limited habitat leads to a lower reproduction and thus a smaller overall spread and density. This effect could be enhanced if baiting was done in the small region of undamaged forest, which could severely limit the spread to nearby habitat.

It would be an interesting avenue of future work if management could find a way to use this area-limiting property in an efficient way. For instance, if we know the population level and the position of the MPB population, a burn or clearcut could be made to reduce or stop the MPB spread. Unfortunately, trees do not show the obvious red-top from mortality until after MPB have

emerged from the given tree (position unknown) and population levels of MPB are difficult to determine [SW06]. Thus, this may be very difficult to put into practise. This property, however, may lead to some interesting results where MPB in management zones at lower densities may lead to higher impacts than MPB at higher densities.

When comparing the indirect results of clearcutting and burning we made several assumptions which could be investigated further. First, we assumed that the scorched area (very damaged trees) was unusable by MPB for reproduction and was not attractive to the MPB (*Mary Reid, personal communication*). These assumptions are not currently verified but research is being done to explore these assumptions further. Second, in interpreting the scorched region in the control landscape as equivalent to a clearcut region, we assumed that movement in a clearcut patch would be identical to movement in a scorched region. It is possible however, that diffusion in the two patches is different [Rei09] (Chapter 3). A scorched region still contains the tree trunks necessitating, possibly, more tortuous beetle flight paths [Rei09], and thus a different diffusion speed than in a clearcut. Finally, our simulations assumed that dispersal was identical in the scorched, partially damaged, and undamaged stands (apart from the attractive effects of kairomone and pheromone). In a study by Reid [Rei07], however, it was found that movement may increase in burned regions.

Our simulation results were based on a very synchronous emergence. Other emergence rates and times were tested, and it was found that lower emergence rates led to higher initial source densities needed for the MPB to reproduce. Thus, the population densities reported in this chapter will vary significantly based on the emergence profile of the MPB, which can vary dramatically based on temperature [GPLB04]. Intuitively, lower emergence rates, and less synchronous emergence leads to a lower success in MPB reproduction. Our results can thus be considered worst case scenarios from the point of view of emergence. For more accurate predictions of aggregation, growth and spread rates more realistic emergence functions should be considered [GPLB04, RPBN12]. For an extremely realistic emergence function, age-dependent differential equations could be used to predict emergence

times and densities [CP11].

When we ran multi-year simulations, we were able to map the density of source trees per hectare from one year to the next. We found that the mapping function had an unstable critical point at 2.3 source trees per hectare. Below this threshold, the MPB population decreases to extinction. We interpret "extinction" in this model as endemic infestation. Above the critical threshold, the population grows to epidemic levels. This behaviour is consistent with the result found in Chapter 2 predicting endemic population densities when attack levels are below 0.67 source trees per hectare, and epidemic population densities above 4 source trees per hectare. Incipient epidemic levels, which transition between endemic and epidemic levels, were in between 0.67 and 4 source trees per hectare. A extension of this work could consider the Allee threshold present in the discrete portion of our model and investigate the effects of the aggregation (due to MPB pheromone) on this threshold.

Our simulation model predicts that if source trees are spread more than 325 m apart, there will be no population of MPB the following year, assuming that a single source tree of MPB is not a sufficient density to successfully reproduce to the following year. This result shows an interesting correspondence with previous pattern formation work (Chapter 2). In this work, MPB attack clusters were found to be spaced 353 m on average, which is slightly larger than the 325 m predicted by our model where source trees would have little correspondence. Therefore, this pattern formation wavelength could result from the attack clusters being too far apart to overlap and interact. In other words if source trees are too far apart spot formation may arise with no spread.

Our simulations of MPB population spread in the presence of a clearcut show that a clearcut width of 1 km is sufficient to prevent spread of MPB populations as large as 25 source trees/hectare. We caution, however, that our results are predicated on the assumption that dispersal occurs at the same speed in clearcut and forested regions. Our result is thus only applicable to local MPB dispersal behaviour. It is entirely possible that with increased wind speeds in large clearcut regions, beetles can be carried across

with relative ease, or are more readily lifted into high air currents that carry the beetles long distances over the forest canopy [dCA12]. Our model does not apply to this mode of dispersal and further studies are needed to determine the effectiveness of large clearcuts as barriers to dispersal. Indeed our results in Chapter 3 found that diffusion may be higher in fragmented habitats.

A further extension of our work would be to consider a mix of direct and indirect control strategies [BS03]. We suggest that a successful approach might be to use a prescribed burn to limit MPB spread and growth through the introduction of gaps, and then use baiting and tree removal to severely limit the spread of MPB. The introduction of gaps in the susceptible landscape will limit the spread of MPB, and the baiting and tree removal concentrates, but also further limits the ability of the MPB to cross gaps in the susceptible landscape.

From an economic perspective, our models do not factor in the cost of each management activity. In addition to MPB dispersal studies, optimal control models factoring in the cost of prescribed burning, clearcutting, and baiting and tree removal are needed to determine the most cost-effective combination of strategies.

We note here that burning, clearcutting and targeted tree removal all engender changes to the landscape that are irreversible on a short timescale (decades), and can also be very costly. Simulation approaches like ours can be used to predic the influence of both direct and indirect management strategies. We have been able to successfully explain the non-intuitive MPB spread rates and patterns in response to management activities in Banff NP, and thus provide an informative context for future management decisions. More modelling efforts of this sort are needed, so that we can minimize the use of destructive management tactics, especially as the MPB epidemic continues and spreads into the boreal forest [dCA12].

# Chapter 5

# Conclusion

The ultimate goal of this body of work was to understand the dispersal and attack patterns of the MPB under the influence of management activities. We have succesfully accomplished this goal on the stand spatial scale (1 ha to 1 $km^2$) through the three projects described in this thesis. All of these projects use a original spatially explicit mathematical model which has been developed based on the existing theoretical and empirical work [WP97, RB83].

In Chapter 2, we used our model framework to predict the spacing between MPB attack clusters at incipient epidemic densities. We used MPB attack data from the Sawtooth National Recreation Area to verify our theoretical predictions, providing strong support for our modelling approach. This gave us possible insight into source tree densities at which MPB transition population levels from endemic to epidemic.

A key aspect of MPB dispersal dynamics is movement through fragmented habitats. We thus considered small-scale regions to develop a detailed understanding of movement across heterogeneous regions. This approach led us to the combination of experimental and theoretical work found in Chapter 3. The dispersal behaviour of the MPB through fragmented habitats is largely unknown [BAL93], and therefore our work testing different hypotheses on MPB movement in various habitats is crucial. We were able to link theoretical and experimental predictions to select the most likely mechanisms of movement of MPB in fragmented landscapes.

The culmination of this work appears in Chapter 4 where we investigated the impacts of various direct and indirect management activities on the spread and impact of the MPB. We determined what is the optimal direct management strategy as a function of MPB population density and the

success in detection (and removal) of green-attack trees. We furthermore determined that the best choice of indirect management strategy changes based on the assumptions made regarding the reproduction (of MPB) and attractiveness of partially burned trees. This aspect of MPB biology is as yet unknown, but our work shows that it is a critical consideration in MPB management. Finally, our simulation model was able to provide valuable management predictions for the spacing between source trees, clearcut distance needed, and clustered source tree density required to reduce the MPB population density to endemic levels. Our theoretical framework successfully explained the non-intuitive MPB spread rates and patterns observed in response to management activities in Banff National Park, and thus provides an informative context for future management decisions.

The two most important extensions of our model framework are the effect of temperature on the MPB and the variable resistance of host trees.

All stages of the MPB life cycle explicitly depend upon the surrounding temperature [SW06, GPLB04, CP11]. Recent work by Powell et al. [PB09] used a temperature-dependent model to predict population growth based on the ambient temperature. This incorporation of temperature into the emergence dynamics of the MPB would lead to a more accurate prediction of MPB population growth and spread in real landscapes.

In this work, we restricted our attention to landscapes where trees within a patch were all exactly the same in terms of their attractiveness and resistance to MPB. Our only variable quantity was susceptible tree density. However the importance of weakened trees for nucleation of MPB attack is well-recognized in the literature [WP97, NL08]. The successful growth of a MPB population to epidemic levels can begin at these "nurse trees", which are weakened by such factors as drought or lightning strikes. Incorporation of this factor into the model framework could take place by allowing $k_p$ to spatially vary.

In summary, this body of work has led us to new insights into the movement of MPB in fragmented habitats, the patterns of MPB attack, and the effects of direct and indirect management activities on MPB impact and spread. We have been able to provide valuable management predic-

tions, without engaging any costly and irreversible changes to the landscape. More extensive use of modelling efforts akin to our study are needed to inform management decisions in the future, especially as the MPB continue to spread in Alberta [dCA12].

# Bibliography


[BAL93] B.J. Bentz, G.D. Amman, and J.A. Logan. A critical assessment of risk classification systems for the mountain pine beetle. *Forest Ecology and Management*, 61(3/4):349–366, 1993. → pages 4, 33, 67, 109

[BB91] E.O. Budrene and H.C. Berg. Complex patterns formed by motile cells of escherichia-coli. *Nature*, 349(6310):630–633, 1991. → pages 5

[BB95] E.O. Budrene and H.C. Berg. Dynamics of formation of symmetrical patterns by chemotactic bacteria. *Nature*, 376(6535):49–53, 1995. → pages 5

[Ben06] B.J. Bentz. Mountain pine beetle population sampling: inferences from lindgren pheromone traps and tree emergence cages. *Can. J. For. Res.*, 36:351–360, 2006. → pages 66, 67

[BLB+06] H.J. Barclay, C. Li, L. Benson, S. Taylor, and T. Shore. Effects of fire return rates on traversability of lodgepole pine forests for mountain pine beetle and the use of patch metrics to estimate traversability. Natural Resources Canada, 2006. → pages 69

[BPBL00] Z. Biesinger, J. Powell, B. Bentz, and J. Logan. Direct and indirect parametrization of a localized model for the mountain pine beetle-lodgepole pine system. *Ecological Modelling*, 129:273–296, 2000. → pages 9, 37, 49, 67, 73

[BPL96] B.J. Bentz, J.A. Powell, and J.A. Logan. Localized spatial and temporal attack dynamics of the mountain pine beetle in lodge-

pole pine. *Intermountain Research Paper*, 494, 1996. → pages 6, 14

[BS03] J.E. Brooks and J.E. Stone. *Mountain Pine Beetle Symposium : Challenges and Solutions*. Natural Resources Canada, Canadian Forest Service, Pacific Forestry Centre, Victoria, BC, 2003. → pages 6, 108

[BSW84] A.A. Berryman, N.C. Stenseth, and D.J. Wollkind. Metastability of forest ecosystems infested by bark beetles. *Res. Popul. Ecol.*, 26:13–29, 1984. → pages 3

[Bur77] D.G. Burnell. A dispersal-aggregation model for mountain pine beetle in lodgepole pine stands. *Res. Popul. Ecol.*, 19:99–106, 1977. → pages 2, 6

[CC82] S.P. Courtney and S. Courtney. The edgeeffect in butterfly oviposition : causality in anthocharis cardarnines and related species. *Ecological Entomology*, 7:131–137, 1982. → pages 33, 67

[CDO07] D.S. Chapman, C. Dytham, and G.S. Oxford. Landscape and fine-scale movements of a leaf beetle: the importance of boundary behaviour. *Oecologia*, 154(1):55–64, November 2007. → pages 32, 33, 66

[CMM+10] L.R. Carrasco, J.D. Mumford, A. MacLeod, T. Harwood, G. Grabenweger, A.W. Leach, J.D. Knight, and R.H.A. Baker. Unveiling human-assisted dispersal mechanisms in invasive alien insects: Integration of spatial stochastic simulation and phenology models. *Ecological Modelling*, 221:2068–2075, 2010. → pages 30

[CP11] C.A. Cobbold and J.A. Powell. Evolution stabilises the synchronising dynamics of poikilotherm life cycles. *Bull. Math. Biol.*, 73:1052–1081, 2011. → pages 107, 110

[CPB12] B.A. Crabb, J.A. Powell, and B.J. Bentz. Development and assessment of 30-m pine density maps for landscape-level modeling of mountain pine beetle dynamics. *USDA FS Rocky Mountain Research Station Research Note*, 2012. → pages iv, 20

[dCA12] H.-M.C. de la Giroday, A.L. Carroll, and B.H. Aukema. Breach of the northern rocky mountain geoclimatic barrier: initiation of range expansion by the mountain pine beetle. *J. Biogeogr.*, 39:1112–1123, 2012. → pages 65, 108, 111

[ER04] C.M. Elkin and M.L. Reid. Attack and reproductive success of mountain pine beetles (Coleoptera: Scolytidae) in fire-damaged lodgepole pines. *Environ. Entomol.*, 33(4):1070–1080, 2004. → pages 69

[Fah07] L. Fahrig. Non-optimal landscapes animal movement in human-altered landscapes. *Functional Ecology*, 21(6):1003–1015, 2007. → pages 32

[FCC99] W.F. Fagan, R.S. Cantrell, and C. Cosner. How habitat edges change species interactions. *The American Naturalist*, 153(2):165–182, 1999. → pages 32

[GB89] D.R. Gray and J.H. Borden. Containment and concentration of mountain pine beetle (Coleoptera: Scolytidae) infestations with semiochemicals: validation by sampling of baited and surrounding zones. *Journal of Economic Entomology*, 82:1399–1405, 1989. → pages 103

[GGG80] D.R. Geiszler, V.F. Gallucci, and R.I. Gara. Modeling the dynamics of mountain pine beetle aggregation in a lodgepole pine stand. *Oecologia (Berl.)*, 46:244–253, 1980. → pages 2, 6

[GH08] J.G.P Gamarra and F. He. Spatial scaling of mountain pine beetle infestations. *Journal of Animal Ecology*, 77:796–801, 2008. → pages 6

[GPLB04] E. Gilbert, J.A. Powell, J.A. Logan, and B.J. Bentz. Comparison of three models predicting developmental milestones given environmental and individual variation. *Bulletin of Mathematical Biology*, 66:1821–1850, 2004. → pages 2, 29, 37, 106, 110

[GTLS] T. Gauduchon, R.C. Tyson, F. Lutscher, and S. Strohm. The effect of habitat fragmentation on populations with cyclic dynamics and a discontinuous density across patch interfaces. In preparation. → pages 32, 67

[Hae05] J.W. Haefner, editor. *Modeling biological systems*. Springer, New York, NY, 2005. → pages 29, 126

[HC03] K.J. Haynes and J.T. Cronin. Matrix composition affects the spatial ecology of a prairie planthopper. *Ecology*, 84(11):2856–2866, 2003. → pages 32, 33, 66

[HC06] K.J. Haynes and J.T. Cronin. Interpatch movement and edge effects : the role of behavioral responses to the landscape matrix. *Oikos*, 113:43–54, 2006. → pages 32, 33, 66

[HFSL06] J. Hughes, A. Fall, L. Safranyik, and K. Lertzman. Modeling the effect of landscape pattern on mountain pine beetles. Technical Report BC-X-407, Natural Resources Canada, Canadian Forest Service, Pacific Forestry Centre, Victoria, British Columbia, 2006. → pages 3, 6, 12, 53, 64

[HLZ+08] B. H. Aukema, A. L. Carroll, Y. Zheng, J. Zhu, K. F. Raffa, R. D. Moore, K. Stahl, and S. W. Taylor. Movement of outbreak populations of mountain pine beetle: influences of spatiotemporal patterns and climate. *Ecography*, 31:348–358, 2008. → pages 6, 29

[HM45] G.R. Hopping and W.G. Mathers. Observations on outbreaks and control of the mountain pine beetle in the lodgepole pine stands of western Canada. *The Forestry Chronicle*, pages 1–11, June 1945. → pages 104

[HP08] J. Heavilin and J. Powell. A novel method of fitting spatio-temporal models to data, with applications to the dynamics of mountain pine beetles. *Natural Resource Modeling*, 21(4):489–524, 2008. → pages 3, 6, 101

[HP09] T. Hillen and K. Painter. A user's guide to pde models for chemotaxis. *J. Math. Biol.*, 58(1):183–217, 2009. → pages 12

[Hug02] J. Hughes. *Modeling the effect of landscape pattern on mountain pine beetle*. PhD thesis, Simon Fraser University, 2002. → pages 33, 34, 65, 66

[Jon77] R.E. Jones. Movement patterns and egg distribution in cabbage butterflies movement patterns and egg distribution. *Journal of Animal Ecology*, 46(1):195–212, 1977. → pages 33, 67

[LeV97] R.J. LeVeque. Wave propogation algorithms for multidimensional hyperbolic systems. *Journal of Computation Physics*, 131:327–353, 1997. → pages v, 44

[LeV07] R.J. LeVeque. *Finite Difference Methods for Ordinary and Partial Differential Equations*. SIAM, Philadelphia, PA, 2007. → pages 44, 45, 46, 48

[LP00] M.A. Lewis and S. Pacala. Modeling and analysis of stochastic invasion processes. *J. Math. Biol.*, 41:387–429, 2000. → pages 30

[LT96] R.J. LeVeque and R.C. Tyson. Clawpack version 2.0, 1996. → pages v

[LWBP98] J.A. Logan, P. White, B.J. Bentz, and J.A. Powell. Model analysis of spatial patterns in mountain pine beetle outbreaks. *Theoretical Population Biology*, 53:236–255, 1998. → pages 6

[MAD10] S. Matsumura, R. Arlinghaus, and U. Dieckmann. Foraging on spatially distributed resources with sub-optimal movement,

imperfect information, and travelling costs: Departures from the ideal free distribution. *Oikos*, 119:1469–1483, September 2010. → pages 32

[MKW03] C.W. McHugh, T.E. Kolb, and J.L. Wilson. Bark beetle attacks on ponderosa pine following fire in northern Arizona. *Environ. Entomol.*, 32(3):510–522, 2003. → pages 69

[ML] G.A. Maciel and F. Lutscher. How individual movement response to habitat edges affects population persistence and spatial spread. Am. Nat., in press. → pages 67

[MP91] R.G. Mitchell and H.K. Preisler. Analysis of spatial patterns of lodgepole pine attacked by outbreak populations of the mountain pine beetle. *Forest Science*, 37(5):1390–1408, 1991. → pages 6

[MSL+00] R.N. Mack, D. Simberloff, W.M. Lonsdale, Evans H., M. Clout, and F. Bazzaz. Biotic invasions: Causes, epidemiology, consequences, and global control. *Issues in Ecology*, 5:1–20, 2000. → pages 31

[Mur77] S.J. Muraro. Preliminary results of using fire to control mountain pine beetle. Canadian Forestry Service, Pacific Forestry Centre, 1977. → pages 69

[Mur03] J.D. Murray. *Mathematical Biology*. Springer-Verlag, Berlin, Heidelberg, 2003. → pages 5, 12, 13, 30

[NL08] W.A. Nelson and M.A. Lewis. Connecting host physiology to host resistance in the confer-bark beetle system. *Theor Ecol*, 1:163–177, 2008. → pages 110

[NPL+08] W.A. Nelson, A. Potapov, M.A. Lewis, A.E. Hundsdorfer, and F. He. Balancing ecological complexity in predictive models: a reassessment of risk models in the mountain pine beetle system. *Journal of Applied Ecology*, 45:248–257, 2008. → pages 3

[NSS05] R.K. Nagle, E.B. Saff, and A.D. Snider, editors. *Fundamentals of Differential Equations and Boundary Value Problems*. Pearson, Boston, Ma, 2005. → pages 15

[Ova04] O. Ovaskainen. Habitat-specific movement parameters estimated using markrecapture data and a diffusion model. *Ecology*, 85(1):242–257, January 2004. → pages 32

[PB09] J. Powell and B. Bentz. Connecting phenological predictions with population growth rates for mountain pine beetle, an outbreak insect. *Landscape Ecology*, 24:657–672, 2009. → pages 2, 19, 29, 49, 91, 110

[PD11] L. Pérez and S. Dragićević. ForestSimMPB: A swarming intelligence and agent-based modeling approach for mountain pine beetle outbreaks. *Ecological Informatics*, 6:62–72, 2011. → pages 6

[PJLB00] J.A. Powell, J.L. Jenkins, J.A. Logan, and B.J. Bentz. Seasonal temperature alone can synchronize life cycles. *Bulletin of Mathematical Biology*, 62:977–998, 2000. → pages 2

[PKW+00] J. Powell, B. Kennedy, P. White, B. Bentz, J. Logan, and D. Roberts. Mathematical elements of attack risk analysis for mountain pine beetles. *Journal of Theoretical Biology*, 204:601–620, 2000. → pages 1

[PL90] A.D. Polymenopoulos and G. Long. Estimation and evaluation methods for population growth models with spatial diffusion: dynamics of mountain pine beetle. *Ecological Modelling*, 51:97–121, 1990. → pages 3, 6

[PL05] J.A. Powell and J.A. Logan. Insect seasonality - circle map analysis of temperature-driven life cycles. *Theoretical Population Biology*, 67:161–179, 2005. → pages 2, 29

[PLB96] J.A. Powell, J.A. Logan, and B.J. Bentz. Local projections for a global model of mountain pine beetle attacks. *J Theor Biol*, 179(3):243–260, 1996. → pages 73

[PLBW02] M. Peltonen, A.M. Liebhold, O.N. Bjornstad, and D.W. Williams. Spatial synchrony in forest insect outbreaks : Roles of regional stochasticity and dispersal. *Ecology*, 83(11):3120–3129, 2002. → pages 6

[PM10] S Petrovskii and K McKay. Biological invasion and biological control: A case study of the gypsy moth spread. *Aspects of Applied Biology*, 104:37–48, 2010. → pages 30

[PMW98] J.A. Powell, T. Mcmillen, and P. White. Connecting a chemotactic model for mass attack to a rapid integro-difference emulation strategy. *SIAM Journal of Applied Mathematics*, 59(2):547–552, 1998. → pages 3, 6, 7, 8, 40, 71

[RB83] K.F. Raffa and A.A. Berryman. The role of host plant resistance in the colonization behaviour and ecology of bark beetles (Coleoptera: Scolytidae). *Ecological Monographs*, 53(1):27–49, 1983. → pages 8, 9, 37, 71, 73, 109

[RB86] K.F. Raffa and A.A. Berryman. A mechanistic computer model of mountain pine beetle populations interacting with lodgepole pine stands and its implications for forest managers. *Forest Sci.*, 32(3):789–805, 1986. → pages 2

[Rei07] M. Reid. Environmental effects on host selection and dispersal of mountain pine beetle. Natural Resources Canada, 2007. → pages 69, 106

[Rei09] T.G. Reid. Dispersal studies of mountain pine beetles. Master's thesis, University of Calgary, 2009. → pages 34, 43, 66, 67, 106

[RFSS04] W.G. Riel, A. Fall, T.L. Shore, and L. Safranyik. A spatiotemporal simulation of mountain pine beetle impacts on the

landscape. Technical Report BC-X-399, Natural Resources Canada, Canadian Forest Service, Pacific Forestry Centre, Victoria, British Columbia, 2004. → pages 2, 3, 6

[RH98] L.C. Remer and S.B. Heard. Local movement and edge effects on competition and coexistence in ephemeral-patch models. *The American naturalist*, 152(6):896–904, December 1998. → pages 33, 67

[RNJ+09] C. Robertson, T.A. Nelson, D.E. Jelinski, M.A. Wulder, and B. Boots. Spatial-temporal analysis of species range expansion: the case of the mountain pine beetle, Dendroctonus ponderosae. *Journal of Biogeography*, 36(8):1446–1458, 2009. → pages 6

[RPBN12] J. Regniere, J. Powell, B. Bentz, and V. Nealis. Effects of temperature on development, survival and reproduction of insects: experimental design, data analysis and modeling. *J. Insect Physiol.*, 58(5):634–647, 2012. → pages 106

[RWNW] C. Robertson, M.A. Wulder, T.A. Nelson, and J.C. White. The effect of landscape pattern on mountain pine beetle spread. `http://rose.geog.mcgill.ca/ski/system/files/fm/2009/Robertson_abstract.pdf`, Downloaded on March 10, 2013. → pages 33, 34

[SB03] N. Schtickzelle and M. Baguette. Behavioural to habitat patch boundaries responses restrict dispersal and generate emigration-patch area relationships in fragmented landscapes. *Journal of Animal Ecology*, 72(4):533–545, 2003. → pages 32

[SBTR99] L. Safranyik, H. Barclay, A. Thomson, and W.G. Riel. A population dynamics model for the mountain pine beetle, *Dendroctonus Ponderosae* Hopk. (Coleoptera : Scolytidae). Technical Report BC-X-386, Natural Resources Canada, Canadian Forest Service, Pacific Forestry Centre, Victoria, British Columbia, 1999. → pages 2, 6

[SC01] C.B. Shultz and E.E. Crone. Edge-mediated dispersal behavior in a prairie butterfly. *Ecology*, 82(7):1879–1892, 2001. → pages 33, 67

[SG89] A.J. Stock and R.A. Gorley. Observations on a trial of broadcast burning to control an infestation of the mountain pine beetle *Dendroctonus ponderosae*. *The Canadian Entomologist*, pages 521–523, June 1989. → pages 69

[SKT95] N. Shigesada, K. Kawasaki, and Y. Takeda. Modeling stratified diffusion in biological invasions. *The American Naturalist*, 146(2):229–251, 1995. → pages 30

[SL54] D.E. Smith and M.L. Latham. *The geometry of Rene Descartes with a facsimile of the first edition*. Dover Publications, New York, New York, 1954. → pages 17

[SL00] S. Samman and J. Logan. Assessment and response to bark beetle outbreaks in the rock mountain area. Technical Report RMRS-GTR-62, U.S. Department of Agriculture, Forest Service, Rocky Mountain Research Station, Ogden, UT, U.S., 2000. → pages 28

[SLSH01] L. Safranyik, D.A. Linton, T.L. Shore, and B.C. Hawkes. The effects of prescribed burning on mountain pine beetle in lodgepole pine. Technical Report BC-X-391, Natural Resources Canada, Pacific Forestry Centre, Victoria, British Columbia, 2001. → pages 69

[SRT] S. Strohm, M.L. Reid, and R.C. Tyson. Edge effects on mountain pine beetle movement. In preparation. → pages 35

[SS92] T.L. Shore and L. Safranyik. Susceptibility and risk rating systems for the mountain pine beetle in lodgepole pine stands. Technical Report BC-X-336, Forestry Canada, Pacific and Yukon Region, Pacific Forestry Centre, Victoria, British Columbia, 1992. → pages 2

[ST09] S. Strohm and R.C. Tyson. The effect of habitat fragmentation on cyclic population dynamics: A numerical study. *Bulletin of Mathematical Biology*, 71:1323–1348, 2009. → pages 32

[ST12] S. Strohm and R.C. Tyson. The effect of habitat fragmentation on cyclic population dynamics: A reduction to ordinary differential equations. *Theoretical Ecology*, 5(4):495–516, 2012. → pages 32

[SW04] R.L. Schooley and J.A. Wiens. Movements of cactus bugs: Patch transfers, matrix resistance, and edge permeability. *Landscape Ecology*, 19:801–810, October 2004. → pages 32

[SW06] L. Safranyik and B. Wilson, editors. *The Mountain Pine Beetle*. Natural Resources Canada, Canadian Forest Service, Pacific Forestry Center, Victoria, BC, Canada, 2006. → pages 1, 2, 6, 8, 19, 28, 33, 37, 68, 104, 106, 110

[TLM99] R. Tyson, S.R. Lubkin, and J.D. Murray. Model and analysis of chemotactic bacterial patterns in a liquid medium. *Journal of Mathematical Biology*, 38(4):359–375, 1999. → pages 5

[TR08] M.K. Trzcinski and M.L. Reid. Effect of management on the spatial spread of mountain pine beetle (*Dendroctonus ponderosae*) in Banff National Park. *Forest Ecology and Management*, 256:1418–1426, 2008. → pages 68, 69, 78, 103

[TSL00] R. Tyson, L.G. Stern, and R.J. LeVeque. Fractional step methods applied to a chemotaxis model. *Journal of Mathematical Biology*, 41:455–475, 2000. → pages 44, 45

[Tur52] A.M. Turing. The chemical basis of morphogenesis. *Phi. Trans. R. Soc. Lond. B*, 237:37–72, 1952. → pages 5

[Tys96] R.C. Tyson. *Pattern formation by E. coli - Mathematical and numerical investigation of a biological phenomenon*. PhD thesis, University of Washington, 1996. → pages 15, 30, 44, 45

[WP97] P. White and J. Powell. Phase transition from environmental to dynamic determinism in mountain pine beetle attack. *Bulletin of Mathematical Biology*, 59:609–643, 1997. → pages 2, 3, 6, 8, 29, 35, 37, 53, 64, 66, 69, 109, 110

[WSM04] J. Whittington, C.C. St. Clair, and G. Mercer. Path tortuosity and the permeability of roads and trails to wolf movement. *Ecology and Society*, 9(1), 2004. → pages 33, 67

# Appendix

# Appendix A

# FFT Analysis and Parameter Sensitivity

## A.1 FFT analysis of MPB data

An example of the FFT analysis of the data (in 2007) is shown in Figure A.1. The detailed results of the FFT analysis of the data are shown in Figures A.2, A.3, and A.4. Each year the landscape was analyzed for regions of incipient epidemic densities of MPB. The size and number of regions chosen in each year is displayed in Figure A.5.

## A.2 Parameter Sensitivity

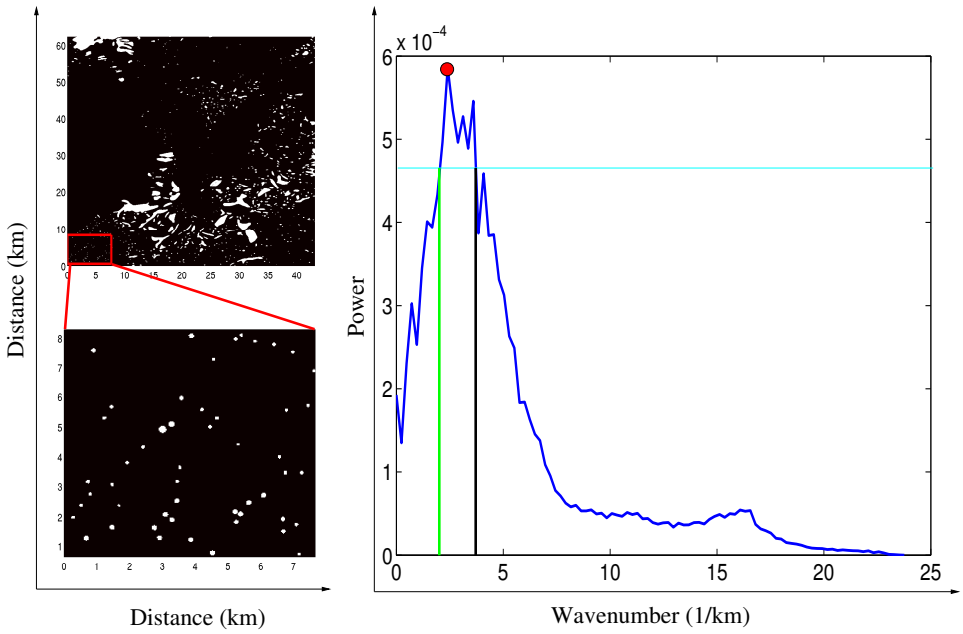


Figure A.1: The SNRA (top left) is plotted for 2007, where white areas denote regions of MPB attack. The red highlighted region (left bottom) is analyzed using Discrete fast Fourier transforms to determine the power spectral density (right). In this graph, the dominant wavenumber ($\nu_d$) is represented by a solid red dot, and the upper ($\nu_u$) and lower ($\nu_l$) bounds on the dominant wavenumber are displayed with vertical green and black lines, respectively.

Table A.1: Table of parameter sensitivity for the non-dimensional model (2.4). The simple-index, S, computes the ratio of the standardized change in the wavenumber to the standardized change in the parameter values [Hae05]. $S^+$ denotes a 10% increase in the parameter value while $S^-$ denotes a 10% decrease in the parameter value. Negative values correspond to the wavenumber increasing (decreasing) while the parameter is decreasing (increasing). Values of zero signify no change in the wavenumber with the parameter change.

| Par | $\overline{\lambda}$ | $b_1$ | $\overline{\delta_q}$ | $\epsilon$ | $\overline{k_p}$ | $\overline{\mu_p}$ | $\overline{\nu_a}$ |
|---|---|---|---|---|---|---|---|
| $S^-$ | 0.0423 | 0.0423 | 0.1273 | 0.2562 | 0 | -0.3303 | 0.1273 |
| $S^+$ | 0 | 0 | 0.1022 | 0.2538 | -0.0517 | -0.4193 | 0.1022 |

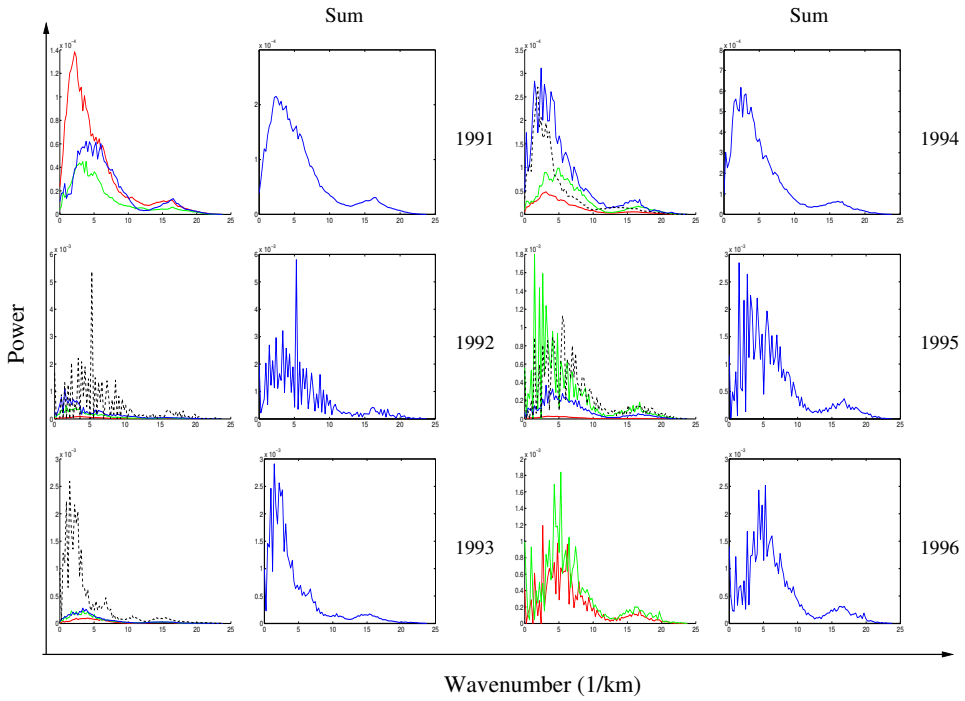


Figure A.2: Plots of power against spatial radial wavenumber, $\nu_r$, for years 1991-1996 (progressing top to bottom, then left to right) for all data analyzed. Different colours represent the analysis of a different region on the landscape. The right figure in each year is the sum of the power spectral densities over all regions in a given year.

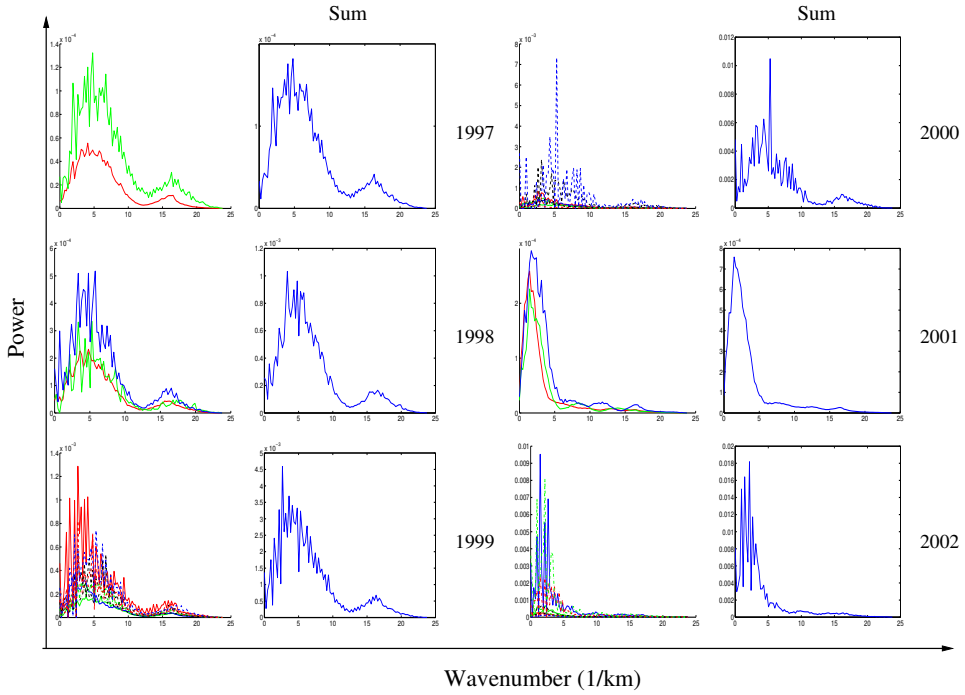


Figure A.3: Plots of power against spatial radial wavenumber, $\nu_r$, for years 1997-2002 (progressing top to bottom, then left to right) for all data analyzed. Different colours represent the analysis of a different region on the landscape. The right figure in each year is the sum of the power spectral densities over all regions in a given year.

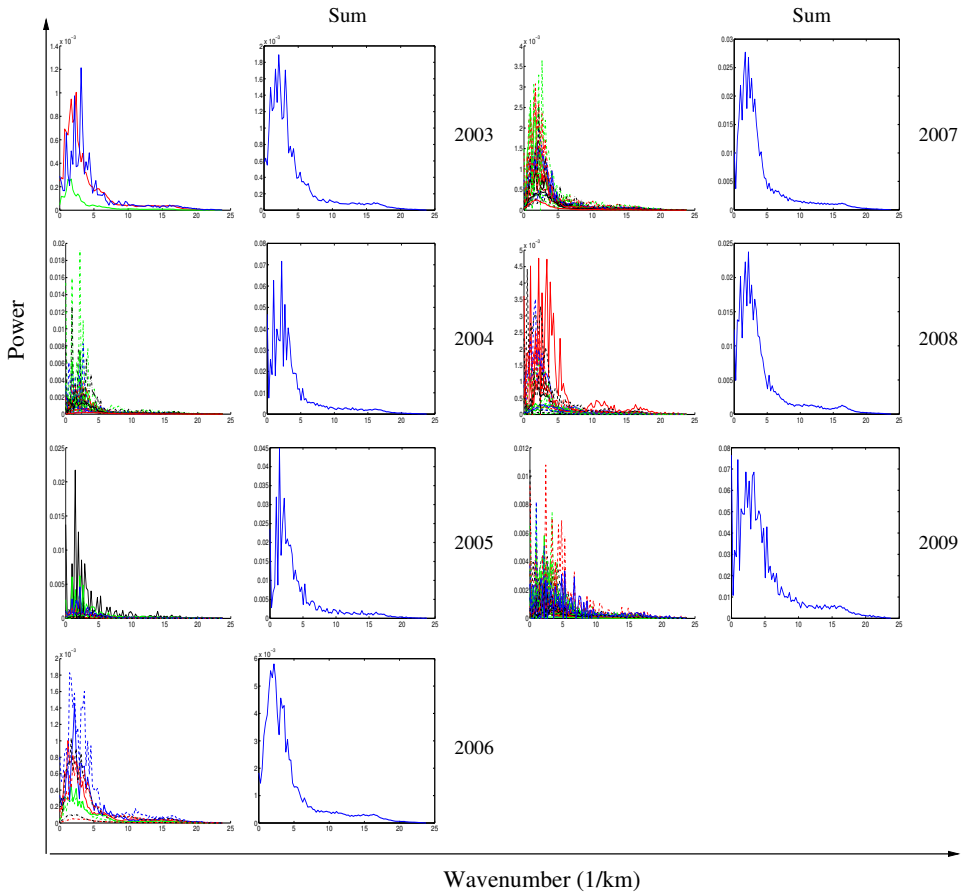


Figure A.4: Plots of power against spatial radial wavenumber, $\nu_r$, for years 2003-2009 (progressing top to bottom, then left to right) for all data analyzed. Different colours represent the analysis of a different region on the landscape. The right figure in each year is the sum of the power spectral densities over all regions in a given year.

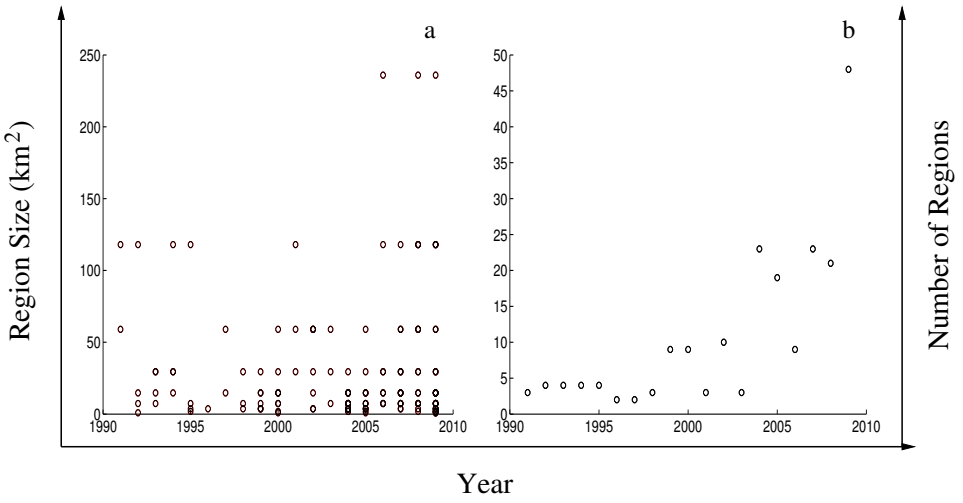


Figure A.5: The size (km$^2$) (a) and number of regions (b) over the time period 1991-2009. Multiple regions of the same size in the same year are represented by a single dot for clarity.

# Appendix B

# Burn Simulations

We simulated the burned 1-dimensional domains for three different initial conditions, beginning in the left undamaged patch (Figure B.1), beginning in the left damaged patch (Figure B.2), and beginning in the central scorched patch (Figure B.3). The plots depict the nesting MPB density at the end of every year over the spatial landscape.

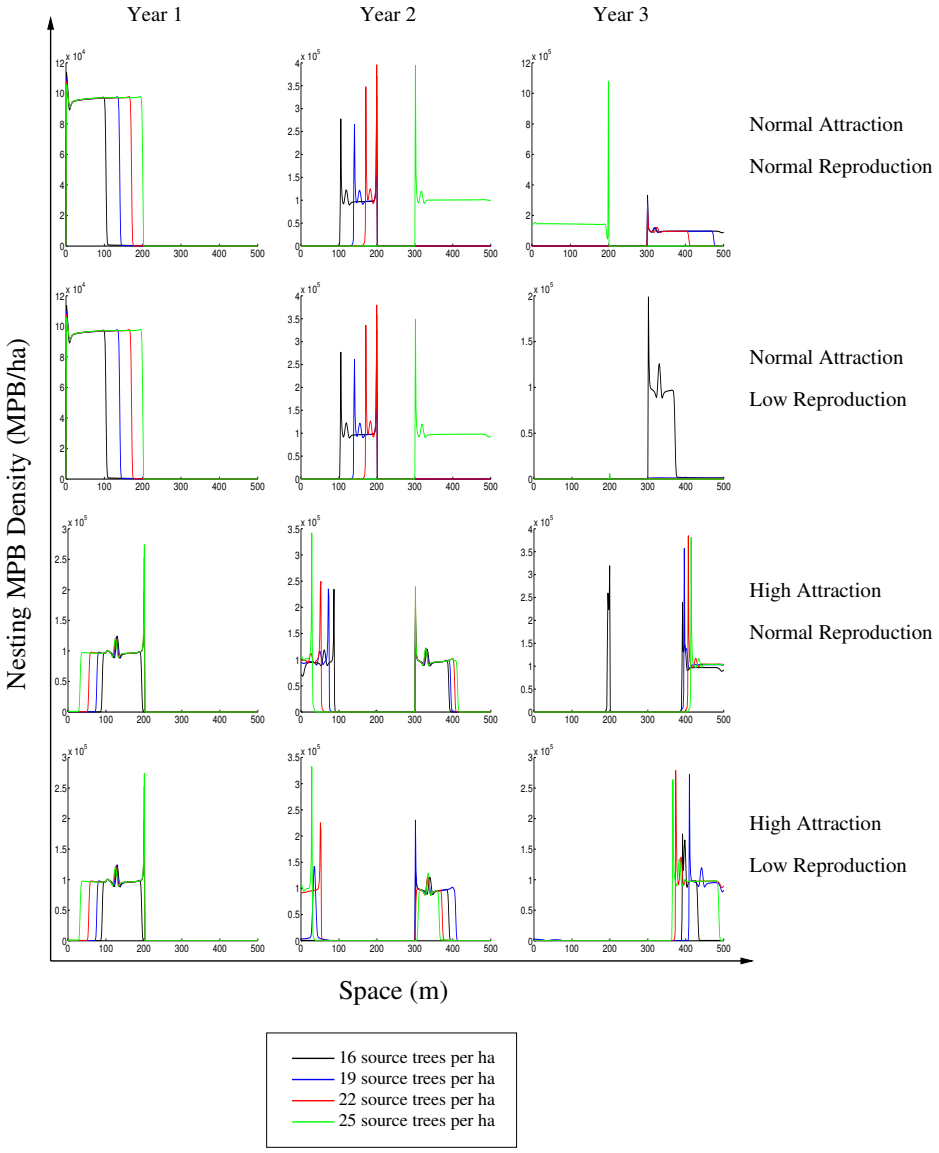


Figure B.1: Nesting MPB population density over space for various initial density of source trees. The assumptions on the reproduction (low or normal) and reproduction (normal or high attraction) change for each row of figures. This simulation assumes population of MPB emerge from the left undamaged forest region.

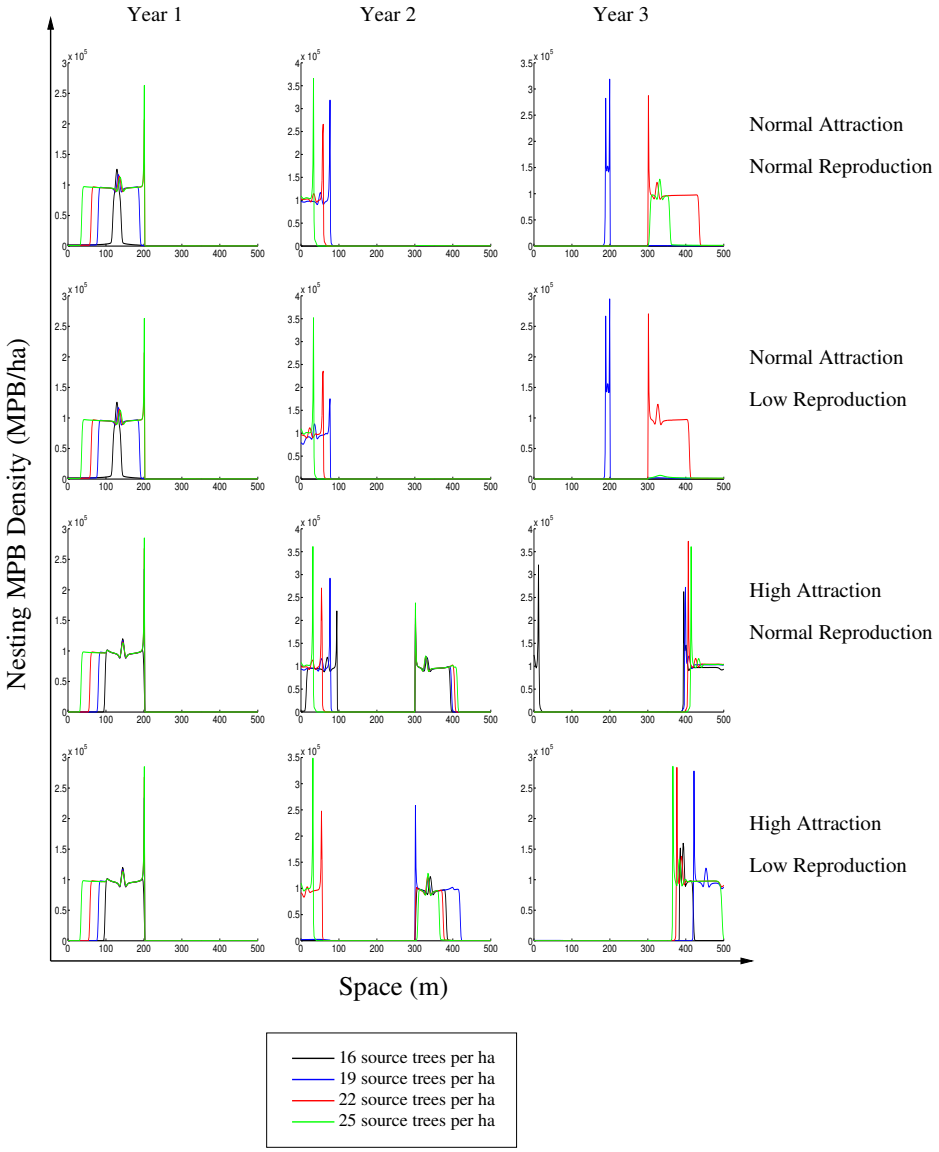


Figure B.2: Nesting MPB population density over space for various initial density of source trees. The assumptions on the reproduction (low or normal) and reproduction (normal or high attraction) change for each row of figures. This simulation assumes population of MPB emerge from the left partially burned region.

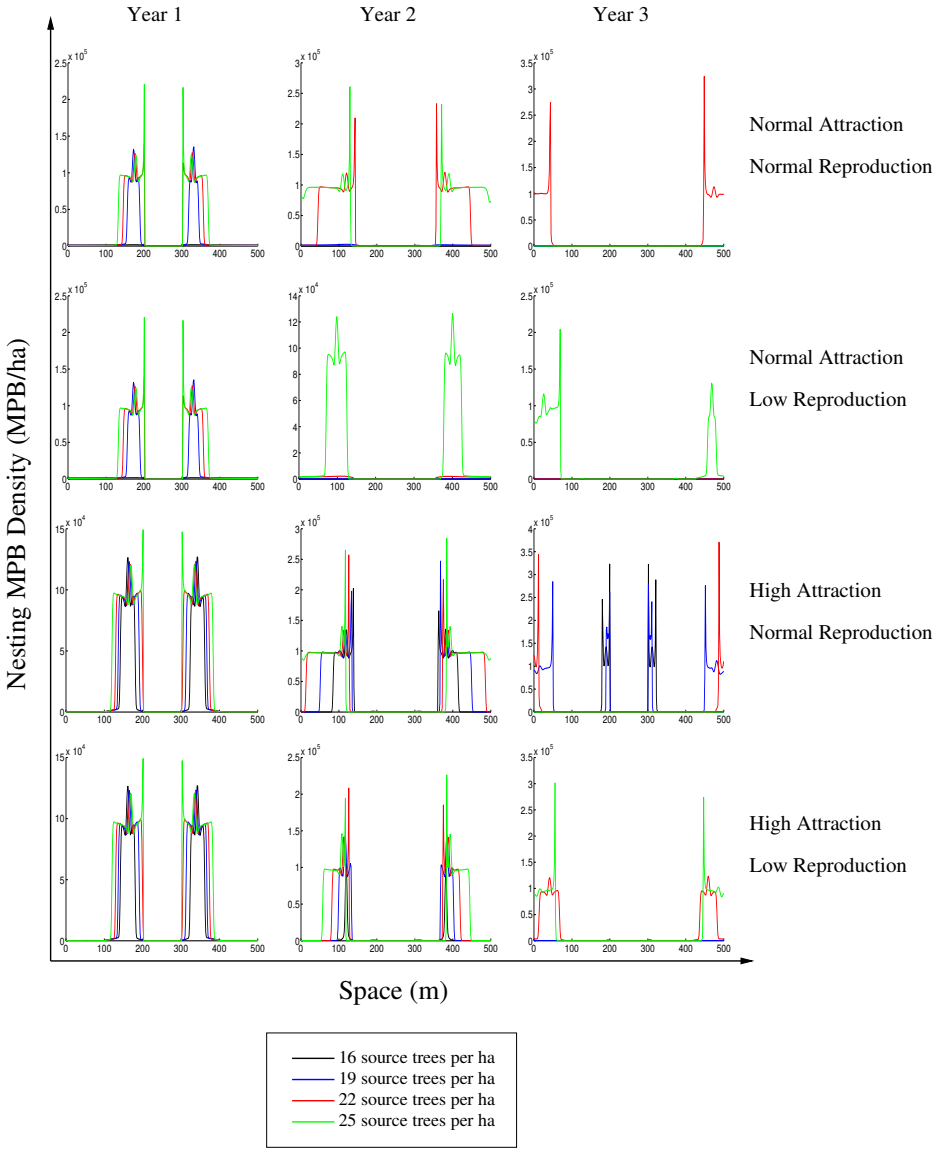


Figure B.3: Nesting MPB population density over space for various initial density of source trees. The assumptions on the reproduction (low or normal) and reproduction (normal or high attraction) change for each row of figures. This simulation assumes population of MPB emerge from the central scorched forest region.